Evaluating the use of laser processing and polishing techniques to generate micro-patterned surfaces for controlling fibroblast cell behaviour

Michael David Irving

A thesis submitted in partial fulfilment of the requirements of Liverpool John Moores University for the degree of Doctor of Philosophy

June 2017

ABSTRACT

The aim of this thesis was to develop novel micro and nano polymer substrates through different surface patterning techniques to compare their effect on human lung fibroblast (LL24) and bovine aorta endothelium (BAE-1) cell behaviours. The cells ability to adhere, proliferate and migrate were studied through the use of MTT assays and live cell tracking. Laser processing in a directional manner resulted in polyurethane surfaces having a ploughed field effect with micron-scale features a novel surface. In contrast, abrasive polishing in a directional and random manner resulted in polyurethane surfaces having sub-micron scale features orientated in a linear or random manner.

The cell results showed that for both the LL24 and BAE-1 cells the laser and randomly organised abrasive surface prompted cell adhesion when compared to the linear polished surface and non-patterned surfaces. The linear polished features did not enhance cell proliferation for wither cell type when compared to the flat surface. For cell migration a clear difference can be seen between the cell types with the LL24 cells showing a decrease in cell migration on the laser and random abrasive surface. The BAE-1 cells showed enhanced migration on the non-patterned surface when compared to the other surfaces.

This work was expanded to include different polished surfaces through the use of different grades of polishing paper. The results for the LL24 cells showed that though the polished surfaces promoted adhesion when compared to the non-patterned surface there was no clear difference between the surfaces for cell proliferation and migration. The BAE-1 cells results showed a similarity to the LL24 cells with the polished surfaces promoting adhesion when compared to the non-patterned surface. There was a clear distinction for the proliferation results with the LL24 cells showing enhanced proliferation on the scratched surface, this is in contrast to the BAE-1 cells which were enhanced on the non-patterned surfaces compared to the scratched surfaces.

A final study was performed to introduce the use of machine grinding to generate surfaces with micro-sized features and their ability to affect cell behaviour. Results are presented which show that polyurethane castings of the ground surfaces can promote LL24 cell adhesion and migration, demonstrating that this method can be a cost effective technique to be used in this field.

Table of Contents

ACKNOWLEDGMENTS

Since my A-Level days I have always dreamed of a career in science, following the completion of this work I am now closer then I have ever been to achieving that dream. Even though my name is at the front of this work it would not have been possible with the support of those around me.

First and foremost, I need to thank my parents, there support throughout my whole life has enabled me to push on down this path. Your guidance and advice has helped shape my life to this point and though there have been some pit falls and stumbles along the way it is your support that kept me going. I hope you know how much I appreciate you both and I will always be grateful.

Next I must thank my amazing fiancée Chloe, this has been the toughest work I have ever undertaken and having you beside me has helped keep the weight of it all off my shoulders. This final year were writing and working has been intertwined, your help has been even more important. I love you and thank you for everything.

Next I would like to thank Mark Murphy, having your expertise to call on has made my life so much easier during this programme. Your support with my presentations, papers and most importantly this thesis has been invaluable. You have also been a friend and have helped break the sometimes monotonous times with football talk, even if you are a blue.

My step into the world of engineering was a tough one and it would have been all the more difficult without the help of Paul French and Martin Sharp. The use of lasers was almost out of a world of science fiction when I started, but you were able to help me develop the surfaces now used in this work.

A lot of thanks must go to Francis Lilley and Dave Burton,. MATLAB was a foreign language to me at the beginning but through your guidance and a lot of editing the development of surface analysis work began to take shape. The only regret would be that we were not able to complete that work and I hope both of you stay well and continue doing what you enjoy.

Peter Moran there is also a big thank you to you for your provision of my samples, the key starting from which all was built on. Your support with my first published paper is also much appreciated, your providing of the ground samples and the explanation of the grinding process made it possible.

Finally, a thank you to Simon Dixon and the people of Biomer for the provision of the polymer substrate I used in my work. The quick resupply ensured no delays happened and I was able to work consistently throughout.

LIST OF ABBREVIATIONS

2D Two dimensional

3D Three dimensional

AFM Atomic force microscopy

ArF Argon fluoride

ASIC Application-specific Integrated Circuit

BAE-1 Bovine aorta endothelium-1

BHK Baby hamster kidney

Cs Continuous wave

CO^2 Carbon Dioxide

DMEM Dulbecco's Modified Eagles Medium

DMF Dimethylformamide

DRAM Dynamic Random Access Memory

EBL Electron beam lithography

ECACC European Collection of Authenticated Cell Cultures

ECM Extracellular matrices

ERK Extracellular signal regulated kinase

F_2 Fluorine

fs Femtoseconds

H_2O Hydrogen Dioxide

HeLa Human Epithelial Cervix cells

hASCs Human Adipose Derived Stem Cells

HOBs Primary Human Osteoblast cells

J/cm^{-2} Joules per square centimetre

kHz Kilohertz

KrF Krypton fluoride

kV Kilovolts

LL24 Human Lung Fibroblast Cells

LSM Laser Scanning Microscope

M Metal

MC3T3-E1 Mouse Monoclonal Osteoblastic Cell Line

MDCK Madin Darby Canine Kidney Cells

MHz Megahertz

MG-63 Osteoblast-like Cells

mJ Millijoules

MMPs Matrix Metalloproteinase

m/s Meter per second

NA Numerical aperture

NIH3T3 National Institute of Health Mouse Embryonic Fibroblasts

OSX Osteoblast-specific Transcription Factor Osterix

pBrS poly 4-bromostyrene

PBS Phosphate Buffer Solution

PDMS Polydimethylsiloxane

PLGA Poly (lactide-co-glycolide)

pMMA Polymethylmetacrylate

PR Photoresist

PS polystyrene

Ra Roughness Average

RBP2 Retinol Binding Protein 2

RMS Root mean square

RPM Rotation Per Minute

Rt Average Maximum Height

Rz Mean Roughness Depth

Sa Surface Roughness Values

SLA Sand blasted

SD Standard deviation

SEM scanning electron microscopy

Si silicon

SOC System-on-Chip

THF Tetrehydrofuran

Ti Titanium

Ti-A Titanium Alloy

Ti-6Al-4V Grade 5 titanium alloy (titanium with chemical composition of 6% aluminium, 4% vanadium)

TIMPs Tissue Inhibitor of Matrix Metalloproteinases

UV Ultraviolet

W watt

X-ray X-radiation

Figure List

List of Tables

Chapter 1 - Introduction

1.1 Background

Mammalian cells have evolved to interact with their physical environment and this interaction is crucial for many important cellular behaviours including; adhesion, migration and proliferation. *In vivo*, cells depend on an interaction with a 3D scaffold known as the extracellular matrix (ECM). It is thought that the geometrical organisation and mechanical compliance of the ECM is extremely important in helping to regulate the aforementioned cell behaviours. As a consequence, there has been a significant research effort that has focussed on the development of cell substrates having both two dimensional (2D) and three dimensional (3D) structures that mimic the features of the ECM. This has largely been achieved through patterning materials to develop 'functional' or 'smart' surfaces that can be used to better control cellular responses *in vitro*.

Development of such surfaces has been shown to have significant impact on improving the integration of prosthetic implants. For example, modification of dental implants, to alter surface roughness properties, has been shown to improve implant integration [12]. Similarly, increasing the surface roughness of breast implants has been shown to increase the surface adhesive properties for fibroblast cells and it has been suggested that this increased cell adhesion will improve wound healing following implantation, thus limiting the risk of capsular contracture [13]. Therefore, there is a clear benefit and need to develop such materials for use in biomedical applications.

Much of the work in this area has focussed on developing surfaces having specific features with defined geometries and sizes, for example micro and nano-scale grooves [14],

pillars[15] and pits [16]. These surfaces have been shown to influence cell adhesion[17], proliferation and migration [18] of a range of cell types including fibroblasts [16], osteoblasts [19], endothelial [20], epithelial [21] and neurons[22].

Many methods are available for modifying topography to develop functional surfaces. One of the most widely used techniques is through the use of a template mask, which is placed over the surface that is due to be processed, leaving a predetermined pattern, post processing. This method is seen in lithography based techniques including; electron beam lithography [16, 23, 24], colloidal lithography [25], photolithography [14, 26, 27], Langmuir–Blodgett lithography [28] and X-ray lithography [29, 30]. Such methods are advantageous, as they allow the development of substrates having a range of well-defined geometries however, they often require expensive equipment and are generally time-consuming processes.

This thesis describes the use of laser processing, abrasive polishing and machine grinding techniques to develop surfaces that can be used to manipulate the adhesion, migration and proliferation of fibroblast cells. Laser processing has been shown to be an effective method for micro-patterning for cell control, due to it being a rapid, direct-write and flexible process [31] which, is also capable of processing large areas [32]. In contrast the use of polishing methods and grinding for developing textured surfaces for manipulating cell behaviour have been largely overlooked, even though they are comparatively cheap processes that can be used to produce surfaces having feature of comparable sizes to the lithographical based methods listed above.

1.2 Aims and objectives

The aims of the work presented in this thesis were:

1. To develop novel surface topographies through the use of different surface patterning technologies namely laser processing, surface polishing and machine grinding.

2. To characterize these polyurethane surfaces using different microscope techniques.
3. To investigate the effects of these novel surfaces on LL24 and BAE-1 cell adhesion, migration and proliferation.

The general objectives of the work presented in this thesis were:

1. To use two laser types to compare the effect of processing on steel through changing of parameters such as laser power, speed, pass number. To use different grades of silicon carbide paper to produce different sized features on steel, and to change the depth of cut on the grinding wheel to produce features of different size following a pass over steel.
2. To use a scanning electron microscope to observe surface topographies while also using white light interferometry and atomic force microscopes to measure the topographical features and gain measurements of average surface roughness (Ra), the average maximum height value (Rt) and mean roughness depth.
3. To use cell culturing techniques and different bioassays including MTT assay and time lapse photography to determine the effect of the different surfaces on cell behaviour.

1.3 Impact of Research

The impact of my research comes in two areas. Firstly I have been able to demonstrate the suitability of two techniques limited in technological terms, the surface polishing and machine grinding for development in modifying cell behaviour. This opens up the research area to those unable to develop higher cost manufacturing machinery such as lithographic methods. Secondly I have been able to determine a link between the cell processes of adhesion and migration through surface topography. The link seen between surfaces that

promote and adhesion and migration while limiting proliferation is something that should be taken into account for any future surface development research. Finally I have continued the trend shown by other researchers that cells are negatively affected by uniform patterns. This can be seen throughout all comparisons between the linear and random surfaces were cells show increased adherence to the random surface.

1.4 Structure of the Thesis

This thesis is concerned with modifying surface topography to enhance the adhesion and growth of cells whilst also investigating the effect on cell migration. It will compare three different surface patterning techniques and their unique patterns on the modification of the above mentioned processes. Two cells are used for this investigation, human lung fibroblast cells (LL24) and bovine aortic endothelial cells (BAE-1), such work has potential to improve medical implant technology and the tissue engineering processes.

Chapter two will be used as a background to the work, it will introduce the science behind maintaining of cell structure and the role of the extracellular matrix to ‘set the scene’, and highlight the impact that surface topography has on controlling cell behaviour and function.. It will discuss the different structural proteins within the cell including; the cytoskeleton and their functions with respect to cell structure, adhesion and migration. It will also introduce the naturally occurring extracellular matrix structure and topography, which is inspiring scientists to either reproduce or generate new user designed surface topography to maintain or improve cell bio-functionality. Finally, this chapter will introduce the role of integrin receptors and focal adhesion which are important structures that provide the structural link between the cytoskeleton and the ECM.

Chapter three will critically discuss the current technologies available which are commonly used to fabricate surfaces having micro and nano-sized topographical features and which have been used for biomedical studies. It will explore a range of technologies that are expensive and highly specific in their ability to produce defined features such as lithography and laser based techniques, as well as technologically less complicated methods such as mechanical polishing and surface grinding. This will be followed by a discussion on how cells respond to such surface topography.

Chapter four of the thesis will discuss the experimental design/approach to the work highlighted in this thesis. It will present the different techniques that have been used and the reasoning behind those using these techniques. It will also introduce the model cell lines used and justification for choosing these cell lines. Finally, this chapter will also discuss the experimental approach with respect to bioassays used and cellular behaviours studies.

Chapter five will detail the materials and methods used to conduct the research carried out in this thesis.

Chapter six will present the results. These results are based on developing and characterising surfaces using a range of advanced imaging techniques and from bio-experiments that were carried out in order to investigate the effects of surface topography on cell behaviours including; cell adhesion, cell morphology, proliferation and migration.

Chapter seven will discuss the results. This chapter will draw upon the relevant literature to discuss the results and put them into context with the aim of understanding how the cells interact with the developed textured surfaces.

Chapter eight contains the conclusions drawn from this research work.

Chapter nine will provide some suggestions for future work.

Chapter 2 - Background

2.1 Cytoskeleton organisation and the extracellular matrix

Understanding how cells adhere, migrate and divide is an important facet when developing surface topographies. Such processes have been shown to be controlled, somewhat, by an interconnected network of cell proteins that provide the cell with structural and mechanical integrity, this is known as the cytoskeleton. Its existence was first confirmed in the 1960s by Inoue and Sato in 1964 [33] and Roth and Daniels in 1962 [34], and is a highly organised network of filamentous protein structures made up of actin filaments, intermediate filaments and microtubules [35]. Each filament consists of subunits that can be assembled and disassembled when required. The importance of the cytoskeleton is linked to its ability to connect the nucleus of the cell with the extracellular matrix providing a link between molecules involved in cell communication and those involved in gene expression [35]. The cytoskeleton is also important when analysing cell adhesion, Ingber *et al* 1989 showed a link between the cytoskeleton and the cells attachment to the substrate. When judging cell attachment, it was determined that an increase in cytoskeleton tension was linked to improved cell attachment and that the flatter a cell was the more tension was seen in the cytoskeleton and thus the stronger its attachment was [36].

2.2. Cytoskeleton filaments

The cytoskeleton is made up of three different filaments; these are microtubules, intermediate filaments and actin polymers. Microtubules are the largest of the three with a typical diameter of 25nm (figure 1a) [37], it is tubular in shape and made up of globular tubulin subunits that vary in length. The filaments are able to shrink and grow rapidly as required and are able to form highly stable structures when attached between molecules to

prevent depolymerisation, this leads to a highly organised network within the cell which contributes to the integrity of the cell both structurally and mechanically [37]. Microtubules have also been involved in the motility of cilia and flagella, the movement of chromosomes and organelles, cytokinesis while also being involved in maintaining cell shape and internal organisation [38, 39].

2.3 Actin

As seen in figure 1b actin is the smallest of the cytoskeleton filaments but the most abundant being only 7nm in diameter and making up between 1-5% of the total cellular protein. It is found in two forms, as a globular monomer (G-actin) and as a filamentous polymer (F-actin), which consists of twisted linear chains of G-actin subunits [40]. When bundled together or set into networks of filaments, actin provides support to the cell membrane and is linked to the determination of cell shape and mechanical integrity [37]. Actin is also involved in cell motility; directed growth of the polymer chain at the leading edge of the cell maintains the direction of movement. Multiple actin filaments can form parallel bundles known as stress fibres one end inserts into the plasma membrane forming a focal adhesion point between the cell and the substrate. [41].

2.4 Intermediate Filaments

Intermediate filaments are the second largest of the cytoskeleton proteins at between 8-10nm in diameter (figure 1c). The function of intermediate filaments is to withstand mechanical stress when the cell is deformed, this is based on the fact that they are found predominantly in cells that undergo regular mechanical stress, such as muscle cells, which is where they were originally discovered. The filaments are composed of long rod shaped proteins such as

keratins or vimentin, they are typically elongated fibrous proteins composed of an amino-terminal globular head, a carboxyl terminal globular tail and central rod domain [37].

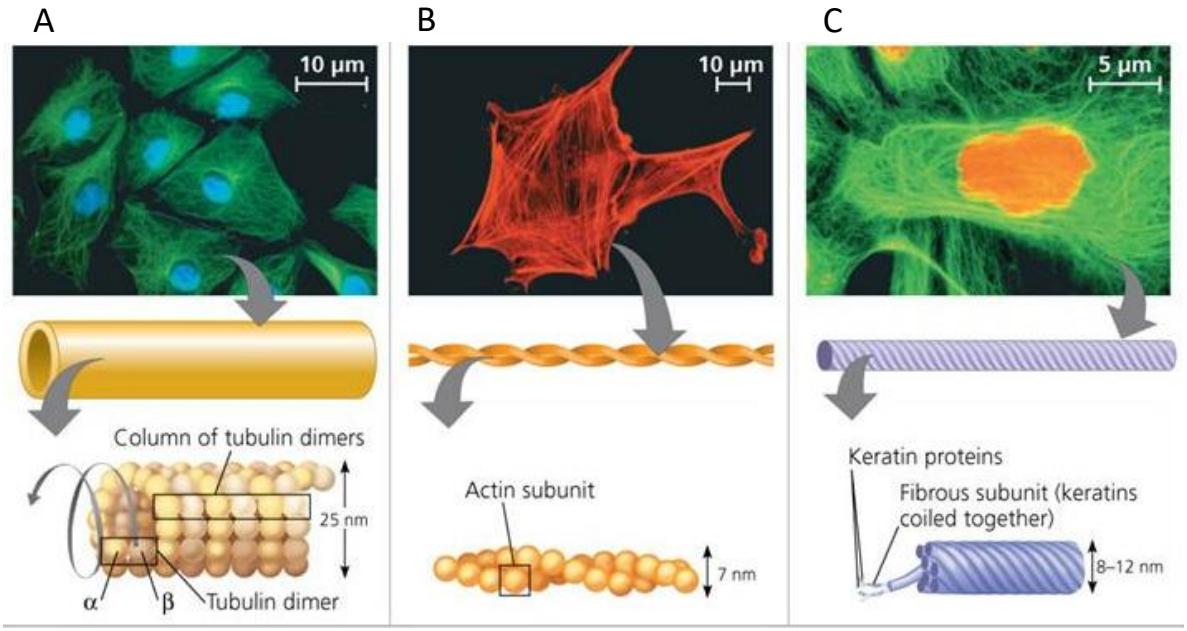

Figure 1 Fluorescent microscope images of fibroblasts, different proteins have been tagged; A, tubulin B, actin C, Keratin [1]. Reproduced with permission of Pearson.

2.5 Focal Adhesions

Focal adhesions as highlighted in figure 2 form at points of attachment between the cell and the ECM through the clustering of integrin receptors which recruit structural and signalling molecules. They are made up of a number of structural proteins including talin, vinculin, tensin and alpha actin, while also being made up of the signalling proteins focal adhesion kinase, c-Src, p120cas and paxillin [42]. The role of focal adhesions has been linked to cell attachment and migration through their ability to sense substrate rigidity [43, 44] while also being able to transmit forces from stress fibres through to the ECM. This ability to respond to the surfaces through mechanosensing and mecahnotransduction feedback loops regulates focal adhesion and cytoskeleton assembly [45, 46]. This is then responsible for regulating cellular functions such as migration[47], spreading [48] and differentiation[49, 50].

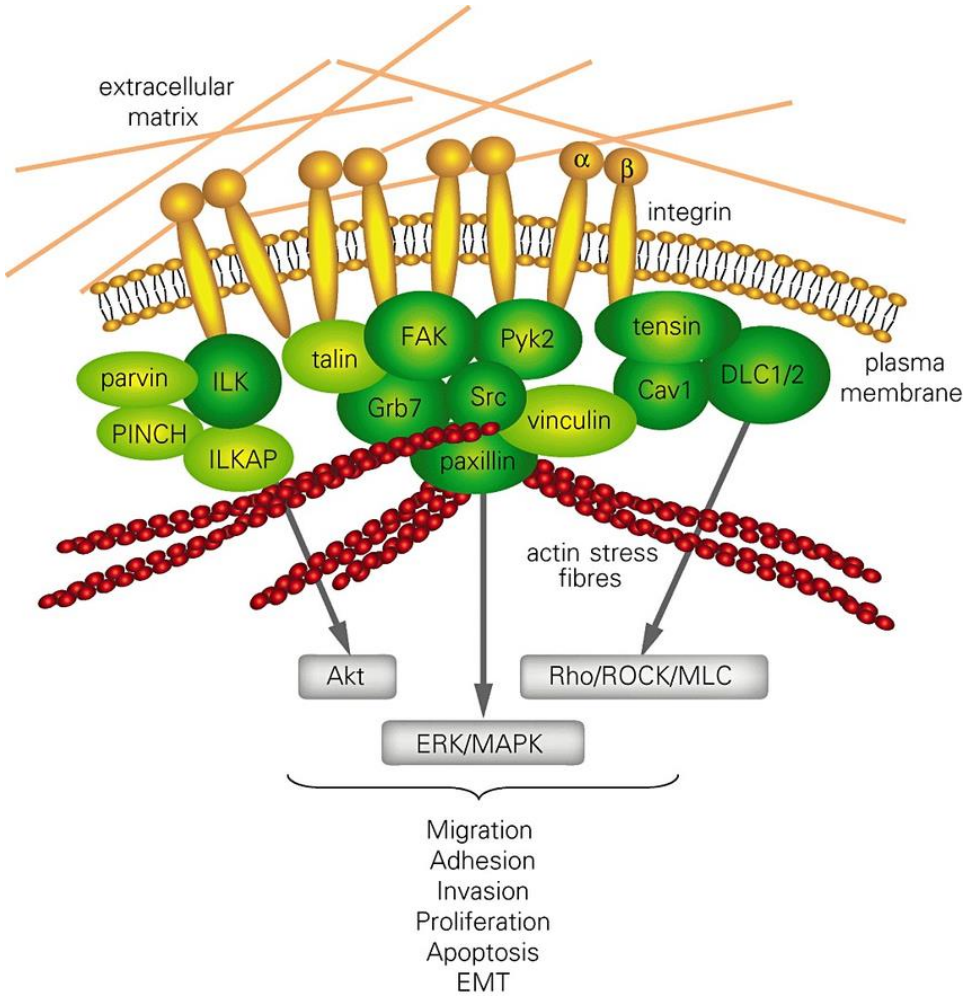

Figure 2 Schematic diagram illustrating a focal adhesion complex. [2]. Reproduced with permission of John Wiley and Sons.

2.6 Extracellular matrix

The reasoning behind designing surface topographies to modify cell behaviour is linked to the ECM (figure 3). The ECM is a highly organized structure that consists of different extracellular macromolecules including collagen, elastin, fibronectin and laminin. The ECM *in vivo* provides structural support and physical cues for cell attachment, migration, proliferation and gene expression. While it also able to generate highly complex three dimensional ECM sheets which contain a range of structures such as grooves, pits, pores,

pitched ripples and fibres in both the micro and nano size range that can also fold into a tertiary organisation with features on the mesoscale. In animal tissues the ECM exists in two forms: the basement membrane and the stromal matrix [51]. Studies have shown that the ECM has specific organisations, architecture and feature dimensions depending on the tissue it was taken from. This specificity is important to support local tissue bio-functionality.

The basement membrane structure is formed by cross linking of laminin, type IV collagen, entactin and perlecan [52] and it provides adhesion sites that support the overlying epithelial cells and compartmentalises the epithelial cells from other cell types. However, the organisation, architecture and feature dimensions vary depending on its specific location in the animal tissue. This was demonstrated by Kawabe *et al* 1985, who upon examination of the basement membrane of human plantar skin noted that the structure is comprised of millimetre scale primary and secondary grooves and dermal papillae. The primary grooves exhibited a microscale reticulated appearance with a net-like arrangement of collagen fibrils which contained holes, these holes were the ducts of eccrine sweat glands [53]. The human bronchial basement membrane was investigated by Howat *et al*., and was revealed to have a porous topography [54, 55]. Whilst, Li *et al* investigated porcine oesophagus basement membrane morphology which showed that it was constructed from interwoven fibres and pores which were unevenly distributed [56]. Such studies highlights the difference in ECM structure with tissue location and the ability of cells from different tissue types to respond to different ECM structures/topography.

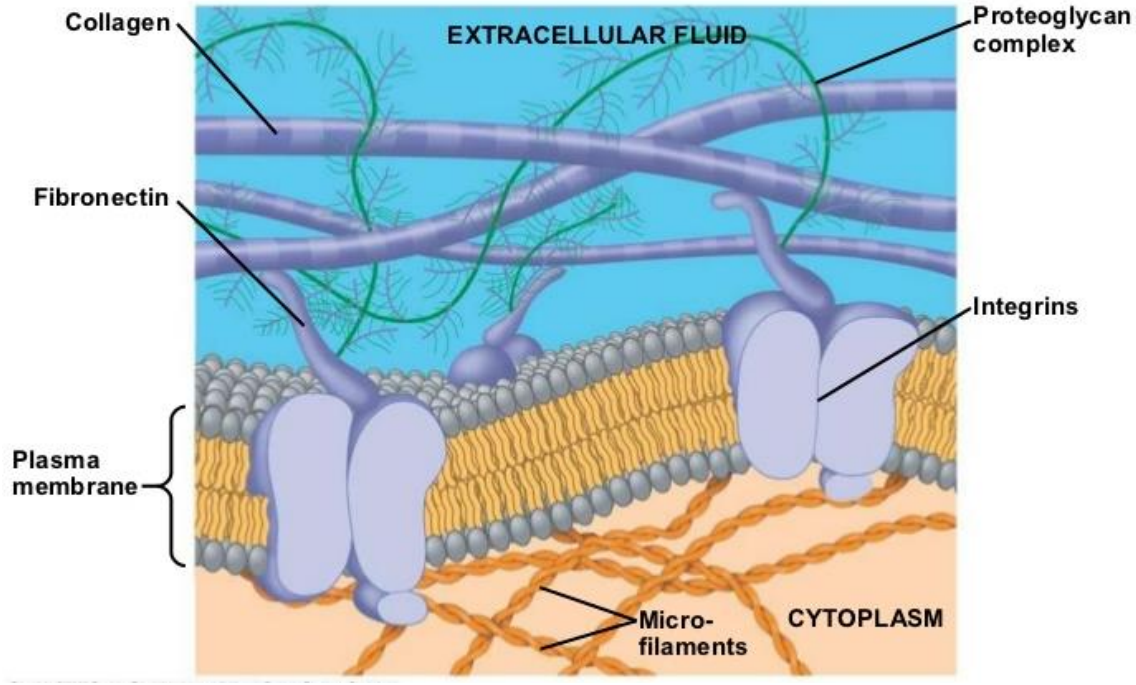

Figure 3 Extra cellular matrix of an animal cell [1]. Reproduced with permission of Pearson.

2.7 Practical applications for ECM

The importance of the ECM in cellular processes, specifically its role in wound healing, has been identified and has led to the development and commercially available ECM based materials. Currently there is a variety available such as INTERGA®, OASIS® AND Unite®. The process of wound healing is divided into four stages inflammation, proliferation, granulation and matrix remodelling [57], the matrix remodelling process is a result of the depositing of a collagen matrix by fibroblast cells. This is followed by scaffold degeneration and remodelling at the damage site as the cells regenerate. INTERGA® has been shown to be useful for deep partial-thickness and full-thickness burn wounds, full thickness skin defects with different aetiologies, chronic wounds and soft tissue defects. It is composed of cross linked bovine tendon collagen glycosaminoglycan and a semi-permeable polysiloxane. OASIS® which is derived from porcine a cellular small intestinal submucosa, provides an

optimal environment which allows cellular and vascular infiltration for tissue bio-functionality and structural restoration.

These examples of the practical use of ECM substitutes demonstrates the importance such features can have on wound healing, that the topography of these products improves the healing rate of burns following application. This shows that by investigating the effect different topographies have on cell behaviour it has the potential to further improve patient wellbeing. The next chapter will provide examples of work that has been undertaken to investigate the effect of a range of topographies on a number of different cells and how it affects their behaviour. A range of different patterning techniques will also be investigated to compare the patterning processes and the resulting topographies.

Chapter 3 - Literature Review

3.1 Different Techniques for surface patterning and the cellular response to those features

3.1.1 Photolithography

The process of lithography has come a long way since its origin back in 1798 with the development of a lithographic printing process by Alois Senefelder [58]. From limestone, ink and correction fluid to photoresist, ultra violet (UV) lamps and silicon, the lithographic process has become a major industrial process.

Currently lithography employs an optical projection printing process and as such it follows the Rayleigh criterion, limiting the resolution capabilities:

$$R = k1\frac{\lambda}{NA}$$

Were the constant (k1) is dependent on the process being used [59]. In integrated circuit technology $k1$ values can range from 0.5 to 0.8. Numerical aperture (NA) of optical lithography tools range from 0.5 to 0.6.[59]

Improvements in lithographic resolution have come from decreases in the printing wavelength (table 1) as well as the development of improved resist materials that exhibit high imaging contrast. Currently the best lithographic performance is at 248nm [59] and unless further development of resists for 193nm or shorter wavelengths can be developed, continued feature size shrinkage through wavelength reduction is not feasible. The ability to generate features below the µm scale makes lithography an important process within the semiconductor industry and further advancement, through next generation techniques to produce sub 100nm features, will continue its importance.

Table 1 The different illumination sources for photolithography

Illumination source	Mercury lamp		Excimer laser		
	G-line	I-Line	KrF laser	ArF laser	F_2 laser
Wavelength	435nm	365nm	248nm	193nm	157nm
Smallest lateral dimension that can be produced	500nm	350nm	250nm	180nm	120nm

There are however limits to using the process, for example the mask used to produce the required pattern is typically manufactured 4-5× larger then final features. This is primarily due to limits to the mask making procedure, and can lead to the problem of mask error enhancement factor.

Another limit includes the cost of manufacturing. The cost of lithography can be split into different areas:

The 'Tool Cost', which is divided by the number of wafer printed (throughput) in an hour; The 'Cost of the Mask', which is divided by number of wafers printed by that mask and the 'Process Cost' includes the cost of resist application and development. Tool cost can also include the cost to operate an exposure tool, depreciation, labour space etc. The Mask cost can vary significantly depending on the industry being examined; DRAM manufacturing can produce 3000-5000 wafers per mask, microprocessors around 1500 and ASIC/SOC downwards of 500 per mask. What also must be taken into consideration is that each new design will require a new mask for its production, this means that with each alteration the cost increase as the number of masks required does also [59]. This must be factored in when deciding on whether to use a lithographic technique particularly when a high rate of design

change is planned. The combination of these costs make lithography based processing an expensive method for testing cell behaviour modification. The optimization process would require many new masks for short term use until an optimum one can be identified and focused on for testing. This cost would need to be offset by the methods ability to produced features on a nano scale and its ability to generate specific features.

3.1.2 Lithography Methods

Though not universal, the method for patterning surfaces using photolithography is similar across all experiments (figure 4). Initially, the relevant substrate material is chosen which is usually materials such as perspex [60], polystyrene [3] or silicon [61]. The material is then coated in a metal layer (figure 4.1) usually of aluminium [60], chrome [3] or titanium [61]. Next, a photoresist layer is added (figure 4.2) which is typically spin coated on to the surface and then baked, though temperature and time of baking is not universal. Two types of resist are used, positive or negative. Positive resists are more commonly used from which the areas exposed to UV light are dissolved during development. Negative resists, in contrast, become insoluble when exposed, to UV light [62]. The next step is to use UV light and a 'mask' to generate the required pattern on the photoresist layer (figure 4.3-4). The 'mask' is typically a quartz substrate with a chrome pattern which prevents the light passing through[62] and is patterned by a scanned electron or laser beam primary pattern generator [59]. The exposure time can vary between 1 and 30 seconds depending on the pattern and resist. The next stages involve removing the exposed photoresist then the underlying exposed metal layer (figure 4.5-9).

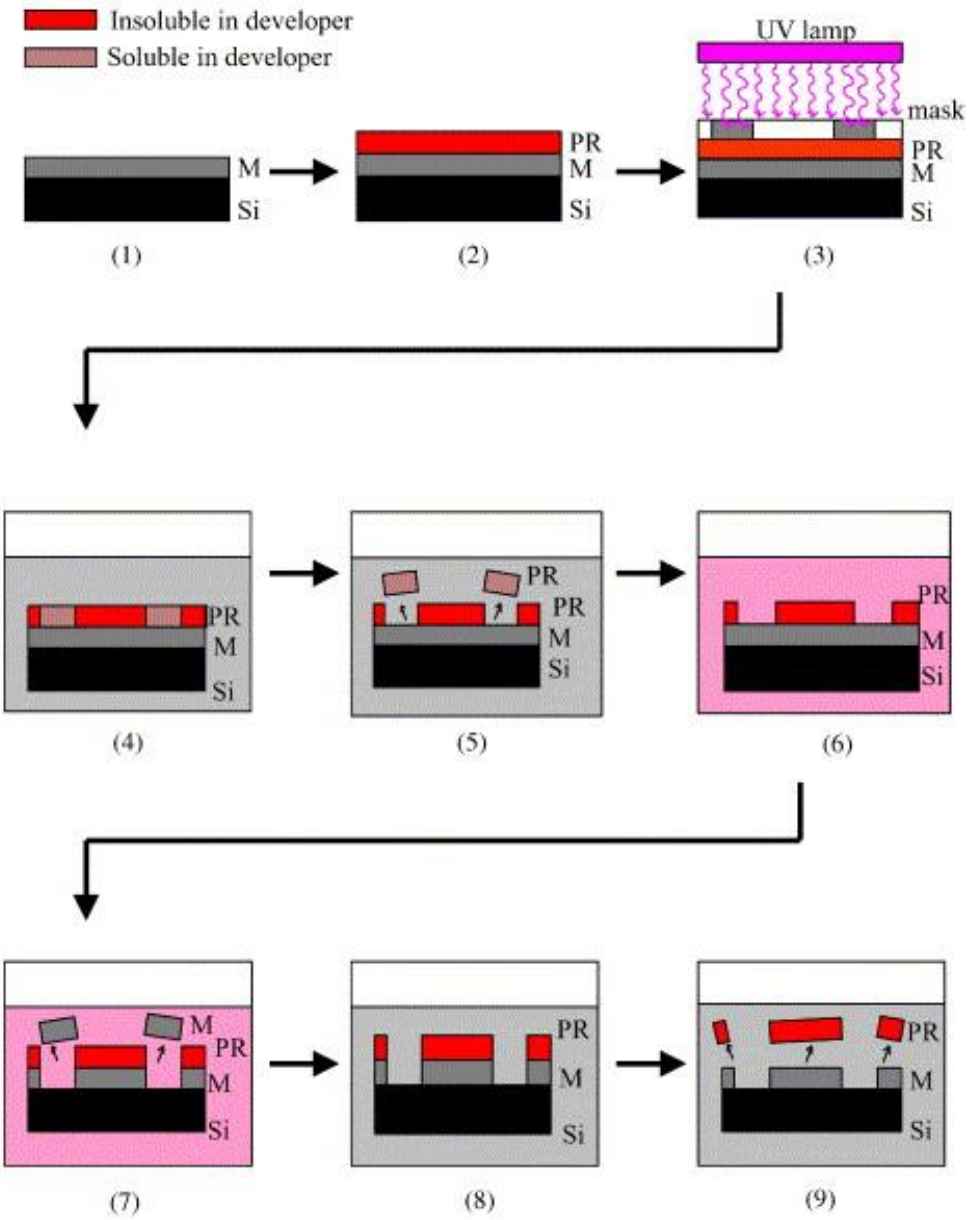

Figure 4. The steps involved in the photolithography process following the creation of a photomask and surface preparation of the silicon wafers. These photolithographic techniques allow the preparation of silicon wafers having desired micro-patterns. PR=photoresist, M=metal, Si=silicon wafer [3]. Reproduced with permission of Elsevier.

3.1.3 Lithography methods in surface patterning

There has been numerous examples of using lithography to develop patterned surfaces for biomedical applications, , these have included simple steps [60], microgrooves [3, 61], micro pillars [4] and micro pores [63].

In 1987 Clark *et al* demonstrated the effect of simple micron-sized steps generated by photolithography on baby hamster kidney cells (BHK) and chick embryo hemisphere neural cells (CH). This work demonstrated that by increasing the step height a corresponding decrease in the cells ability to climb the step is seen, it would also suggested that groove depth is possibly the most important factor influencing the orientation of cells [60].

Work by Recknor *et al* in 2003 used photolithography to pattern polystyrene (PS) to have grooved features with the dimensions of 10/20/3µm for groove width /groove spacing /groove depth (µm) as seen in figure 5. The effect of the grooves combination on astrocyte behaviour was tested and compared to non-patterned PS. Clear differences were noted between the morphology of the cells growing on the patterned surfaces, in that the cells were observed to be highly elongated. In contrast, the cells growing on the non-patterned surface were polygonal in shape with cellular processes extending out from the cell in a radial fashion. Also, when analysing cell alignment it was determined that on the grooved surface the number of cells that were aligned within 20 and 10° of the groove direction was significantly higher compared to cells on the non-patterned surface [3]. These results demonstrating that the astrocyte cells responded to physical stimulus.

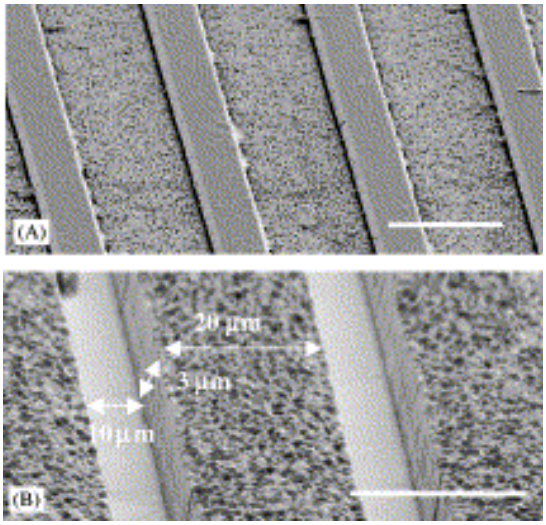

Figure 5) A 20/10/3µm silicon wafer used as microdie. (B) A scanning electron microscope (SEM) image of a PS film having groove dimensions of 10/20/3µm created by solvent casting onto the microdie. Scale bars=20µm [3]. Reproduced with permission of Elsevier.

Similarly, in 2003 Andersson *et al* also tested the effect of groove substrate on cell behaviour. In this work the substrate patterned via photolithography was titanium with mean groove dimensions of 184nm depth, 14.8µm ridge width and 14.8µm groove width. In this study T24 bladder epithelial cells were used and the effect of surface grooves was compared with non-patterned surfaces and surfaces containing pillars created through colloidal lithography. In this study it was found that there was no difference in cell number across the surfaces. However, there was found to be significant differences in the expression levels of the cytokines IL-6 and IL-8 proteins associated with the cells response to bacterial infection, with the levels being much lower in the cells growing on the pillar surfaces compared to the grooved and non-grooved surface, which was found to express similar levels of the cytokines. There was also a difference in morphology, cells on the pillars had a smaller area, were less round, and had more outgoing membrane projections compared to cells on flat. The author suggests that these results suggest a link between the surface topography,

specifically the pillars and the integrin binding to the surface bound ECM components altering the cell morphology. This alteration could result in the changes in cytokine release. [61].

Photolithography has also been used to develop surfaces having micro-pillars and micro-wells. Turner *et al* (2000) generated pillars of specific widths as can be seen in figure 6, (0.5, 0.75, 1.25, or 2.0μm) and specific inter-pillar distance (0.5, 1.0, 1.5, 2.0, 2.5, 3.0, 3.5, 4.0, 4.5, or 5.0μm) with a height of 1μm, into a silicon substrate. For the wells the spacing distance varied (0.5, 0.75, 1.25 or 2.0μm), but their width was 0.5μm and 1μm deep. This study showed that on the pillars/smooth surface 70% of cells preferentially attached to the pillared surface, were as only 40% of cells did the same on the surface containing wells. When comparing morphologies cells were seen to be more spread on the pillared surface compared to the cells growing on both the smooth and welled surfaces. The author hypothesises that this is due to the amount of surface area available to the cell, the pillars promoted attachment, seen with the increase in spreading were as the wells did not. The well topography, the author suggests, may have may have resulted in trapped pockets of medium that would result in nutrient depredation and thus limited cell growth [4].

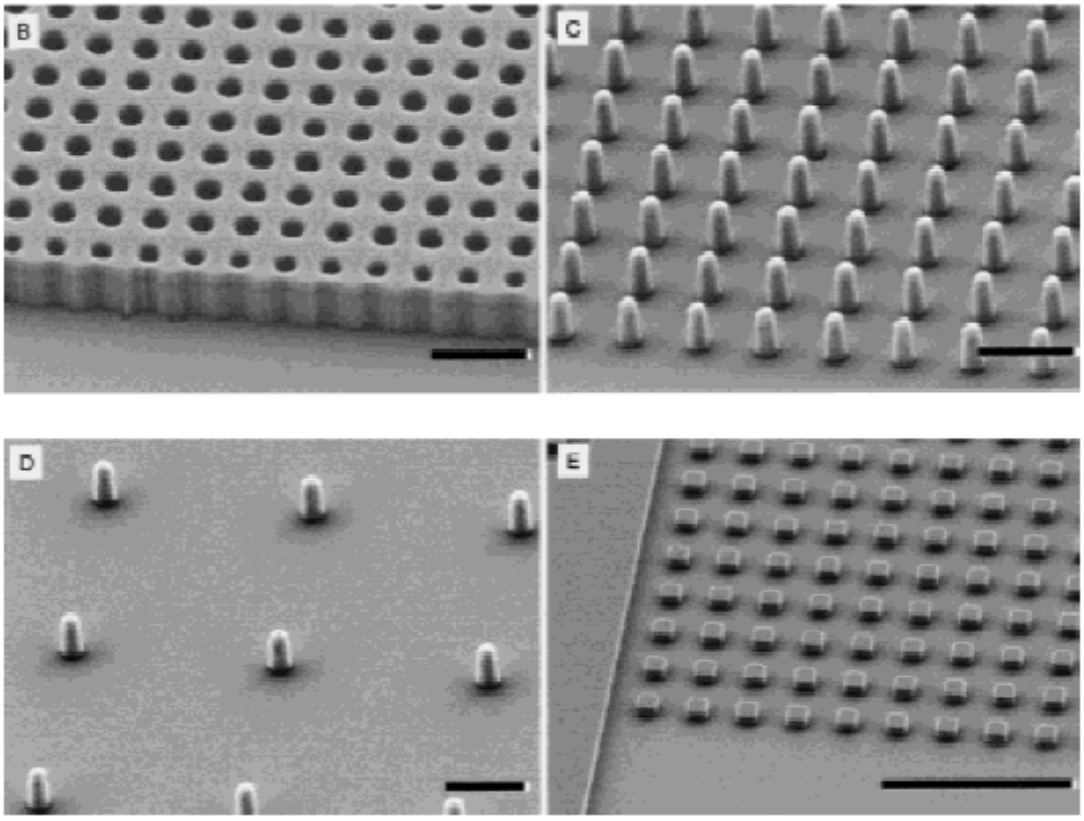

Figure 6. Scanning electron micrographs of pillar arrays, w = width, g = interpillar gap. Higher-magnification images illustrate characteristics of the pillar arrays with wells [(B) w = 0.5 mm, g = 0.5 mm] and different densities of pillars [(C) w = 0.5 mm, g = 1.0 mm; (D) w = 0.5 mm, g = 5.0 mm; and (E) w = 2.0 mm, g = 3.5 mm]. Scale bars: (A) 100 mm; (B–D) 2 mm; (E) 20 mm [4]. Reproduced with permission of John Wiley and Sons.

Micro-pores have also been investigated by Salem *et al* in 2000 that also used photolithography, to generate pores with diameters of between 5 and 90µm. The features ability to effect endothelial and fibroblast cells behaviour specifically morphology and growth. It was found that for endothelial cells, it was shown that maximum coverage on the surface was seen after 120hrs, but at no point did the cells cover the pores having diameters greater than 80-90µm wide. From 30-60µm the pores were partially covered by the cells, while for pore width of 30µm and less, cells were observed to grow over and cover the pores.

In contrast, for the fibroblast cells the maximum coverage was found after 72hrs and their ability to cover the larger pores of 80 and 90μm was dependant on the total cell confluency, the pores were increasingly covered as the number of cells attached to the surface increased. As time continued up to 48hrs, fibroblast cells were unable to cover or partially cover the pores, but at maximum coverage of 72hrs between 20 and 30% of pores were covered [63]. Investigation into these results showed that at the cytoskeleton of the endothelial cell stopped at the pore edge, this was in contrast to the fibroblast cells whose cytoskeleton remained unchanged over the pore. The author suggests that this is a result of the generation of the actin cytoskeleton, in endothelial cells it is generated at the pore edge resulting in concentrated focal adhesions possibly limiting cell movement. The fibroblasts did not form focal adhesion solely at the pore edge thus allowing greater mobility; they were also seen engaging with other cells using them as support structures to cover the pores [63].

3.2.1 Election beam lithography

Electron beam lithography (EBL) is used extensively in the manufacturing of ultra large scale integration technology, application specific integrated circuits and special logic devices for main frame computers. Its method is similar to photolithography with the use of a photoresist layer for surface patterning; however it has the advantage of being able to write directly onto the surface without the requirement of a mask [64]. Another advantage to using EBL is due to its smaller beam size, compared to other patterning devices it is able to generate smaller features with features on the order of < 10nm being reported [65].

One of the key elements to EBL is the resist used; a review by Yifang Chen sets out how the resist chosen has an impact on the resolution of the features produced. Figure 7 shows the

resolution limit of the most frequently used resists, and that sub 10nm features are possible with at least three of the available resists [5].

Limits to using EBL are speed of writing and the effect of deposited energy distributions. Though EBL has the ability to generate features at the nanometre resolution it is a slow process therefore, when applying this application to industry throughput capability becomes a problem. To solve this two writing procedures were designed; the raster and vector scan. The raster scan works in a fixed direction but, by controlling the beam activity one can generate the required pattern on the surface also the mean writing time is constant and not dependant on pattern density. Vector scan allows for much finer resolution in smaller scan areas; it does this through passing the electron beam only through the area were the pattern is required by deflecting the beam towards it. This changes the rate dependency to the pattern density rather than the pattern size [64].

The proximity effect can be split into two types; inter and intra, were for inter a crowded pattern area can result in the deposited energy being larger than the pattern size. And for intra, for isolated patterns the energy deposited being smaller than the pattern area.

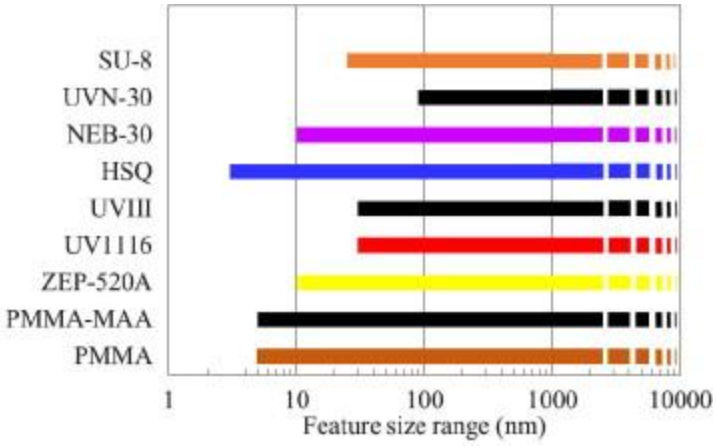

Figure 7 Bar chart for the feature size ranges of the most frequently used e-beam resists, taken from [5]. Reproduced with permission of Elsevier

3.2.2 Electron Beam lithography and modifying cell behaviour

Similarly to other lithographic methods there has been an effort to test the effect of EBL patterning on cell behaviour. This is due to the techniques ability to generate features on a on the nanometre scale (figure 7) while also having the ability to generate a range of feature geometries including nano-pits, micro-grooves [19] and nano-grooves [66], all of which have been used in biomedical science for testing the modification of cell behaviour**.** Research in this area has shown that cells do respond to the features produced by EBL, thus highlighting its promise in the development of biomedical products e.g. implant technologies.

Examples of such research come from Rajnicek *et al* who in 1997 tested the effect of micro-grooves created via EBL into fused quartz on neurons from embryonic *Xenopus* spinal cord and embryonic rat hippocampus. Their work showed that the two different cell types displayed very different responses to the grooved surfaces. The *Xenopus* spinal neurites grew parallel to grooves, which had depths ranging from 14nm to 1100nm, with widths of 1, 2, or 4µm. This was not a surprise to the author as *in situ Xenopus* neurites follow channels formed from between neighbouring neruepithelial cells that range from approximately 0.6 to 3µm across, all significantly bigger than the size of grooves used in this research.

This was in contrast to the hippocampal neurites, which grew perpendicular to shallow, narrow grooves while parallel to deep, wider ones. The hippocampal neurites changed their orientation from perpendicular to parallel between the 2 and 4µm wide grooves despite the depth remaining unchanged. Rajnicek *et al* determined that the age of the hippocampal neurite has an impact on the cell orientation; older neurites were shown to align parallel to grooves at a greater concentration then younger neurites on the same grooves [67].

Curtis *et al* performed two studies working with EBL in 2001 and 2004 and both studies involved using fibroblast cells for his experiments (rat epitenon and primary human in 2001 and 2004 respectively). In 2001 titanium was patterned and polymer casts taken to produced pillars and pits, all of which were 50nm in diameter with different centre to centre spacing's of 75, 150, or 300nm. These surfaces were compared to grooves, 40nm high created in silica. The work demonstrated that ordered topography reduces cell adhesion markedly when compared to the discontinuities of the groove features [16]. This work was continued in 2004, were pits were created within nickel and subsequently transferred into polymer substrates through hot embossing. The diameters of the pits were 35, 75 and 120nm with a pitch of between 100, 200 or 300nm, respectively. This work compared the effect of pits in ordered and random orientation as can be seen in figure 8 which shows the different surfaces used. This work demonstrated that cells adhere less to the ordered surfaces, with the random surfaces showing similar adhesion levels to the planar surface [6]. In both papers the author suggests that these results may be linked to the surfaces ability to bind to proteins, or in ability in the case of the ordered feature surfaces. They do accept that this is yet to be proven and would require further investigation.

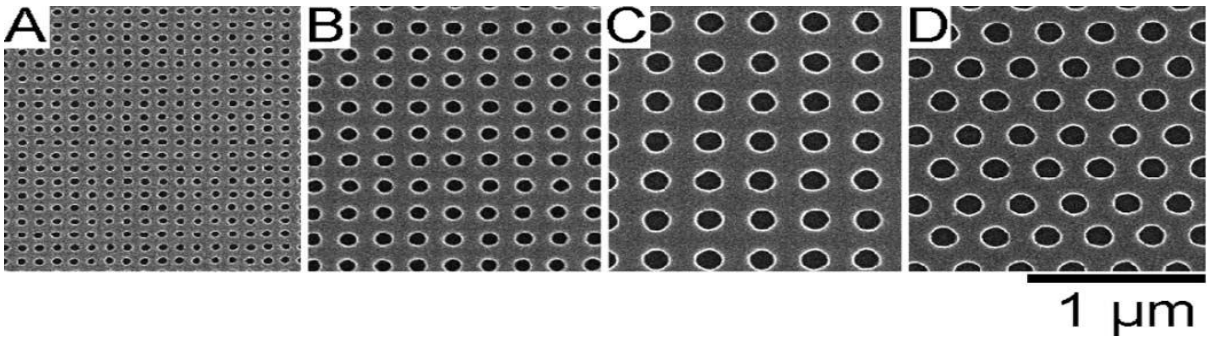

Figure. 8 SEM images of the three square arrays. (A)–(C) Orthogonal and rectilinear nanopitted silicon masters. (D) Hexagonally packed D nanopitted silicon masters. These masters were produced by high-resolution e-beam lithography [6]. Permission granted by IEEE.

Similarly, Biggs *et al* have also extensively worked on modifying cell behaviour using surface patterning, specifically ELB. This work in 2007, 2008 and 2009 focused on nano-pits created in both ordered and random orientations. In 2007 the work demonstrated that primary human osteoblasts (HOBs) were well spread on the planar surface but on the highly ordered square and hex-symmetries the cells were less spread with rounded, having stellate morphologies. Were as the less ordered surfaces promoted cell spreading with large lamellae [68]. Biggs suggests that this is a result of a number of factors; that the size of the nano features is approaching the size of molecular proteins possibly affecting the adsorption of proteins needed for cell adhesion to occur. Ordered nanotopography has been shown to induce a state of 'super hydrophobicity' resulting in decreased protein adsorption.

Similar research was carried out in 2008, were square and hexagonal pits were fabricated onto silicon and then imprinted into Poly(methyl methacrylate (pMMA). These structures were compared to nano-craters and nano-islands which were generated via spin coating polystyrene (PS) and poly 4-bromostyrene (pBrS) solutions which generated 47nm deep craters and islands 45nm high. In this study human osteoblast cells were also used and similarly to 2007 demonstrated extensive cell spreading on the planar substrate as well as on the nano-crater/island substrates. On the square and hexagonal nano-pits the cells displayed an elongated morphology with limited cell spreading. In this study the nano pits were nanopits was associated with decreases in the expression of genes involved in signaling and functional pathways. On the nano island/crater surface the opposite was true [69]. This work was further developed in 2009, where ordered nano-pits were generated which were 100nm deep with a diameter of 120nm and centre to centre spacing of 300nm. In this study the pits were arranged in both square and hexagonal symmetries, nano-grooves were also generated via photolithography for a contrasting feature to compare with. As with the previous studies

HOBs were used and showed a well spread morphology on the planar surface, compared to the square and hexagonal nano-pits, which showed reduced adhesion and spreading. The reduced adhesion correlated with a down regulation in the extracellular signal-regulated kinase (ERK) signalling cascade. ERK has been shown to positively regulate osteogenic differentiation through bone morphogenic proteins and other growth factors [19]. All of this work demonstrates that cells react unfavourably to ordered surface patterns, when compared to random features or planar surfaces.

3.3.1 Laser patterning

Laser (light amplification by stimulated emission of radiation) patterning, particularly direct laser patterning, is the use of a laser to create patterns through the irradiation of the surface. Using lasers for surface patterning has its advantages, as you can control where the patterning takes place and at what rate energy is deposited. For direct patterning this is usually carried out using solid state or carbon dioxide laser systems, due to their good beam quality. Unlike the previously mentioned methods laser patterning requires more optimisation. This has been shown in work done by Ulerich *et al* who demonstrated that surface patterning by a laser is a result of surface ablation and which relies on the laser pulse density, the hatching space and the direction of movement of the substrate, all of which require investigation. Further modification is determined by laser power, scanning rate and number of passes, which effect surface roughness and feature depth. Using a Nd:YVO4 laser to pattern polished Titanium (Ti64) it was shown that for patterning grooves their depth is affected by translation distance, laser energy per pulse, and number of passes, while width is affected by translation distance. As seen in figure 9, with a decreased translation distance grooves were generated with steep walls (figure 9 b), while at large translation distances the grooves were shallower but had lower slopes (figure 9 d). To demonstrate the effect of laser

power on surface roughness Ulerich *et al* used increasing pulse energies of 3.6μJ, 23μJ, 82μJ, and 130μJ and compered the resulting features. It was found that increasing the pulse energy resulted in features of a significantly smaller length scale compared to features generated using lower pulse energies and an increase in surface roughness. It is suggested that this is due to the lower energies merely melting the surface with thermocapillarity, thus causing a net change in the surface features. While at high energy the material begins to experience larger recoil pressures and material is now ablated and re-deposited to the surrounding areas with each pulse (figure 10) [7].

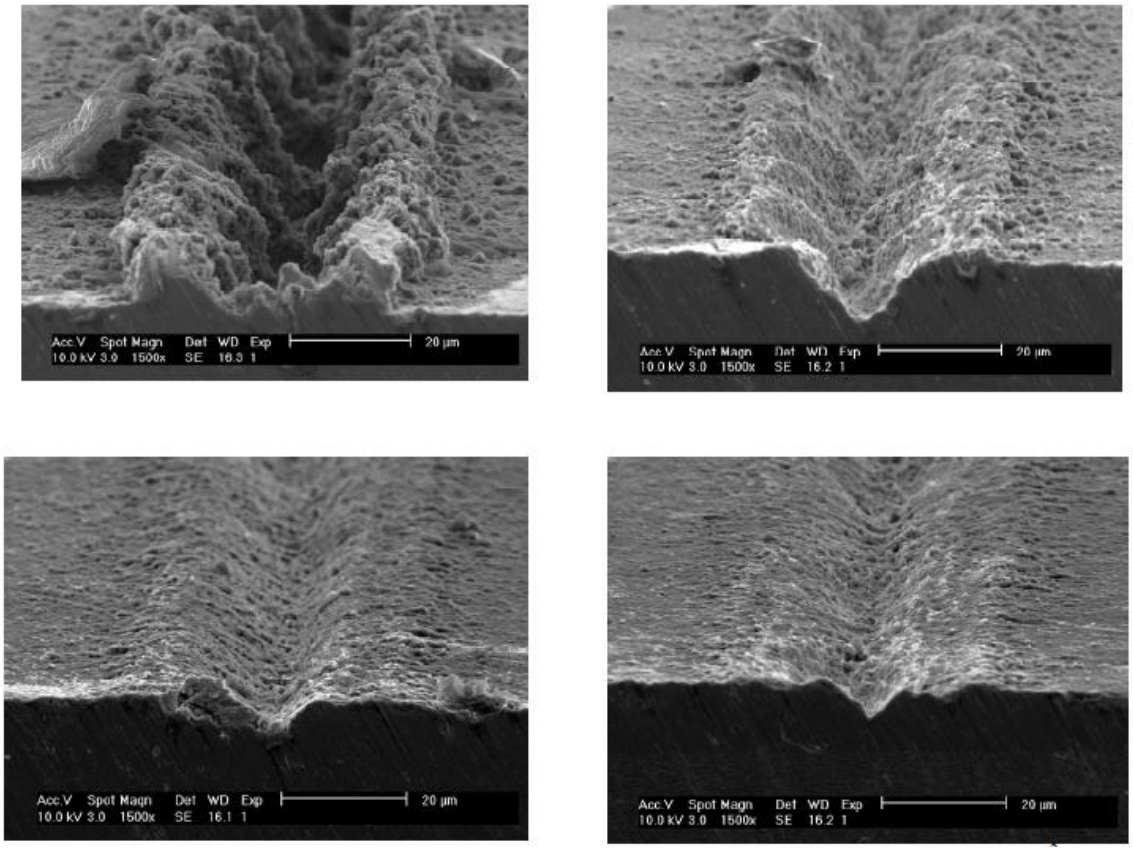

Figure 9 Effect of changing translation distance on surface features at 56 J/cm^2 showing the effect from a translation distance of A) 2μm, B) 4μm, C) 6μm and D) 8μm. Scale bar is 20μm. [7]. Permission granted by Ulerich *et al*., 2007.

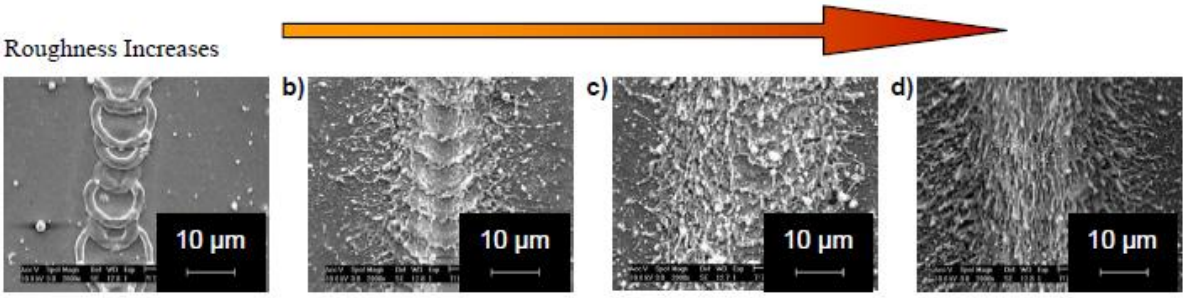

Figure 10 Grooves generated with a translation distance of 6µm and pulse energies of a) 3.6µJ, b) 23µJ, c) 82µJ and d) 130µJ. Scale on all images 10µm [7]. Permission granted by Ulerich *et al*., 2007.

When analysing laser surface modification there are two mechanisms; photo-thermal and photo-chemical. Whether the surface modification is photo-thermal or chemical is linked to the laser induced excitation rate and the thermalisation rate; if the excitation rate is low in comparison to the thermalisation rate then the absorbed laser energy is transformed directly into heat (photo-thermal). In contrast if the excitation rate is high compared to the thermalisation rate then the excitation energy can be at a level to break bonds within the surface. This mechanism is non-thermal and referred to as photochemical processing [70]. One of the main mechanisms linked to photo-thermal processing on materials is ablation; this is the removal of material from a substrate by the direct absorption of laser energy. Ablation is dependent on the laser being above a threshold fluence, which is linked to the properties of the substrate material, such as microstructure and morphology. It is also dependant on laser wavelength and pulse duration [70]. When examining the ablation of surfaces using short laser pulses in the µs/ns range, the surface is observed going through melting, evaporation and plasma formation.

Practical applications for lasers was initially based around heat treatment of metallic parts for reduced wear [71], a technique which is commonly used to harden or temper load bearing

surfaces and which results in reduced wear, decreased friction and increased longevity [72]. Lasers have also been used for surface cleaning, the ability to control the lasers processing depth enables the removal of any contaminates on the surface, without damaging the underlying original material. Laser cleaning has become a cost effective alternative to water jet, abrasive blasting or chemical cleaning methods [70]. Another successful area of laser use is surface texting. While initially being used to improve mechanical devices such as magnetic disk drives [73] and to improve material tribology [74] laser texturing has seen increasing use in the patterning of medical devices. However, compared to other techniques i.e. lithography, the feature sizes that can be generated are limited to the wavelength of the laser and to produce sub-micron scale features, excimer lasers are then needed due to their relatively short wavelengths 248nm (KrF laser) and 193nm (ArF laser) [75].

3.3.2 Use of laser surface patterning for modifying cell behaviour

There are many examples of surface patterning to modify cell behaviour. In 1992 Clark *et al* used laser holography combined with microelectronic fabrication techniques to generate grooves 130nm wide, with increasing depths 100, 210 and 400nm. His group seeded BHK, Madin Darby Canine Kidney Cells (MDCK) and chick embryo cerebral neurons onto the surface and tested the surfaces effect on cell alignment. This work demonstrated that BHK cell alignment was dependant on groove depth with increasing alignment as the groove depth increased. For MDCK cells alignment was not affected by changing the groove depth, grooves of all dimensions promoted cell alignment equally when compared to the planar surface. However, for the neuronal cells the grooved surfaces showed no effect on cell alignment [76]. This work was continued in 2002 by Clark *et al*, whereby the groove dimensions were kept constant 260nm period (130 nm wide grooves separated by 130nm wide ridges) with 210nm depth and this surface was seeded with myoblasts (undifferentiated

muscle cells). It was demonstrated that when compared to the flat surface the grooved surface promoted alignment along the groove direction, while also limiting migration in the same direction [77]. The results from both Clark studies demonstrates the effect of 'contact guidance' on cell behaviour, were the cells respond to the surface topography in this case aligning on groove features.

Extensive work on laser processing has been carried out by Waugh *et al*. 2009. Their work focused on generating grooves and hatch features. In particular they generated trench and hatch topographical patterns with peak heights of around 1μm on the surface of nylon 6,6, (name due to being made up of hexamethylenediamine and adipic acid, two monomers containing 6 carbon atoms). The grooves had spacing's of 50 and 100μm and this was replicated with the hatch spacing's, also 50 and 100μm. The author's choice of laser results in surface melting (photo-thermal processing) and the laser parameters of 7W and a traverse speed of 600mmecsec^{-1} were used to produce trench features. They observed that all patterned surfaces were rougher then the non-patterned surface (surface roughness (Sa) 0.126μm compared to 0.297-0.636μm). This was linked with an increase in surface contract angle, which increased alongside surface roughness. Focusing on osteoblast cells they determined that after 24 hours the patterned surfaces showed greater cell coverage than the non-patterned surface, with the largest level of coverage observed for the 100μm trench (37% surface coverage compared to 17%, respectively). Interestingly, they did not notice any directionality after 24 hours or after 4days of observation [78].

Further research was carried out by Waugh *et al* in 2011, here a KrF excimer (UV) laser was used for surface patterning (trenches and hatching) and whole surface irradiation on nylon 6,6. The parameters used for the laser patterning were; repetition rate of 25kHz, 10 pulses per site, energy level of 80±7 mJ, while a measured energy at the target sample of 23.67 ± 2.5 mJ, resulting in a fluence of 858 ± 91 mJcm^{-2}. To induce the intended pattern a

projection imaging system was implemented with a focusing lens of ×10 demagnification. The patterns induced using this technique were 50µm trench (ET50), 100µm trench (ET100), 50µm hatch (EH50) and 100µm hatch (EH100) (figure 11).

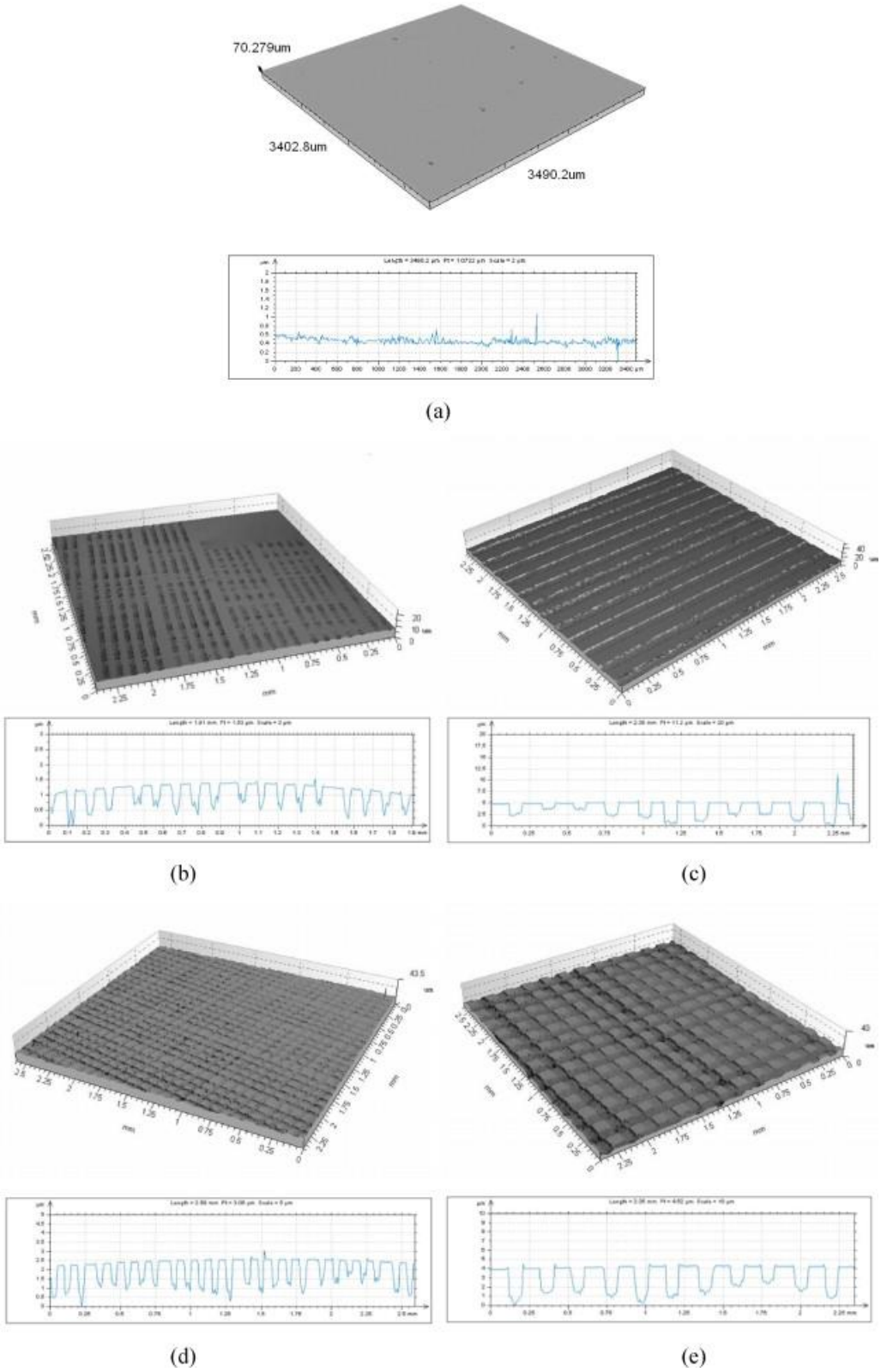

Figure 11 White light interferometer images of KrF excimer laser patterning on nylon 6,6. a) non-patterned, b) 50ET50, c) CT100 d) EH50 and e) H10. [8]. Permission granted by Elsevier.

Whole area processing with the KrF excimer laser was also done by Waugh *et al* 2011. Here a 23×12mm beam was used to irradiate a large section of each nylon 6.6 sample at a time, focused in different area to irradiate the whole sample. For the large area processing experiments, 6 samples were studied as seen in figure 12; these being 100 pulses at 100 mJ (EWA100) (a), 100 pulses at 150 mJ (EWA150) (b), 100 pulses at 200 mJ (EWA200) (c), 100 pulses at 250 mJ (EWA250) (d), 500 pulses at 250 mJ EWA250 500) (e) and 1000 pulses at 250 mJ (EWA250 1000)(f). Little difference is seen when observing the surfaces, this is a result of the large area processing which would be expected to remove a somewhat uniform layer across the surface. As was seen in Waugh *et al* previous work using the carbon dioxide (CO_2) laser in 2009, following laser processing surface roughness increased. This was seen on both the patterned features and the whole surface area irradiation. Surface roughness increased to a greater extent on the patterned surfaces when compared to the whole area irradiation, which showed only a small increase in roughness. When observing cell growth on the different surfaces after 24 hours, it was shown that cell coverage was similar between the laser patterned/processed areas and the un-patterned nylon. The one difference that was observed was with cell morphology, on the KrF laser the cells showed a bipolar cell morpohology, and some form of directionality was seen. This has been linked to the different wettability characteristics of the surfaces as well as the surface oxygen content. [8].

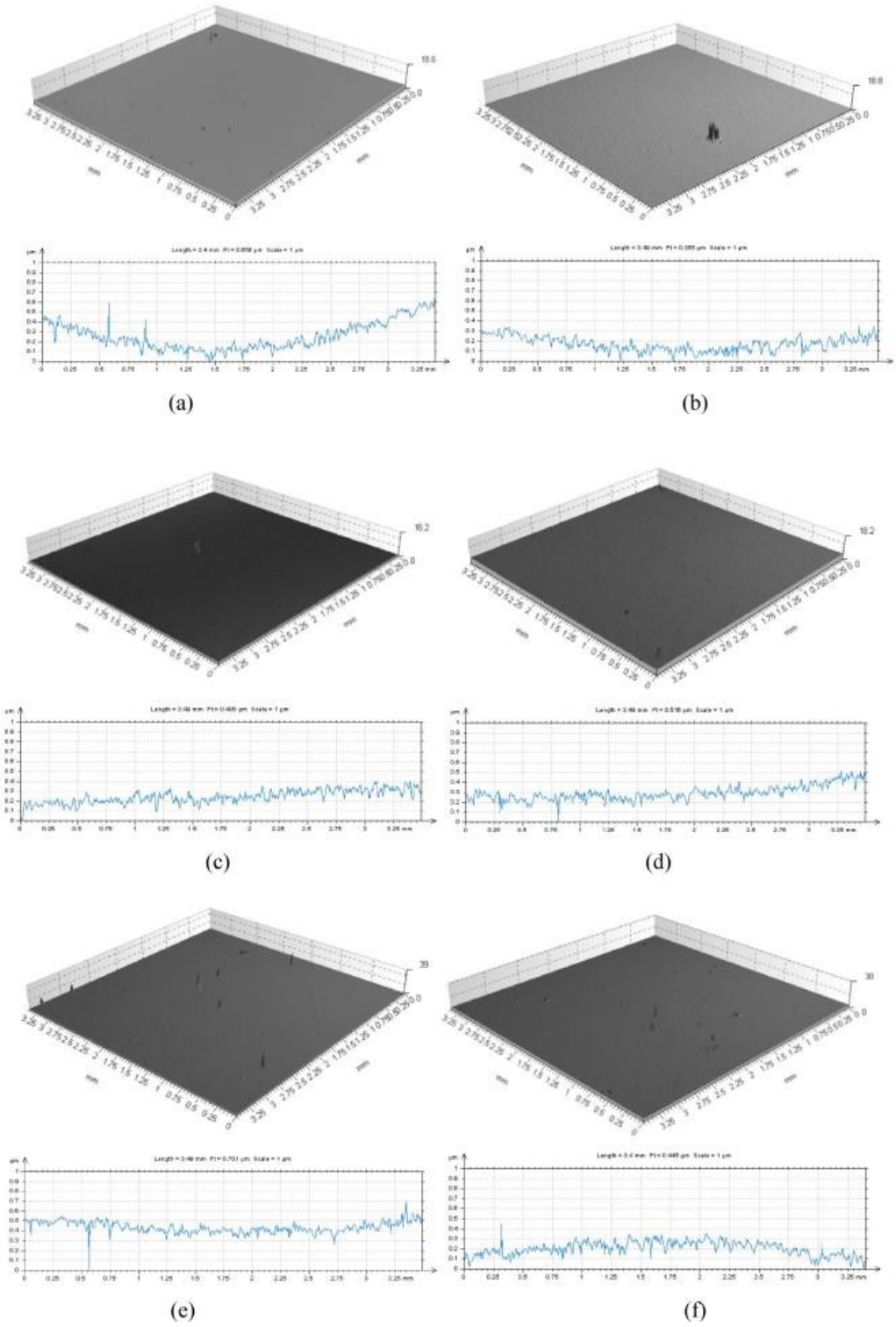

Figure 12. White light interferometer images of KrF excimer laser whole area patterning. a) EWA 100, b) EWA150, c) EWA200, d) EWA250, e) EWA250 500 and f) EWA250 1000. [8]. Permission granted by Elsevier.

Further work by Waugh *et al* in 2012 demonstrated the effect of CO_2 laser processing on nylon 6,6 surface patterning. In this study a continuous wave (Cs) 100W CO_2 laser was used with a 5mm diameter beam, which was passed once across the surface with an irradiance power of 510Wcm^2. Similarly to the group's previous work two processing techniques were used; surface patterning and whole surface irradiation. The patterning produced trenches with 50µm spacing (CT50), hatch width spacing of 50µm (CH50), trenches with 100µm spacing (CT100) and hatch width of 100µm (CH100). To generate different surfaces the parameter that was modified was the scanning speed and the different speeds used were 150, 100, 75, 50, 25 and 20mmsec^{-1}. The fluence used to generate the different surfaces were; 16.84(CWA17), 25.51(CWA26), 34.18(CWA34) 51.02(CWA51), 102.04(CWA102) and 127.55Jcm^2 (CWA128). The laser patterning was shown to increase surface roughness, with the largest peak heights being of the order of 2µm compared to the non-patterned surface, which had peak heights of up to 0.2µm. The roughness values increased considerably with the largest Sa value being 0.63 for the CT50 surface compared to 0.12µm for the non-patterned nylon surface. The whole area irradiation showed a wider range of Sa values, the smallest being 0.1 and the largest 4.4µm, this being a result of the increase in laser fluence and the corresponding effect on the nylon surface. When analysing the effect on osteoblast cell behaviour on the surfaces it was shown that cell coverage was greatest for all the patterned surfaces compared to the non-patterned surface. However, this was not seen in the whole area irradiated samples, which showed surfaces that had increased cell coverage (CWA34 and CWA51), lower cell coverage (CWA102 and CWA128) and similar cell coverage (CWA17 and CWA26) compared to the control samples. This, alongside with the changes in cell morphology, suggests that the different fluence values used for the whole area irradiation may have led to changes in cell signalling. The decrease in cell coverage is suggested to be a result of an increase in the hydrophilic nature of the surface which is

hindering cell adhesion to the surface, or possibly a result of over-melting of the surface due to the high fluence possibly causing toxic elements to form on the surface [79].

The work by Waugh *et al* shows that laser processing has a direct effect on cell behaviour and unlike other patterning techniques the effect is not limited to feature type. All three of the studies showed that by patterning the surface with a laser there is a change in surface roughness, though the extent varies whether the processing was to generate patterns (trenches/hatches) or total surface irradiation. Other values that are altered following laser processing are the contact angle of the surface and the oxygen content. The work by Waugh *et al* suggests that by increasing the surface roughness there is a corresponding increase in the surface contact angle. The contact angle can affect cell behaviour as suggested in Waugh *et al* 2011, were surface with hydrophilic contact angles were linked to decreases in cell coverage (EWA250 500 and EWA250 1000 with contact angles values of 42.9 and 37.6 respectively) [8]. While in Waugh *et al* 2012, surfaces CWA102 and CWA128 had the lowest levels of cell coverage while also having contact angle values of 46.6 and 43 respectively [79]. Oxygen content was also seen to be modified following laser irradiation, with an increase in oxygen content shown in all instances. For the patterned samples the change in oxygen content was similar due to the constant nature of the laser processing however, on the whole area irradiation it was shown that as the laser fluency increased so did the resulting oxygen content.

Another surface feature type that can be successfully generated by lasers are micro and nano-pits, as reported in work by Voisin *et al.* Pattenation in this instance was achieved by combining a ATLEX 300i excimer laser with a monolayer of silica beads to focus the laser light onto a polymer surface. The ArF laser emitted pulses between 4-6 nano-seconds at a wavelength of 193nm and the fluence at incident on the microspheres was 115mJcm^{-2} and 60mJcm^{-2}. This study generated both micro and nano-pits to test their effect on osteoblast

cell metabolic activity and proliferation. The different pits had dimensions of 982 ± 123μm wide and a depth of 114 ± 48μm, and a diameter 426 ± 47nm with a depth of 56 ± 14nm. The roughness values for the micro-structured surface were reported to be 24.2 ± 6.6nm and 25.3 ± 8.7 nm for the nano-structured surface respectively. The results of the study found that the cells were significantly more spread on the micro-structured surface compared to the nano-structured surfaces and untreated surface. There was no difference seen when comparing the nano-structured and the untreated surface. When analysing cell growth it was found that the micro-pitted surface encouraged cells to spread over a significantly larger area as well as increased substrate colonization. It was also observed that on the micro-structured surface, there was an increase in the number of cells displaying extensions when compared to the other surfaces, which showed very few extensions from the cells. This would indicate a weaker interaction between cell and substrate [80].

Laser surface patterning has also been used to control cell adhesion on specific substrate areas. Vijayakumar *et al* used a diode pumped Yb doped fibre oscillator laser system which produces pulses at a central wavelength of 1030nm with varying pulse widths ranging from 214 to 1428 femtoseconds (fs) at an operating average power of 16W. This generated variable pulse width laser pulses between 4 MHz and 25.07 MHz. As is seen in figure 13 this laser system was used to pattern pure titanium through ultra-short pulses, which resulted in sharp non-uniform peaks coupled with changes in the ratio of oxygen on the titanium surface. It was determined that increasing the peak power of the laser pulses resulted in an increase in the patterned area, and that by increasing the laser pulse widths, the oxygen content in the surface also increases. Two cell types were used to test the effect of the laser patterned surfaces namely; mouse monoclonal osteoblastic cell line (MC3T3-E1), osteoblasts and mouse embryonic fibroblasts (NIH3T3). It was found that on the treated titanium cell adhesion and proliferation was altered when compared to the untreated

titanium. On the untreated titanium the two cell types exhibited a flattened morphology, whereas on the treated surface the cell's morphology was more elongated in shape with a significant decrease in adhesion for both cell types [9].

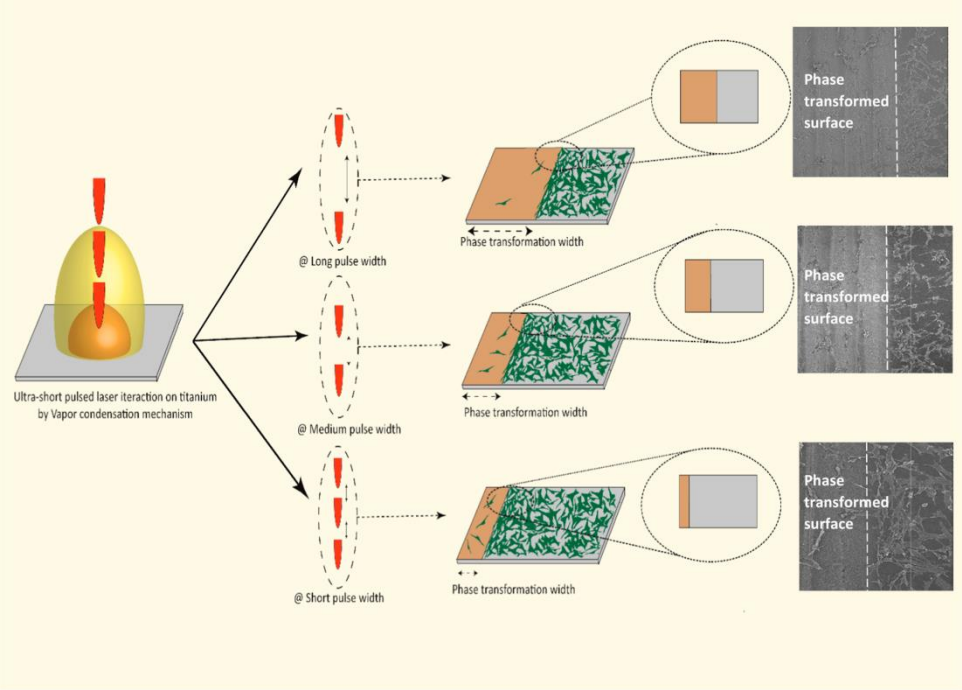

Figure 13 Laser processing resulting in material oxide phase synthesis, through the modulating of laser pulse to separation time. [9]. Permission granted by Elsevier.

Similar work was done by Premnath *et al* using a Megahertz (MHz)-repetition-rate ultrafast laser irradiation of un-doped Si wafers at atmospheric conditions. The Si wafers were then irradiated by a diode pumped, Yb-doped femtosecond laser system at laser pulse repetitions of 4, 8, 13, and 26 MHz and pulse width of 214, 771, and 1428fs. The power of the laser beam and the speed on the scan were kept constant at 10W and 100mmsec^{-1}, respectively. To test the effect of the laser patterning the Si wafers were patterned in an array of lines with a separation of between 100µm to 2mm. The result of the laser patterning was a change in the topography of the substrate (3D nano-structures), a change in substrate chemistry (increase in oxygen content) and a significant drop in wettability (65° for the untreated

silicon to <3° for the treated area). Human Epithelial Cervix cells (HeLa) were used to determine the effect of the modified substrate on the cell behaviour. It was observed that on the treated areas, the number of cells adhering decrease dramatically when compared to the untreated area. Following a seeding time of 24 and 48 hrs it also appears that the treated surfaces repel cells, resulting in an accumulation of cells on the untreated areas. The benefits of designing a surface that repels cell attachment or isolates small numbers of cells is desirable in various biomedical applications such as drug testing, fundamental biological studies and toxicology [81].

3.4.1 Indirect laser patterning

There has been limited use of indirect laser patterning. The work in this thesis follows on from work performed by Dr George Goh [10], who used an SPI laser to develop a grooved-pattern with a secondary microripple patterning running along the grooves in stainless steel. This was then used to cast from, using polyurethane as shown in figure 14. The mean laser power was 10W, the pulse duration was 9ns, the repetition rate was 500kHz, laser scanning speed was 500m/s and the number of passes was 25. The four surfaces analysed for their effect on cell behaviour were 1A, 1D, 3A and 3D the dimensions of which can be seen in tables 2 and 3.

Table 2 Dimensions of polymer surfaces 1A and 1D. [10]. Permission to use granted by Dr Goh.

Measurement area/samples	Polyurethane 1A	Polyurethane 1D
Microfringes width	4.05±0.67µm	n/a
Microfringes height	0.11±0.07µm	n/a
Microfringes gap	4.15±4.15µm	n/a
Microridge width	27.16±2.01µm	n/a
Microridge height	0.9±0.34µm	n/a
Microgroove	11.15±1.72µm	n/a

Table 3 Dimensions of polymer surfaces 3A and 3D.[10] Permission to use granted by Dr Goh.

Measurement area/samples	Polyurethane 3A	Polyurethane 3D
Microripple width	6.23±1.26µm	6.27±0.82µm
Microripple height	0.17±0.06µm	0.21±0.07µm
Microripple gap	5.86±1.09µm	6.59±1.21µm
Microridge width	40.09±1.82µm	23.47±1.74µm
Microridge height	0.71±0.22µm	1.23±0.27µm
Microgroove	19.41±2.54µm	18.36±1.58µm

The surfaces were tested for their effect on cell adhesion, proliferation and migration. Following two hours post seeding, a greater number of BAE-1 cells were found to be retained on 1A then on the control surface while also being higher than the other patterned surfaces, 1D 3A and 3D were not found to be different to the control. When testing cell proliferation 10,000 cells were seeded for 24, 48 and 72hrs onto the different surfaces, at each time point the cell number was determined using a PrestoBlue assay. The results showed that 1A resulted in a significantly higher number of cells at each time point compared to the control surface, there was no difference between 3A, 1D and the control surface. When analysing cell migration it was determined that surface 3D had the greatest mean accumulated distance, while 1A had the lowest. He suggests that the microfringes improved cell adhesion and proliferation through promotion of β-actin expression.

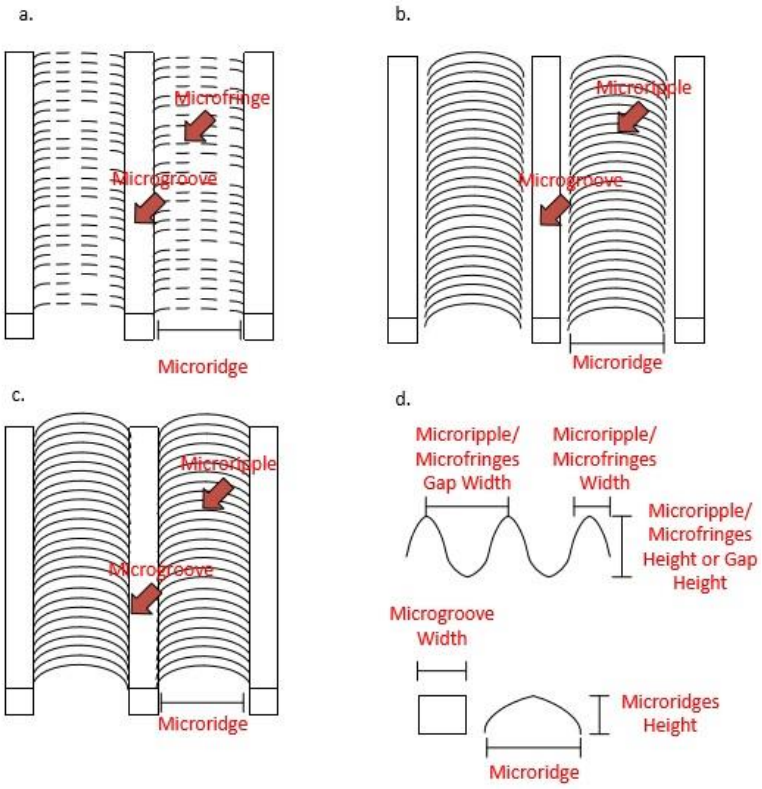

Figure 14 This diagram is used to help describe the laser micro-textured surface dimension measurement and characterisation process. (a) polyurethane 1A with discontinuous microripples, or named as microfringes, (b) polyurethane 3A with microripples, (c) polyurethane 3D with smaller microridge spacing, and (d) surface measurement and guidance.[10] Permission to use granted by Dr Goh.

3.5 Abrasive Polishing

One method that has seen limited use in the quest for controlling cell behaviour is abrasive polishing. Unlike other methods described in this chapter polishing is a method for patterning and which can be achieved using basic and inexpensive manufacturing equipment. As this technique requires limited equipment it also limits the cost of processing when compared to other methods. Also, a clean room is not required and the process does not require multiple steps or a range of chemicals. There, are however limitations associated

with using polishing as a patterning method; theses revolve around the type of features that are producible. Polishing would primarily produce linear features, though the orientation of the features can be altered depending on the direction of polishing and the type of equipment used. There have been some examples of using polishing for surface patterning to modify cell behaviour. For example in 1998 Lincks *et al* patterned two different titanium surfaces, pure titanium (Ti) and Ti-6Al-4V alloy (Ti-A). Discs of the two metals were patterned using polishing and wet sanding to generate rough and smooth surfaces respectively. For the polished surface the titanium discs were lapped with 18T grit then polished with 1200 grit aluminium oxide paper (figure 15 A&C); while the rough surface was prepared by wet sanding with a carborundum brand zirconium oxide resin bonded to a cloth belt (figure 15 B&D). When analysed the surfaces showed very different topographies; the polished surfaces on both the pure and alloy metal showed randomly orientated scratches and micro-pits, which were only observable at high magnification. The rough surfaces on both pure and alloy metal showed parallel longitudinal grooves with both sharp and serrated edges with varying heights and widths. When comparing the surface roughness (Ra) it was shown that the smooth surfaces had Ra values of 0.22 and 0.23µm, while the rough surfaces had Ra values of 4.24 and 3.20µm for the metal and alloy respectively. To test the effect of the different surfaces on cell behaviour MG63 osteoblast-like cells were used. When comparing morphology, it was observed that when grown on the smooth metal surface cells demonstrated a dendritic morphology that exhibited extensions up to 10µm in length, they were spread across the surface in a discontinuous monolayer. In contrast, on the smooth alloy and the rough metal surface, the cells grew in a continuous monolayer, while on the rough alloy cells were able to grow in a multilayer, with many cells producing extensions of up to 10µm, while also showing orientations along the parallel grooves. When compared to the plastic control cell number was also affected on the Ti-R surface which showed a reduction

of 36%, a reduction was also seen on Ti-S though this was not significant. The number of cells on the two alloy surfaces was similar to the control. Further analysis was done on alkaline phosphatase activity, Osteocalcin production, and collagen production. Alkaline phosphatase is an early marker of osteogenic differentiation and is found in higher levels in cells which mineralize their matrix such as osteoblasts, it was found in higher levels on the rougher surfaces. Ostocalcin production was also seen to have increased 1.9 fold on the Ti-R surface compared to the control, this shows that cells on Ti-R are further differentiated then cells on the other surfaces. Collagen production synthesis was found to be greater on the rougher surfaces, this correlates with the production of latent TGF-b, TGF-b a growth factor associated with the collagen deposition in the extracellular matrix of osteoblasts cells, this suggests a more differentiated osteoblastic phenotype for the cells on the rougher surfaces. The results suggest that surface roughness plays an important role in MG63 differentiation [11].

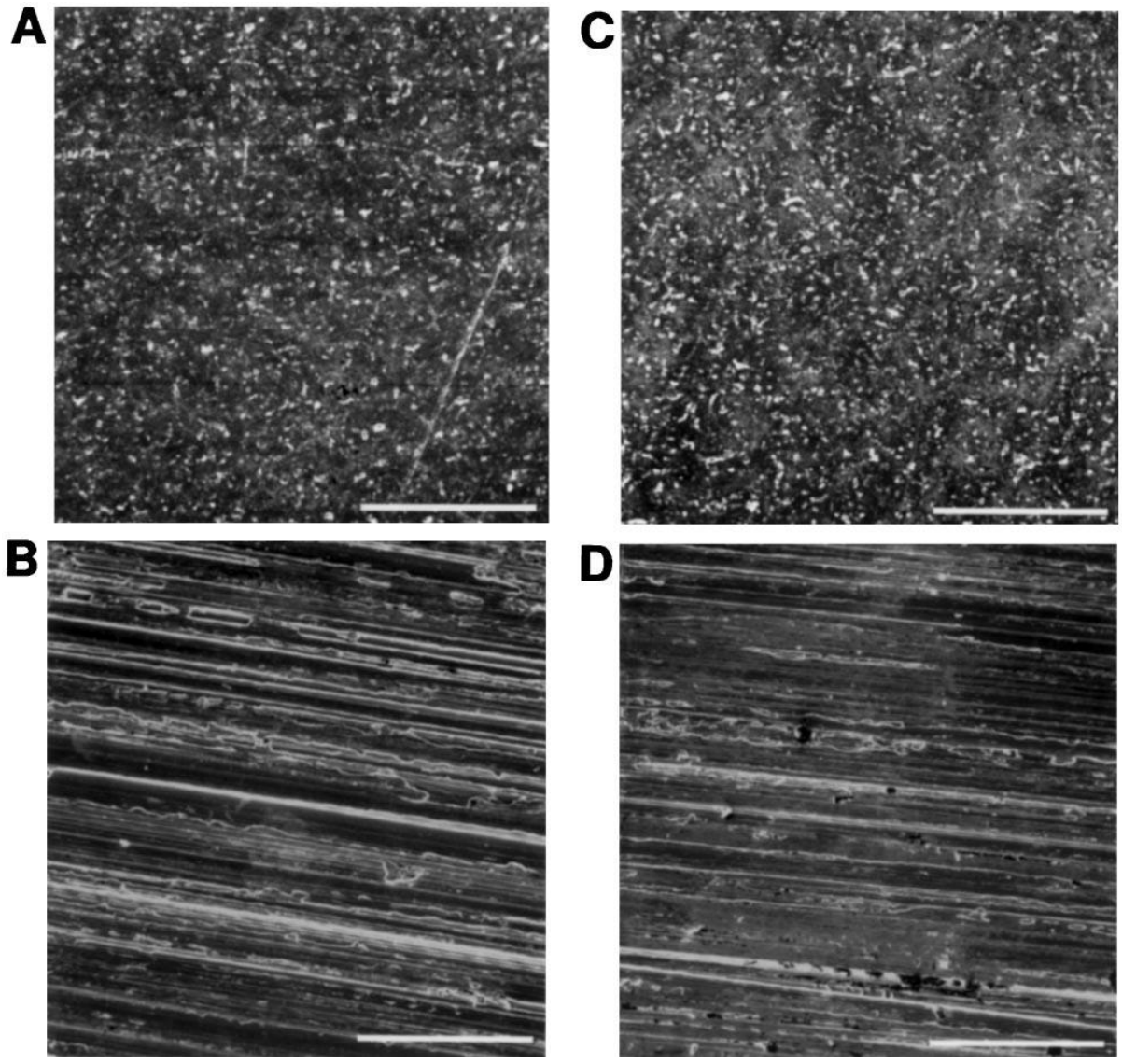

Figure 15 SEM images of the different disk surfaces used. A: Titanium Smooth; B Titanium Rough; C: Titanium alloy smooth; D: Titanium alloy rough. Bar=200µm [11]. Permission granted by Elsevier.

Similarly to the work by Lincks *et al*, Linez-Bataillon *et al* in 2002 compared two patterning methods that would produce rough and smooth surfaces. In this study, sandblasting and surface polishing were used to generate patterned surfaces and the effect of these surfaces on MC3T3 osteoblast behaviour was tested. Briefly, titanium discs (Ti6Al4V) were either sandblasted with 500µm aluminium (Al_2O_3) beads or polished using silicon carbide papers of grade 80, 1200 and 4000. There was also a mirror polish with 0.25µm diamond particle.

The Ra of the different surfaces were compared and were shown to be 0.62, 0.61, 0.43, 0.3 and 0.15µm for the sandblasted, grade 80, grade 1200, grade 4000 and mirror polish, respectively. The cell behaviours tested in this study were proliferation, morphology and adhesion. When comparing cell proliferation it was determined that it is linked to surface roughness; proliferation was shown to decrease as surface roughness increased. The morphologies of the cells were also affected, particularly in the spreading of the cell which increased as the surface roughness decreased. On the sandblasted surface cells were rounded, while on the mirror surface cells showed the greatest level of spreading with large lamellipodia, which indicates that the cell is actively migrating. On the larger grade polishing surface (80) cells showed a level of orientation along the polished lines. The research demonstrated a significant correlation between the material surface roughness and the cell proliferation rate, and the other hand, a qualitative relationship between roughness and cell adhesion [82].

In 2014 Lv *et al* compared the ability for three different titanium surface types to modify the behaviour of human adipose-derived stem cells, these surface types were polished, sand blasted then acid etched (SLA) and nanotubes. The polished surface was built up through a series of polishing steps going through the larger grit size of 240 down to the smallest of 4000, for the SLA and nanotube surfaces the substrates went through the polishing process before following different pathways. The nanotubes were obtained by anodization, with voltages of 10, 20 and 25V respectively. The surfaces were then heat treated at 450°C for 2hrs. For the SLA the polished titanium was sandblasted by 110µm Al_2O_3 particles and then acid etched. The surfaces, when characterized, showed that the nanotubes had outer diameters of 50nm, 70nm and 100nm to correspond to the voltages of 10, 20 and 25V respectively. The surface roughness values of the nanotubes increased as the diameter increased, the 70 and 100nm nanotubes also exhibited a higher roughness value compared

with sandblasting and acid etching. The acid etched and 50nm nanotubes show similar surface roughness while all show a much larger Ra value when compared to the polished surface. To test the effect on cell behaviour, human adipose derived stem cells were used to investigate adhesion and proliferation rates. Following 2hrs of culture on all nanotubes surfaces cells were observed to have extended lamellipodia and had higher number of adhered cells compared to the SLA and smooth surfaces. The SLA surface in comparison promoted cells to form rounded morphologies with only short pseudopodia, and on the smooth surface the cells were rounded with no pseudopodia and had the lowest number of adhered cells. Cell proliferation was also different across the different surface types; the nanotubes showed no difference in proliferation rates compared to the control surface over the first 4 days but, continued to show growth until the 6^{th} day. In contrast, the SLA and smooth surfaces only showed growth until the 5^{th} day and showed a lower optical density compared to the nanotube surfaces. Lv *et al* demonstrated that nanoscale geometry can influence cell differentiation, and 70nm TiO_2 nanotubes are optimal for the osteogenic differentiation of human adipose derived stem cells (hASCs). That nanoscale geometry can regulate the osteogenic differentiation of hASCs, in that the appropriate nanotopography can upregulate the methylation level of H3K4 at the promoter regions of osteogenesis-associated genes by inhibiting of retinol binding protein 2 (RBP2) expression. [83].

3.6 The comparison between polishing and grit blasted surface patterning

The use of polishing and grit blasting to develop surfaces for cell growth is limited. However, it has been shown to be useful for developing surfaces that can control cellular processes. For example, in 2011 Mendonca *et al* seeded mesenchymal stem cells onto polished or grit blasted titanium discs. The titanium was polished using increasingly small grit size down to

600 and either left as the polished surface or grit blasted with 100μm aluminium oxide particles. The surface roughness between the surfaces was compared and it was shown that the polished surfaces were much smoother with a Sa value of 37.8nm compared to the grit blasted surface, which had a Sa of 378nm. To determine the effect of the different surfaces on cell behaviour Mendonca *et al* analysed cell spreading and the changes in gene expression. After four hours cells on both surfaces were well spread, but it was only on the polished surface that the cells exhibited a fibroblast like morphology. Whilst on the rough surface the cells did not exhibit a defined long axis. There were a range of changes in gene expression both up and down regulation; the genes were split into different categories including collagen biosynthesis, processing, post-translational modifications and ECM remodelling. For the genes associated with collagen expression all genes were shown to be upregulated on the rough surfaces. This was similarly seen for the proteases matrix metalloproteinases (MMPs) and tissue inhibitor of matrix metalloproteinases (TIMPs), where they were upregulated on the rough surface compared to the smooth surface. The trend for an increase in gene expression on the rough surfaces was continued with the osteoblast marker genes; this included Runx2, a key transcription factor for osteoblast differentiation and OSX, another key transcription factor for osteoblast differentiation. This work suggests that a rougher surface can promote stem cell differentiation down the osteoblast pathway [84].

3.7 Grinding

Similar to surface polishing, machine grinding also provides a more financially conservative method for patterning surfaces to try and modify cell behaviour. Grinding can also be set up to provide a rough ground surface, or a defined set of repeated features, depending on the level of detail required. There are limitations to using machine grinding in that the features

producible would be limited to a unilateral direction, unless repeated passes across the surface along different angles was performed for example, through wheel dressing. There is limited evidence as to the success of machine grinding however in 2008 Shimizu *et al* developed surface features through the use of surface grinding and polymer casting. The surfaces were based around iron blocks that were ground in one direction using three different abrasives; these were 9nm diamond suspension, #400 sandpaper and #150 sandpaper. The three surfaces were used as moulds to for polydimethylsiloxane (PDMS) substrates, type I, type II and type III. The surface features were all in a linear pattern and the Ra values for these surfaces were analysed and determined to be 0.03, 0.16 and 0.56µm for type I, II and III, respectively. In this study myoblasts were the cell type used, and when a viability test was done it was observed that the number of cells on each substrate was similar to that of the control, which was a flat PDMS substrate. After 24h of culture on laminin- coated surfaces the orientation of the myoblasts was analysed. On type II and III substrates there was an observable level of orientation along the features. This was not seen on type I, on which the cells extended in random directions, most likely a result of the smaller features produced by the smaller diamond suspension. After 72h of culture cell confluence was achieved on all surfaces, whereas confluence was achieved at the 24h time point on type II and III and were any orientation along the features was observed. That there was no morphological changes to the cells on any of the surfaces suggests that the ground patterns does not significantly affect the differentiation of the myoblasts as differentiation is associated with changes in myoblast morphology [85].

As outlined in the above chapter there are a range of methods available for the patterning of surfaces with an aim towards biochemical applications and cell control. When comparing the techniques, the lithographic ones are multistep processes that are time consuming and expensive, requiring a clean room to ensure surface suitability. The laser patterning is also

an expensive method requiring a large upfront cost for the equipment setup, it also comes with the added safety concerns that come with laser use. The other methods described arelow cost, low tech, and though their ability to provide different surface patterns is limited to grooves the examples given earlier show that they are still able to influence cell behaviour.

The rest of this thesis will introduce the techniques that were used to pattern surfaces and produce topography to modify cell behaviour. It was decided to compare three techniques, two low cost ones in surface polishing and machine grinding and a high tech technique in laser patterning. The novelty in this work was to contribute to the current knowledge in the area of cell control using laser generated topographic nano/micro-structures on polymeric substrates for potential use in the development of biomedical implantation technology and wound healing through the undulating pattern that was produced in this work. This was combined with patterns generated through surface polishing and machine grinding to compare how the different patterns taken from three different techniques influence cell behaviour. The surfaces were characterised using surface metrology techniques and measurements and linking this to the surface topography. This helped to develop a greater understanding of why cells respond to certain features and how such features influence certain behaviours such as cell adhesion, proliferation and migration, this was achieved through carrying out laboratory-based bioassays.

3.8 Use of surface measurement parameters

Limitations of mean based measurements

When it comes to analysing surfaces there are different parameters that can be identified which provide specific values which can be compared. The range of surface parameters values include:

- The Sq parameter, this is defined as the root mean square value of the surface departures
- The Sa parameter, this is the arithmetic mean of the absolute value of the height within a sampling area
- The Sp parameter, this is defined as the largest peak height value from the mean plane within the sampling area. This parameter can be unrepresentative of a surface as its numerical value can vary so much from sample to sample
- The Sv parameter, this is defined as the maximum pit height of the surface
- The Sz parameter, this is defined as the maximum height of the surface,

When taken individually these parameters though useful to an extent show limitations as they do not describe the surface, this can lead to surfaces that look different having similar values for those parameters. There are ways to combat this, by using in conjunction with other parameters such as both the Sq value and the Sz value, it may be possible to indicate whether the apparent roughness is due to isolated features or the overall surface roughness

The importance of surface topography can be shown by the move towards predicting topography within industry. Within the aerospace industry milling is commonly used for repair and manufacturing of high functional parts, and due to the importance of surface topography on functional performance there has been extensive research on predicting surface topography pre manufacturing. An example of which is Arizmendi et al who's analytical model shows the importance of tool runout and its impact on surface topography [86]. Denkema *et al* demonstrates the use of combining kinematic topography from the machining simulation and adds a stochastic topography based on empirical data [87]. This combined approach they feel is beneficial when compared to empirical, analytical/numerical and material removal simulation methods, their limitations are linked to being limited in

experimental scope (empirical) and equations can get too complex to handle by adding more simulation features, such as vibrations or special tool shapes (analytical). Denkema *et al* presents a method which improves the estimation of the aerodynamic effects, such as the wall shear stress, of regenerated surfaces in simulations [87].

There is also a move to predict surface roughness, understanding the interaction between the abrasive and the workpiece would support this predictive process. As mentioned before there are different theoretical methods currently being developed to attempt to do this, these can be separated into empirical and analytical methods. Empirical methods link surface roughness to kinetic conditions [88]6), analytical models are typically characterized by the description of the grinding wheel taking grain distance, width of cutting edge and grain diameter into account. Khare & Agawal present a new analytical surface roughness model which is developed on the basis of stochastic nature of the grinding process, governed mainly by the random geometry and the random distribution of cutting edges on the wheel surface having random grain protrusion heights [89]. Their model was shown to accurately predict the results of experimental values for different kinematic conditions in the horizontal surface grinding of AISI 4340 steel.

Taking this information forward is extremely important when considering cell responses to different surfaces. I have already previously presented how modifying the surface can influence cell behaviour so it is essential that surfaces produced for this research are accurately investigated to try and identify which values are effecting the cells such as peak height or surface roughness.

Chapter 4 – Experimental Design

4.0 Experimental Design

It has been shown that cells respond to surface topography and that growing cells on surfaces having specific feature geometry and size, can significantly affect a range of important cellular behaviours including; differentiation, adhesion, migration and proliferation. Such knowledge has led to researchers trying to develop functional surfaces for use in a range of biomedical applications including dental implants[12], ophthalmic implants[90], coronary stents[91] and even breast implants[13].

Development of such surfaces is usually achieved using advanced and often high cost methods including lithography-based techniques and to a lesser extent laser processing. Both techniques have many benefits and allow the production of surfaces with clearly defined and often intricate patterns with feature sizes at the submicron scale. However, these methods can be expensive and there is scope to explore more cost-effective methods to generate patterned surfaces for cell control. Also, do we need to produce surfaces with highly defined and ordered features to control cell behaviour? Are there simpler, less controlled and more cost effective methods that can be used to develop functional surfaces for controlling cell behaviour for biomedical applications? After all, the ECM to which cells adhere, is in appearance, rather randomly organised and does not contain perfectly symmetrical and highly ordered pillars, pits, grooves etc….

Any material that may be considered as a surface biomedical application should promote cell attachment, flattening; spreading and migration as these steps are important in determining whether cells will go on to proliferate. Therefore, the overarching aims of the work presented in thesis were to:

1. Evaluate the use of abrasive polishing methods and laser processing for producing nano/micro-patterned polyurethane substrates using an indirect processing method.

2. Determine if these substrates can be used to promote important cellular behaviours namely, cell adhesion, migration and proliferation.

Abrasive polishing has largely been under exploited for such applications but potentially offers an alternative method to produce functional surfaces for biomedical applications. Laser processing is an established technique for micro-patterning surfaces for controlling for cell behaviour and thus offers a direct comparison to the abrasive methods for their abilities to produce nano/micro-patterned polyurethane surfaces for promoting cell adhesion, migration and proliferation.

For this work an indirect processing method was used to micro/nano-texture polyurethane surfaces, whereby the original processing (whether by laser of abrasive polishing) was carried out on stainless steel samples, which were then used to cast off the polymer samples, thus generating an inverted pattern on the polymer surface. The polyurethane was used as it is well characterised and biocompatible and thus offers potential use as a coating for biomedical implant technologies (see section 5.3.6 for polymer details).

Three types of micro/nano-textured polymer surfaces were generated through laser processing, surface polishing and machine grinding. The laser surface was an undulating pattern that ran across the surface in parallel lines with non-patterned areas in between the channels. There was a range of polished surfaces, linear lines ranging in size linked to the size of the silicon carbide paper that was used for polishing. These decreased in size from 120, 320, 400, 500 600 and 1200, there was also a comparative random scratched surface through the manual rubbing of the steel mould on the 1200 surface. There were four machine

ground surfaces that were based on the depth of cut on the grinding wheel. These surfaces were then evaluated to see if they would promote cell adhesion, migration and proliferation when compared to cells growing on a non-textured polymer surface.

4.1 Use of LL24 fibroblasts and BAE-1 endothelial cells for research

Fibroblast cells were chosen because they are one of the first cells to encounter foreign implants and are important in biointegration. Also, there is extensive evidence showing that fibroblast cells respond to changes in surface topography both in vitro and in vivo. The LL24 cell line was chosen as it is a well characterised, stable, normal human diploid cell line. Bovine aortic endothelium cells were chosen because they are an economical alternative to the primary endothelial cell which have been used extensively to study endothelial cell behaviour. The use of endothelial cells also provides a link to medical implants as the overgrowth of endothelial cells on stents is a major cause of restenosis and thus stent failure. Should the patterns generated in this work negatively affect endothelial cell behaviour it may be suitable for use in future stent design,

4.2 Surface patterning using laser processing

The use of laser processed surface topography to manipulate cell behaviour is well established for example with work showing that micro-pits generated through an ArF excimer laser can effect osteoblast spreading and growth [80] and that trenches generated through CO_2 laser processing can improve osteoblast growth and signalling [79]. Recent work performed within the General Engineering Research Institute (LJMU), has demonstrated that the SPI 20W 1064nm infrared fibre laser can be used to produce micro-

patterned surfaces with novel micro-ripple features and which can be used to enhance BAE-1 cell adhesion, migration and proliferation [10]

The work described in this thesis used the SPI laser rate to generate novel, directional grooved features with an undulating, rolling hill-like theme along the groove. The features can be easily reproduced and contain limited unwanted features left on the surface following laser ablation, thus ensuring any effects on cell behaviour was as a result of the designed features and not any non-desirable features, that could not be controlled during the processing. The reason for generating such features was that previous work has shown that at the micron scale, grooves can be used to control cell alignment and to direct cell migration [10]. In this work the groove feature was expanded upon with an extra dimensional feature, in this case the undulating rolling hill theme. This enabled the testing of the effect of this secondary feature, which increased the surface area of the groove while also affecting the surface roughness.

4.3.1 Surface patterning using abrasive polishing/grinding

As previously mentioned, abrasive polishing offers a method to improving biointegration by developing micro/nano-patterned surfaces for biomedical applications. Therefore, two related methods were chosen to develop functional surfaces. These were abrasive polishing through use of silicon carbide grit paper or through the use of a high speed grinding wheel.

4.3.2 Expansion of abrasive polishing to examine effect of different grit size

Silicon carbide paper of different grit sizes (120B - largest), 320, 400, 500, 600 and 1200 - smallest) was used to process stainless steel in a directional manner using a METASERV

universal polisher (see figure 17). This produced nano-scratched in the stainless steel which, when cast resulted in polymer surfaces having sub-micron scale directional features. Feature size could be controlled depending on which grit size was used. Varying the size of the features would inform us if feature size has any effect on the aforementioned cell behaviours. However, in order to determine if directionality of the features has any effect on cell behaviour, silicon carbide paper was used to produce polymer substrates having more randomly ordered features on the surface. This was generated using the 1200 grit sized silicon carbide paper. However, instead of using the METASERV universal polisher, the stainless steel was manually rubbed across the 1200 paper to produce a surface with a more random finish. It was thought that this would, to some extent, mimic the ECM with respect to feature directionality and size feat while allowing comparison of cell behaviour when growing on the surfaces with the directional features.

4.3.3 Development of grooved surfaces created through machine grinding

Machine grinding of stainless steel was used to create patterned surfaces. This was achieved using a Jones & Shipman 540 surface grinder and the wheel was dressed at four different depths of 2, 4, 6 and 10µm. The dressed wheel was then run on a single pass across a stainless steel mould to produce four different surfaces. All surfaces showed linear grooves running in a unilateral direction and the size of the features was dependant on the depth of dressing on the grinding wheel, the feature sizes ranged from 1.23 to 1.88µm. As a patterning process machine grinding can be optimized by the depth of dressing and the number of passes across the work piece. Surface grinding was chosen as it is a cost effective method to produce grooves comparative in dimensions and structure to more technical and expensive

lithography-based methods. Should the surfaces show an ability to modify cell responses, then as a process it would be seen as an alternative method for generating grooved surfaces.

4.4.1 Cell Response to Indirect Textured Polyurethane

The work described in this thesis employed different experimental methods and techniques in order to develop patterned surfaces. This was achieved through processing stainless steel and using this as a mould to cast polyurethane thus creating pattered polyurethane surfaces for cell substrates. The work employed LL24 and BAE-1 cells and in particular wanted to understand:

1. Whether the patterned polyurethane causes changes in cell adhesion levels when compared to unprocessed polymer
2. How these surfaces affect cell proliferation, and whether this is different to unprocessed polymer
3. If the different patterning techniques effect cell migration

4.4.2 Investigating the effect of Textured and Non-textured Polyurethane on fibroblast and endothelial cell Adhesion

Two cell types were used to examine the effect of the textured surfaces on cell response, LL24 and BAE-1. Evidence from the literature has shown that by altering the surface topography the cells ability to adhere to the surface is also altered. When seeded onto grooved titanium of different dimensions that had been acid etched fibroblast cells were shown to adhere with more affinity to the grooves surfaces than the smooth surface [27]. It has also been shown that plasma treated polymer surfaces can enhance fibroblast adhesion compared to unmodified polymer [92].

To investigate the effect of differing indirect patterning techniques on cell adhesion, MTT assays were carried out. This involved seeding the cells onto the surfaces and leaving them to attach for either two hours for the fibroblast (LL24) cells or six hours for the endothelial cells (BAE-1). These times were determined empirically, with microscopy observations showing that the fibroblast cells attached and spread on the surfaces after two hours while it took approximately six hours for the endothelial cells to attached and spread on their surface. Cell adhesion was evaluated using time-lapse microscopy and quantified using the MTT assay, which can be used to provide an indication of relative cell density and which is based on absorbance following metabolism of MTT by viable cells.

4.4.3 Investigating the effect of Indirect Textured and Non-textured Polyurethane on fibroblast and endothelial cell proliferation

Research has shown that surface topography can modify cell proliferation. For example, when seeded onto pillars it has been shown that fibroblast proliferation is affected by the inter-pillar gap. It was shown that by increasing the size of this gap there was a reduction in cell proliferation [93]. Grooved titanium has also been shown to have an effect on cell proliferation. Here, acid-etched grooved surfaces promoted cell proliferation over smooth and non-grooved surfaces [27, 94]. This has further been seen on plasma modified polymer which showed greater cell proliferation [92].

To investigate the effect of patterned polyurethane surfaces on cell proliferation the cells were seeded onto the surfaces for 24, 48 and 72 hours, respectively. The MTT assay was carried out after 24, 48 and 72 hours in order to determine what effect the surfaces had on cell proliferation. With this assay a greater number of cells would reflect a greater absorbance value and thus provide a relative estimation of cell density.

4.4.4 Investigating the effect of Indirect Textured and Non-textured Polyurethane on fibroblast and endothelial cell migration

Cell migration has also been shown to be affected by surface topography. For example, surface topography has been show to alter cell migration directionality [95]. The speed of fibroblast movement can also be affected by the dimensions of surface topography. For example, cells growing on grooved surfaces, have been shown to increase and decrease the speed of their movement depending on the size of the grooves. [96]. Whilst fibroblast migration has also been shown to be controlled through the design of micro channels that direct cell movement through the promotion of a polarized morphology while also suppressing backwards movements [97].

In order to investigate the effect of patterned polyurethane on cell migration velocity and distance, time lapse imaging was performed on the cells two hours post seeding on each surface. Images were captured every fifteen minutes for four hours. This enabled offline tracking to be done so as to track individual cells and determine mean cell migration distance (μm).

4.4.5 Investigating the effect of Indirect Textured and Non-textured Polyurethane on fibroblast and endothelial cell morphology

Cell morphology has been shown to be affected by surface topography; this has been seen most clearly in grooved features which have been shown to promote alignment of cells and their elongation [98]. While growing cells on pillars has been shown to promote or inhibit cell spreading depending on pillar size and spacing. For example, on surfaces with small inter-pillar spacing with small fibroblasts cells have been shown to exhibit a well-spread

morphology. However, when the pillar spacing is increased the cells were found to have difficulty in attaching to the surface [93]. In order to investigate the effect of pattered polyurethane on LL24 morphology, cells were seeded overnight before a being fixed to the surface; the fixed cells were then imaged using a scanning electron microscope to determine any changes to the cell morphology when compared to unprocessed polymer.

Chapter 5 – Materials and Methods

5.1 Materials

Table 4. The following materials were used throughout this thesis

European Collection of Animal Cell Cultures (ECACC)	LL24 BAE-1
Biomer Technology Ltd, UK	Series 'A' polyurethane Z1A1 Polyurethane
Sigma, UK	Foetal bovine serum, Bovine serum albumin, Penicillin/streptomycin, Triton X-100, Paraformaldehyde, Fluoromount aqueous mounting medium, dimethyl sulfoxide (DMSO). Mtt tetrazolium dye, Phospophate buffer solution
TED PELLA, Inc, USA	Harris Uni-Core™ punch
Cytoskeleton, Inc., USA	Acti-stainTM 555 fluorescent phalloidin
Appleton Woods, UK	Sterile serological pipettes (5 and 10ml), and glass microscope slides (75×25×1.1mm)

5.2 Major Equipment

Table 5. The Following equipment was used throughout this thesis

Grinding wheel	Jones + Shipman 540 surface grinder
Polisher	Metaserv Universal Polisher
SEM, Netherlands	FEI-Philips variable vacuum scanning electron microscope
Atomic Force Microscope (AFM), America	Molecular Force Probe-3D (MFP-3D) atomic force microscope, with software written in IGOR pro
Bruker, Germany	White light interferometer, vision 64 software
Zeiss, UK	Laser Scanning Confocal Microscope (LSM), model 510 META
SPI Laser, UK	20W Nano Second Pulsed Fibre Laser System
PeCon GmbH, Germany	Tempcontrol 37-2 and CTI-controller 3700
BMG LABTECH, Germany	CLARIOstar microplate reader
Quorum Technologies, UK	Emitech K550x sputter coater

5.3 Methods

5.3.1 Preparation of stainless steel sample moulds

All patterns surfaces were generated upon a biocompatible polyurethane polymer (described in 5.3.6). Patterns were developed on the polymer indirectly, by casting off the flat end surface of a cylindrical stainless steel mould that had been cut from stainless steel rods (grade 316, cylinder height 13mm, diameter 18mm). To prepare the stainless steel moulds for patterning, their flat surfaces were first polished to remove all marks caused by the cutting process. This was achieved using a METASERV universal polisher and silicon carbide sheets of decreasing grit size (60 to 1200B) followed by a polishing cloth. This resulted in the stainless steel cylinder having a mirrored surface finish (mean Ra value of approximately 0.02μm) which could then be used for processing.

5.3.2 Green Laser micro patterning of metal surfaces

The experiments were performed using an Quantronix diode pumped solid state frequency doubled Q-switched laser source (Model - Osprey - 532 - 8 - 0), with a maximum average laser power (P) of 8W, wavelength (λ) of 532 nm. Pulse widths are typically 23ns. The laser beam was collimated and expanded up to 10mm through a Linos variable magnification beam expander. The expanded beam was then delivered to a galvanometer scanning head (GSI Lightning), which consists of two mirrors that control the laser beam path across the work piece. A translational x-y-z table (Aerotech Inc, UK) was used to accurately position the sample at the focal position of the processing lens. The reflected beam was then focused using a 100mm focal length lens (Linos F-Theta-Ronar 532nm+VIS) which produces a focused spot size of approximately 16μm in diameter. The pattern was generated over an $8mm^2$ area. The laser spot was focused onto the stainless steel and programmed to scan in a

raster pattern across the surface with a line spacing of 50µm between each pass. The parameters altered for processing were: laser power, frequency, processing speed and pass number while pulse duration was kept constant at 23ns.

5.3.3 Solid State Laser micro patterning of stainless steel surfaces

The experiments were performed using an SPI solid state pulsed fibre laser system (G3.0 20W Pulsed Fibre Laser HS Series) with a maximum mean laser power (P) of 20W, wavelength (λ) of 1064 nm and variable pulse duration (τ) of 9-200ns. The laser beam was collimated and expanded up to 10mm through a 5x beam expander. The expanded beam was then propagated to a galvanometer (scanning head, GSI Lightning), which consists of two mirrors that control the laser beam path across the work piece. A translational x-y-z table (Aerotech Inc, UK) was used to accurately position the sample at the focal position of the processing lens. The reflected beam was then focused using a 100mm focal length lens (Linos F-Theta-Ronar 1064 nm+VIS) which produced a focused spot size of 30µm in diameter. The pattern was generated over an 8mm^2 area. The laser spot was focused onto the stainless steel and programmed to scan in a raster pattern across the surface with a line spacing of 50µm between each pass. The parameters used for processing were: laser power 4W, pulse duration 9ns, frequency 25 kHz, a processing speed of 500mmsec^{-1} and pass number 20. These parameters resulted in the stainless steel having a grooved surface with features on the micron scale. The laser direction was kept the same for each lane (Figure 16).

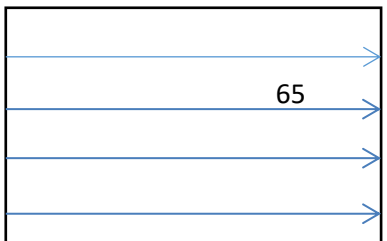

Figure 16 Schematic of laser produced surface showing direction of laser processing

5.3.4 Development of micro and nano-scratched surfaces from polishing

Once polished to achieve an initial mirrored finish (as described above in Section 2.1) the stainless steel cylinder was then polished to achieve a topographical surface patternation, through the use of abrasive paper (1200B). By controlling the motion of the stainless steel cylinders relative to the silicon carbide abrasive paper, surfaces having either directional, or random, sub-micron abrasive marks could be produced, termed here as 'nano-scratches'. The directional features are a result of the METASEV universal polisher's spinning motion (see figure 17), while the more random features are the result of manually rubbing the steel mould across the surface in different directions. The surface topography was subsequently characterised by white light interferometry and scanning electron microscopy. These stainless steel cylinders could then be used as master moulds to cast polymer substrates. In total three different patterns were produced; two polished surfaces including the linear polished and randomly polished.

Figure 17 METASERV universal polisher used for polishing surfaces to mirror surface for laser processing and to 1200B grade discs for polished surfaces.

5.3.5 Development of micro and nano sized features from surface grinding

Stainless steel cylinders were used for the surface patterning; a Jones + Shipman 540 surface grinder (figure 18) was used to pattern the surface. The parameters were 25m/sec peripheral wheel speed with a 2880 RPM constant speed. The wheel diameter was 160mm and was 19mm wide. A WA 60 KV wheel was dressed with a single point diamond, at 2 passes at 100µm/sec at four depths 2, 4, 6 and 10µm. WA means it is made from aluminium oxide, 60 is the grit size per sq mm, K is the hardness level and V means it has been vitrified. To pattern the surface the dressed wheel was run on a single pass at 300µm/sec with a 2 to 5µm depth of cut. This was done with each wheel depth to produce 4 different patterned surfaces, named in this thesis as M1, M2, M3 and M4 respectively.

Figure 18 Jones & Shipman 540 Surface Grinder.

5.3.6 Casting of polymer substrates from stainless steel moulds

Casting the polymer over the stainless steel moulds produces an inverted pattern on the polymer surface. Employing this indirect processing method ensures that only the surface topography/roughness of the material is altered and not the material chemistry. The polymer used here was polyurethane and was provided by Biomer Technology Ltd. The polymer substrates were produced using 8% polyurethane in 2:1 Dimethylformamide (DMF) and Tetrehydrofuran (THF). This was poured onto the stainless steel moulds and cured at 60°C for 2 hours. Following this the mould/cast was allowed to cool before peeling off the polymer from the mould following the grain of the pattern. Prior to cell culture all polymer surfaces were sterilised by washing with 70% ethanol then exposing to UV light for 30 minutes. Finally, the polymers were washed with sterilised distilled H_2O.

5.3.7 Characterisation of surfaces using advanced microscopy techniques

To characterize and measure patterned surfaces a range of advanced microscopy techniques were used. AFM was used because of its ability to provide 3D images of the surfaces as well

as provide surface measurements meant. SEM provided detailed high resolution images of the surfaces and complemented the AFM while also providing detailed measurements of surface features in 2D. LSM was used for live cell imaging to provide migration data through time lapse photography. White light interferometry also provided 3D images of the surface to improve comparisons between the different patterning techniques. The software on the microscope enabled 3D measurements as well as Ra, Rt and Rz measurements.

5.3.8 Cell culture

The cells described in this work are human lung fibroblast cells (LL24) and bovine aortic endothelium cells (BAE-1), which have been purchased from the European Collection of Animal Cell Cultures (ECACC). All cell culture work was carried out under aseptic conditions in a grade II laminar flow cabinet (EBSCO). Cells were maintained at 37°C in a humidified 5% CO_2/ 95% air atmosphere in Dulbecco's Modified Eagles Medium (DMEM) (Sigma-Aldrich, D6429) supplemented with 10% foetal bovine serum (Sigma-Aldrich, 0804) and 1% penicillin-streptomycin.

5.3.9 Routine cell maintenance

Cells were maintained through sub-culturing. Cells were grown in T75 cell culture flasks till 70-80% confluence. Cells were treated with Trypsin for 5 minutes at 37°C to detach them from the flasks. Once detached, cells were transferred to a 25ml universal tube containing 10ml of DMEM. Cells were then centrifuged @2500×g for 5 minutes and the resultant cell pellet was re-suspended in complete culture medium and the cells seeded into new flasks.

5.3.10 Determination of cell number for seeding onto patterned substrates

To ensure equal distribution and repeatability between experiments cell number was determined using a haemocytometer, which is used to determine the number of cells per ml of cell suspension. Briefly, the cells are centrifuged as described above (5.3.9) and the pellet re-suspended in 5ml of DMEM to achieve a uniform cell suspension. Next, 10µl of cell suspension was loaded into the haemocytometer and the cell number calculated with the aid of a light microscope using a ×10 objective lens.

5.3.11 Laser Scanning Fluorescence Confocal Microscopy

All light microscopy and fluorescence images of cells presented in this thesis were obtained using a Zeiss 510 Meta laser scanning microscope, mounted on a Axiovert 200M BP computer-controlled inverted microscope. This microscope is equipped with the following laser lines; blue diode 405nm, Argon ion 458, 477, 488 and 514nm, He-Ne 543nm and He-Ne 633nm. Images were obtained using the following objectives lens; Plan Neofluar 20×/0.30 numerical aperture (NA) and 40×/1.30 NA oil immersion. Cell fluorescence was excited using a wavelength of 543nm.

5.3.12 White light Interferometer

A Bruker Contour GT-K 3D optical microscope equipped with Vision 64 software was used to image the surfaces of the patterned polymers. This enabled feature heights/widths and roughness to be determined. All images were taken using either ×25 or × 50 magnifications.

5.4.13 Atomic Force Microscopy

All AFM data presented in this thesis were obtained using a Molecular Force Probe-3D (MFP-3D) atomic force microscope (Asylum Research, Santa Barbara, California), with software written in IGOR pro (Wavemetrics Inc., USA). The MFP-3D is equipped with a 90μm x-y scanning range, a z-piezo range of 16μm and is coupled to an Olympus IX50 inverted optical (IO) microscope. The MFP-3D-IO was placed upon a TS-150 active vibration isolation table (HWL Scientific instruments GmbH, Germany), which was located inside an acoustic isolation enclosure (IGAM mbH, Germany) to help eliminate external noise.

5.3.14 Scanning Electron Microscope

All SEM images presented in this thesis were obtained using a FEI-Philips variable vacuum scanning electron microscope (Eindhoven). The microscope was an Inspect S model that had a voltage range up to 30Kv and a resolution of 5nm. Both cell types were seeded at a density of 100,000 per surface, and left overnight. The surfaces were washed (×1) with Phosphate Buffer Solution (PBS) to remove cell medium. Next, the cells were fixed with 4% paraformaldehyde in PBS for 10 minutes at room temperature. The fixative was then removed and the surface washed with PBS (×3), followed by being washed in H_2O (×3). The surfaces were coated in gold using a Emitech K550x sputter coater, 2.5 minutes at 25mA using argon gas as plasma. Gold coating is approximately 15 nanometres thick.

5.3.15 Investigation of cell adhesive quality of surfaces

In order to determine if cells had a preference for either the laser processed surface, scratched surfaces (random and uniform) or unprocessed flat polymer surfaces, an adhesion assay was carried out. Polyurethane casts (6mm diameter) were cut using Biopunch (SLS) and placed

in the wells of a 96 well plate. The polymer discs were then treated with UV light for 30 minutes to sterilize the surfaces thus avoiding contamination. The surfaces were washed with PBS (×3) and 10,000 cells seeded onto each polymer. The cells were left to incubate for two hours (LL24) or six (BAE-1) (37°C 5% CO_2), after which the growth medium was removed and the polymer discs washed with PBS (×3). Next, the MTT assay was performed. The first stage was to add 10% MTT (5mg/ml in DMEM to the wells of each plate, they were subsequently left to incubate for 3 hours at 37°C in a humidified 5% CO_2/95% air atmosphere. The medium was removed and replaced with DMSO in order to dissolve the formazan crystals. The plate was then read using a 96 well plate reader at a wavelength of 570nm. For this experiment three control samples were used for each surface, they followed the same protocol but were not seeded with cells.

5.3.16 Investigation of cell proliferative quality of surfaces Cell Proliferation

In order to determine the effects of surface topography on cell proliferation the MTT assay was used to determine relative cell density. Cells were seeded onto 6mm sterile polymer casts (placed in 96-well plates) at a density of 10,000 cells per well and left to incubate for 24, 48, or 72 hours (37°C 5% CO_2). At each discrete time point an MTT assay was carried out as described above and absorbance related to relative cell density was determined.

5.3.17 Investigation of cell migration properties of surfaces

To determine if the different surfaces affected cell migration, time-lapse imaging and subsequent cell tracking was performed over a four-hour period using a Zeiss LSM 510 confocal microscope. Briefly, the polymer surfaces were sterilised in 70% ethanol, washed in PBS then placed into 35mm cell culture dishes. Next 200,000 cell/cm^2 were seeded onto

the polymer surfaces and the dish was placed into the microscope environmental chamber (S-2, PeCon GmbH, Germany). The chamber was maintained at 37°C, 5% CO_2 in a 60-70% humidified air atmosphere using a Temcontrol 37-2 and CTI-controller 3700 (PeCon GmbH, Germany). Images were taken every 15 minutes for 4 hours using a 20× Plan-Apo/0.75 NA DIC objective lens, while scanning using a Helium-Neon (HeNe) laser at 543nm. ImageJ software (National Institute of Health, NIH) with manual tracking plugin (Institute Curie, France) was used to analyse the data produced from the time-lapse image series.

5.3.18 Investigation of cell proliferative quality of surfaces Cell Proliferation

In order to determine the effects of surface topography on cell proliferation the MTT assay was used to determine relative cell density. Cells were seeded onto 6mm sterile polymer casts (placed in 96-well plates) at a density of 10,000 cells per well and left to incubate for 24, 48, or 72 hours (37°C 5% CO_2). At each discrete time point an MTT assay was carried out as described above and absorbance related to relative cell density was determined.

5.3.19 Statistical analysis

All experiments were repeated 3 times. All statistical analysis was carried out using SPSS. For cell adhesion and proliferation studies, an unpaired, independent two-tailed student's t-test was used to determine whether there was a significant difference between the mean absorbance from the cells cultured on the patterned and unprocessed polymer surfaces. For the migration studies an independent two-tailed student's t-test was used to determine if

there was a significant difference between the mean migration distance (μm) of the cells cultured on the patterned polymer and those cultured on the unprocessed surface. All tests were carried out using a 95% confidence limit assuming unequal variances.

Chapter 6 – Results

6.1 Preparing stainless steel for laser processing

Prior to laser processing, the stainless steel surface needed to be polished to remove any markings and scratches on the surface. This required the use of a METASERV universal polisher. The universal polisher was used with decreasingly graded polish papers (60 to 1200B) followed by a polishing cloth. This process helped to remove any unwanted features

from the stainless steel surface and readied the surface for laser processing. As can be seen in Figure 19 (A&B), the original unpolished surface texture showed multiple circular features (approximately 1mm in height) left as a result, of the cutting tool. In contrast, Figure 19 (C&D) shows that the polishing process has removed the circular features, however there are still some scratch marks (approximate height 1µm).

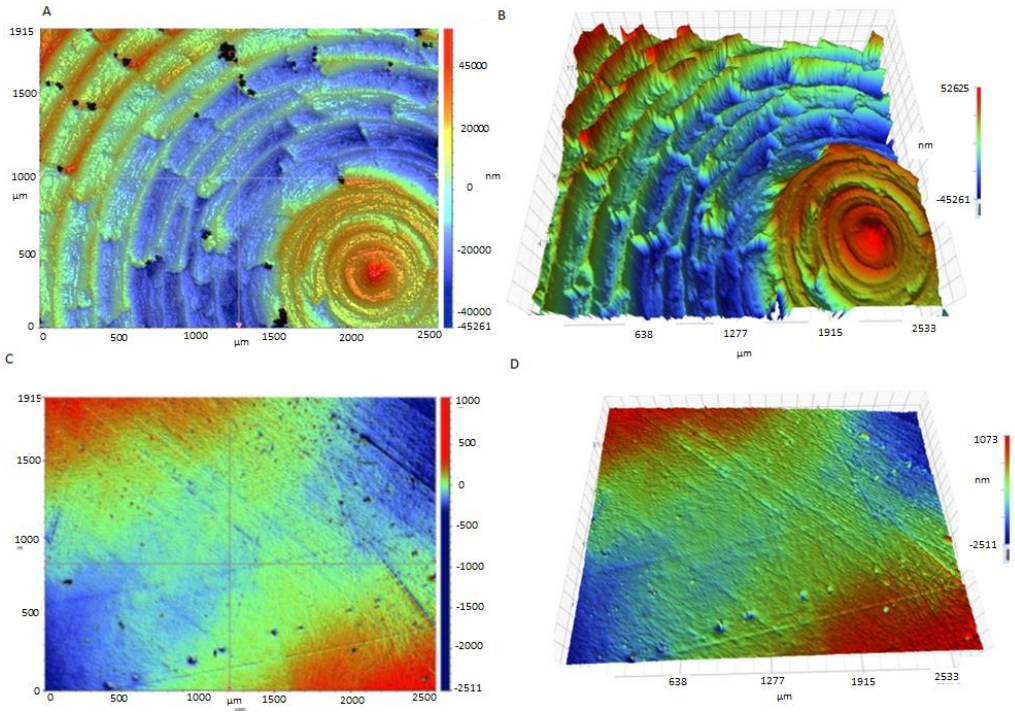

Figure 19 (A&B) White light interferometer images of the stainless steel mould in a plane view and 3D respectively, shows cutting marks and a height gradient of approximately 1mm. C&D Showing steel mould following the polishing process in 2D and 3D respectively and a height gradient shown to be approximately 1µm (Images taken at 10× magnification). Colour bar represents size gradient.

6.2 Visual Analysis of stainless steel patterning using a Quantronix diode pumped solid state frequency doubled Q-switched laser source

Two different laser setups were compared for processing the stainless steel, the SPI laser (solid state infrared laser) and the Green laser (Quantronix diode pumped solid state frequency doubled Q-switched laser source). Both were used in a systematic approach to determine their effectiveness for surface patterning in terms of whether they would produce defined features or an excess of unwanted features. The parameters tested were processing speed, number of passes over the surface and the power of the laser.

To determine what effects of speed of processing on the steel, the parameters of frequency (31.5 kHz) and number of passes (6) was kept constant. The speed of processing was varied, with speeds of 200, 400, 800 and 1200mmsec^{-1} used. This was done to determine what effect the overlap of the laser impact area would have on the surface, at the slower speeds the impact areas overlap more for subsequent impacts and this decreases as the speed increases. The laser power used was kept constant at both 1 and 2W in separate experiments as this would enable a direct comparison between the surfaces. The processing area was 5mm^2 for each sample.

Looking at figure 20, which used a power of 1W, decreasing the speed resulted in a decrease in the space between laser impact points. It can be observed that, at the lower slower speeds 200 and 400mmsec^{-1} the features produced are channels, with a continuous feature running the length of the image. However, when the processing speed is increased to 800mmsec^{-1} the channels become more pit-like and discontinuous.

Figure 21 shows that at 2W the results of laser processing are similar to the 1W results, as speed increases less material is removed in the processing resulting in features that at the slower speed look defined as a channel but with extensive features surrounding the channels. As the speed increases to the 800mmsec^{-1} and 1200mmsec^{-1} respectively the channel becomes less defined.

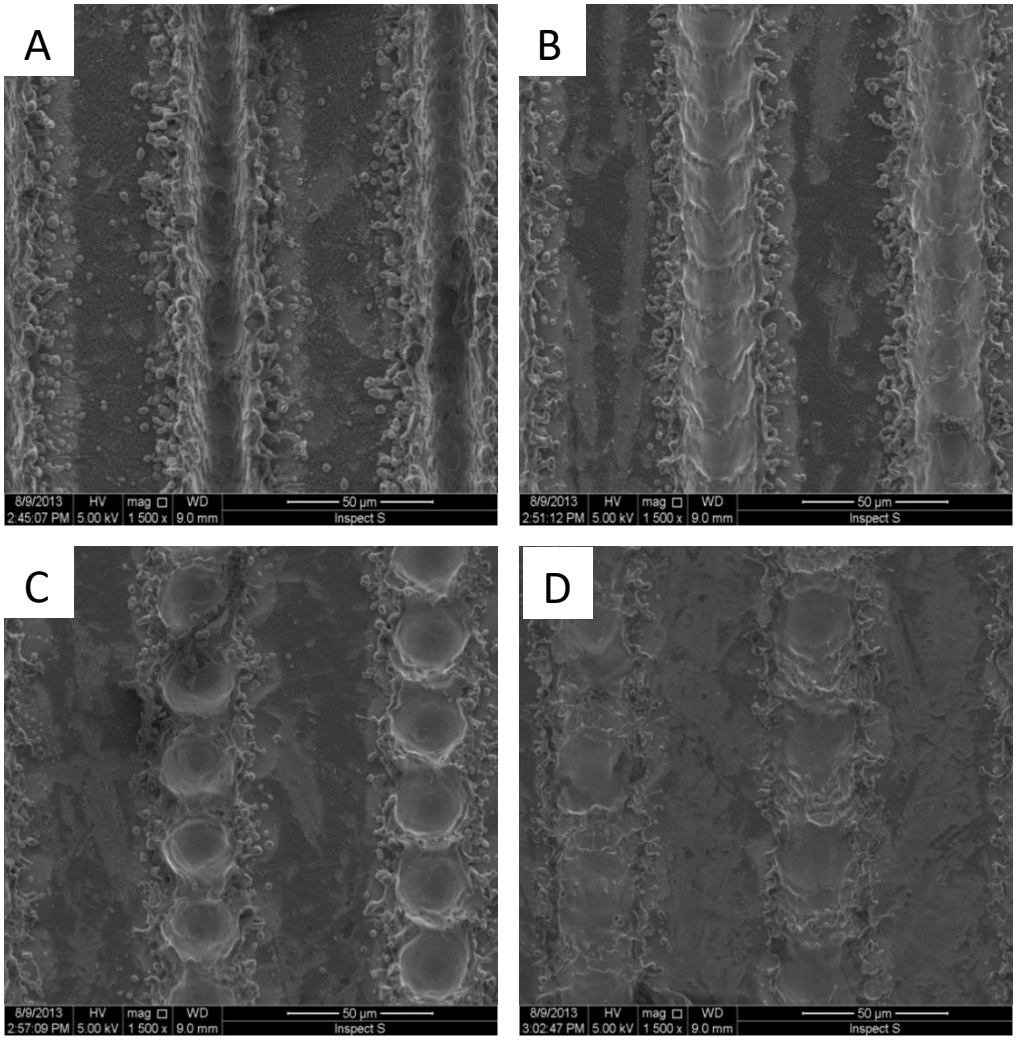

Figure 20 Green laser processed stainless steel, using a power level of 1W with variations in scanning speed- A) scanning speed of 200mmsec^{-1}, B) 400mmsec^{-1}, C) 800mmsec^{-1} D) 1200mmsec^{-1}.

In order to investigate the effects of processing pass number the material was processed with the following pass numbers 1, 3, 6 and 10. These pass numbers were used with constant speed of 500mmsec^{-1}, as well as a constant power of 2W and a frequency of 31.5 kHz. By changing the pass number, the amount of impact the laser has with the surface changes correspondingly. As can be seen from figure 22 as the passage number increases so does the level of processing of the surface. This increase in processing can be seen in the level of external features surrounding the processed area after each increase in pass number.

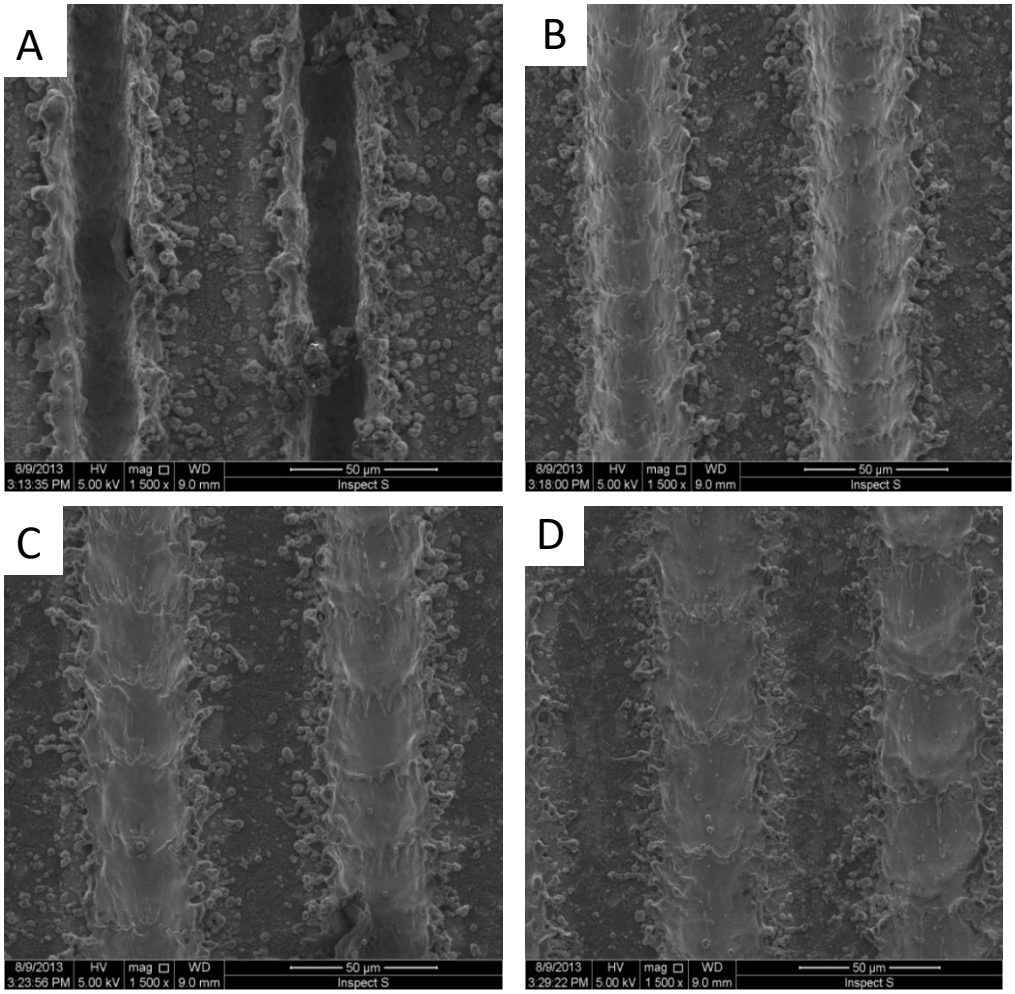

Figure 21 2W laser processing power with variations in scanning speed. A) 200mmsec^{-1}, B) 400mmsec^{-1}, C) 800mmsec^{-1} and D) 1200mmsec^{-1}.

In order to investigate the effects of changing the power level of the laser on the material, stainless steel was processed with the power level of 0.5, 1, 1.5 and 2W. The passage number was kept constant at 6 and a speed of 500mmsec^{-1} and a frequency of 31.5 kHz was used. As can be seen from figure 23, at 0.5W there is evidence of impact with continuous circular pit-like features along the processed area. There are limited features seen around the processed area, suggesting limited material removed during processing. When comparing the features at the different power levels an increase in power resulted in an increase in the level of external features seen.

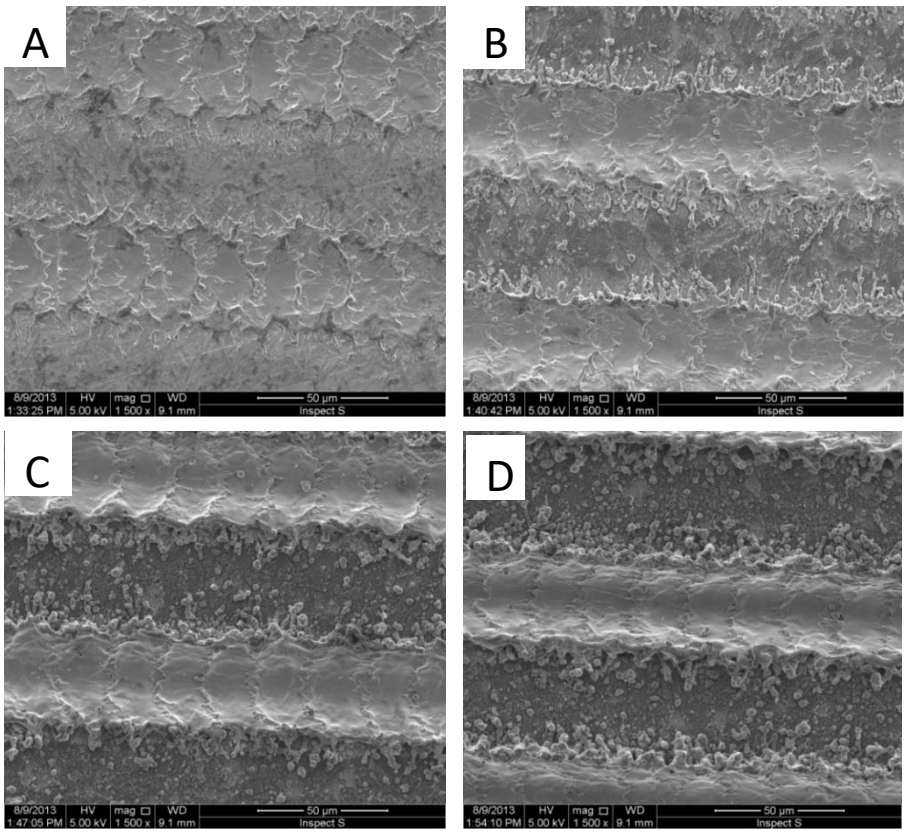

Figure 22 SEM image of stainless steel following laser processing at different pass number, A) 1 pass, B) 3 passes, C) 6 passes and D) 10 passes. The power was kept at 2W with speed kept constant at 500mmsec^{-1}.

When analysing the images taken following the green laser processing what is observed is that increases in parameters (i.e. laser speed, power or the number of passes there) resulted in an observable increase in the level of features surrounding the processed features. This is a limitation of this method (or laser type) as it means that control of feature development is limited. The resulting channel features are a suitable feature for testing cell behaviour but the laser patterning technique is not, therefore a second laser type was evaluated, the SPI laser. The important difference between the two lasers is seen in the spot size, the green laser has a smaller spot size which results in the energy being focused on a smaller area. This would suggest a difference in features type being produced by the lasers, the SPI may produce ones more suitable.

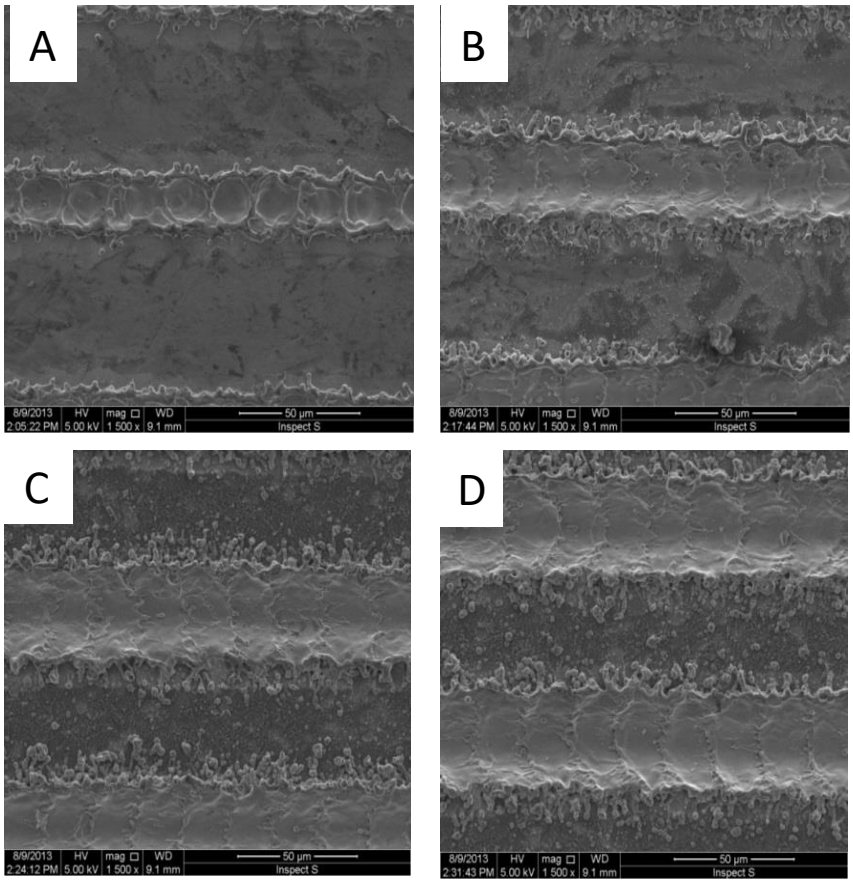

Figure 23 Changes in laser processing of stainless steel with changes in laser power, A) 0.5W, B) 1W, C) 1.5W and D) 2W. The passage number was kept at 6 with speed kept constant at 500mmsec^{-1}.

6.3 Sold State Infrared Laser

The second laser type used was the solid-state infrared laser (SPI). Similarly, to the green laser the parameters speed, power and pass number were changed in order to determine their effect on feature generation on stainless steel. The processing was done in lines across the surface with the laser direction constant from left to right to produce channel like features.

Initial tests were performed at two speeds; 250 and 500mmsec^{-1}, with the power kept constant at 2W and frequency at 25 kHz. These two speeds were used to give a basis from

which to work from, that had been covered in previous work with the green laser. A new variable used in the testing of the SPI laser is the hatch width, or width between laser processing channels, this was changed from 10 to 100µm in 10µm increments. This was done to determine the effect the spot size of the laser would have on the features being produced, while the hatch value remains within this area the features will be affected.

As can be seen from figure 24, at 250mmsec^{-1} the smaller hatch widths (20µm) showed no obvious distinction in laser channels, this is due an overlap in the laser spot size. It was not until 40µm that a clear separation between the channels was seen, by 80 and 100µm hatch width a clear distinction can be seen between the different laser channels.

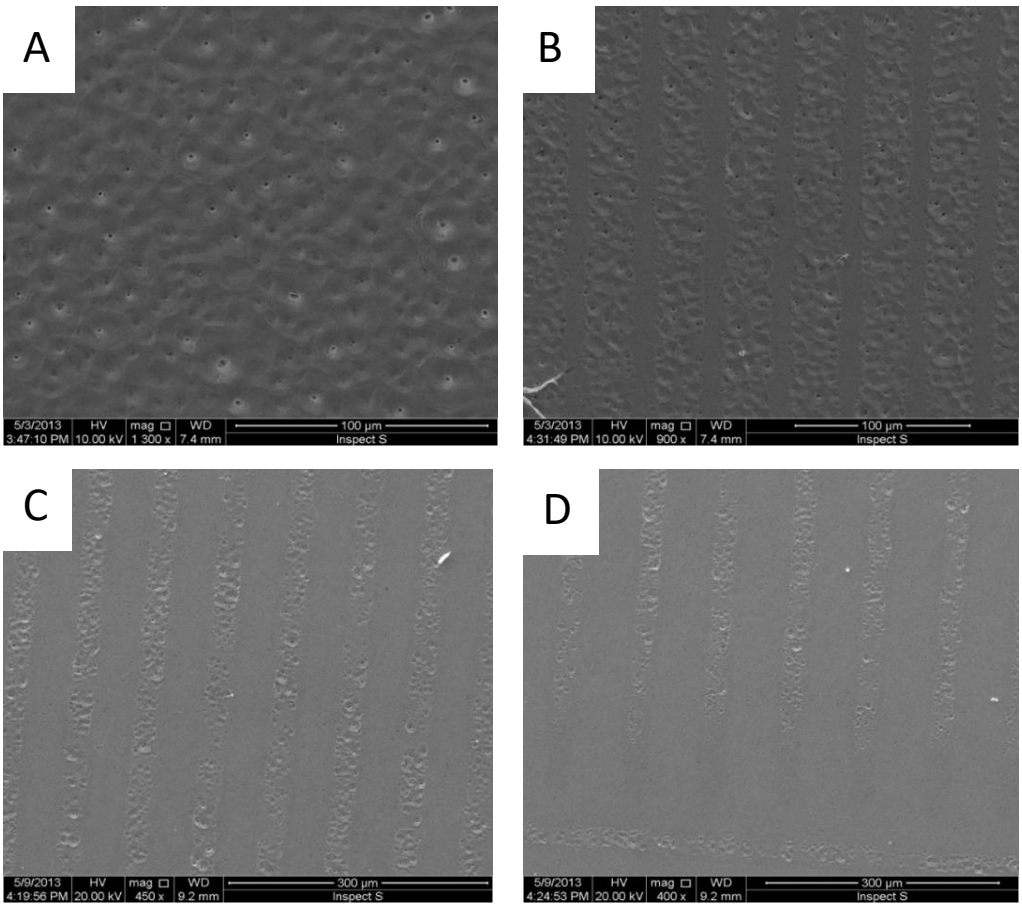

Figure 24 2W laser processing at 250mmsec^{-1}, the hatch spacing value was altered, A) 20µm, B) 40µm, C) 80µm and D) 100µm.

At 500mmsec^{-1} the results are similar to those seen at 250mmsec^{-1}; in that at 20µm there is no distinguishing the different channels, at 40µm there is some limited channel development seen. At 80 and 100µm there (figure 25) is a clear path seen between the different laser channels. When comparing the two speeds there seems to be a difference in the impact areas, this is more noticeable when comparing the 40µm at both speeds. At 500mmsec^{-1} more individual impact points are seen, this may be due to the speed of processing separating those points negating the effect of any overlap that is seen at the slower speed.

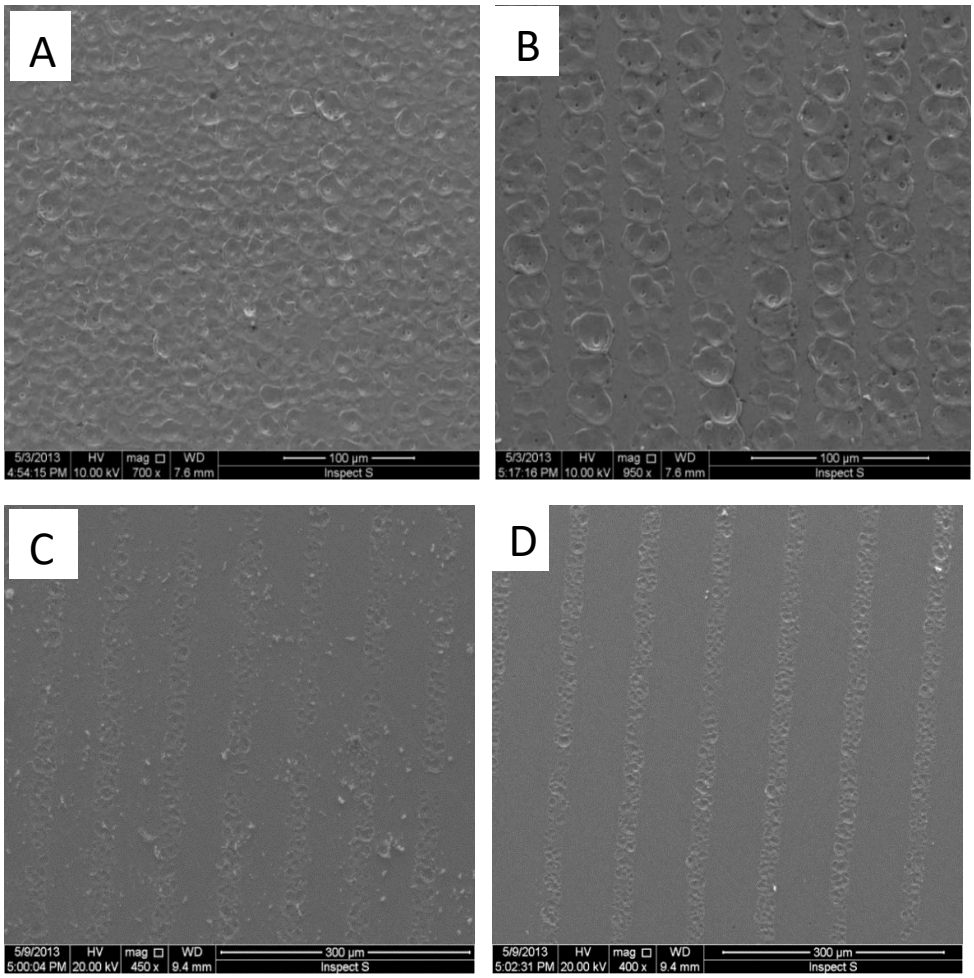

Figure 25 2W laser processing at 500mmsec^{-1}, the hatch spacing value was altered, A) 20µm, B) 40µm, C) 80µm and D) 100µm.

In order to investigate the effects of laser power on feature processing the laser power was increased to 4w while the frequency was kept at 25 kHz, the speed was 500mmsec^{-1} and the

number of passes kept at 5. This was done with three hatch spacing values, 30, 40 and 50µm, all of which are larger than the limiting factor of the laser spot size allowing for the generation of channels, this will enable the effect to be seen without any cross over from the parallel channels.

Figure 26 shows that at 30µm hatch spacing there was little space seen between the channels generated, there was also limited external features seen. This is not the same at 40 and 50µm were the level of built up surrounding features is shown to be extensive, this suggests that by keeping the hatch spacing close it is possible to remove any features built up after the previous channel.

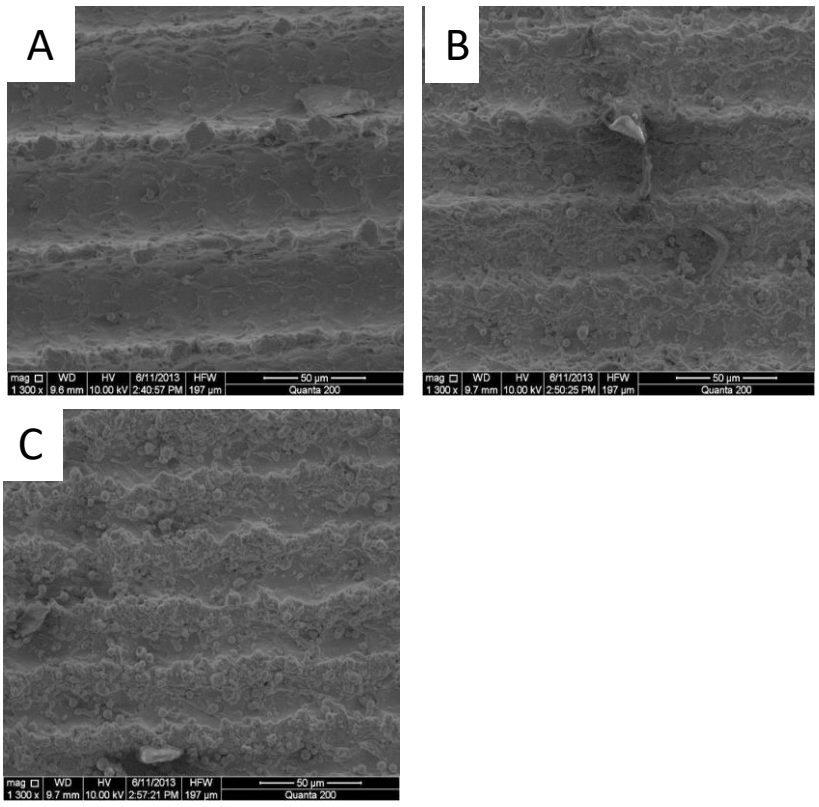

Figure 26 4W laser processing with the speed and pass number kept constant at 500mmsec^{-1} and 5 passes respectively. The hatch value was altered A) 30µm, B) 40µm and C)50µm.

After initial testing of the SPI laser it was determined that the SPI laser was a more suitable laser to use due to its ability to produce channel features that can be easily distinguishable

while also resulting in limited unwanted features. This is in contrast to the green laser that though able to produce very distinguishable features it was limited by the level of surrounding features seen. Having decided upon the SPI laser as the more suitable device further analysis of its patterning ability was needed, specifically the effect of varying laser speed and the number of passes.

By a process of varying the scan parameters, imaging and visual inspection, it was determined that using a rate of 500mmsec^{-1} produced the most uniform features. This can be seen from Figure 27, in which there seem to be an obvious difference in the number of pits (less on the 500mmsec^{-1} surface). Increasing the pass number to 20 (figure 29) improved the feature definition when compared to small pass numbers (figure 27) but, when the pass number increased further to 30, 40 and 50 passes the definition began to decrease. Upon inspection of the images, it was noted that surface pitting (Figures 28 and 29) caused by the laser processing, littered the surface of the sample. Surface pits were seen on all surfaces and were seen to increase in frequency as the laser speed was reduced and as the pass number increased. As can be seen from Figure 28, the surface pits have a diameter of the order of 10µm and a depth of approximately 700-800nm. The dimensions of these pits are comparative to the cellular size and would undoubtedly have an effect upon the cells. Therefore, one of the aims was to reduce this effect.

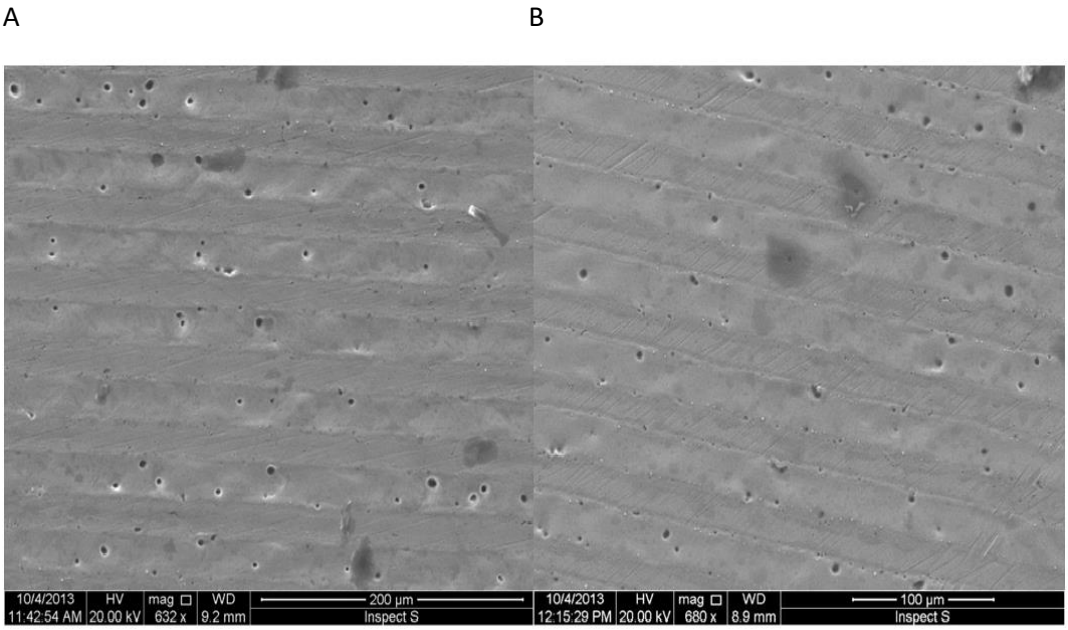

Figure 27 Shows the results of varying the speed of laser processing (A) 200mmsec^{-1} and (B) 500mmsec^{-1}. Both surfaces were processed with 4W, 9ns and 15 passes.

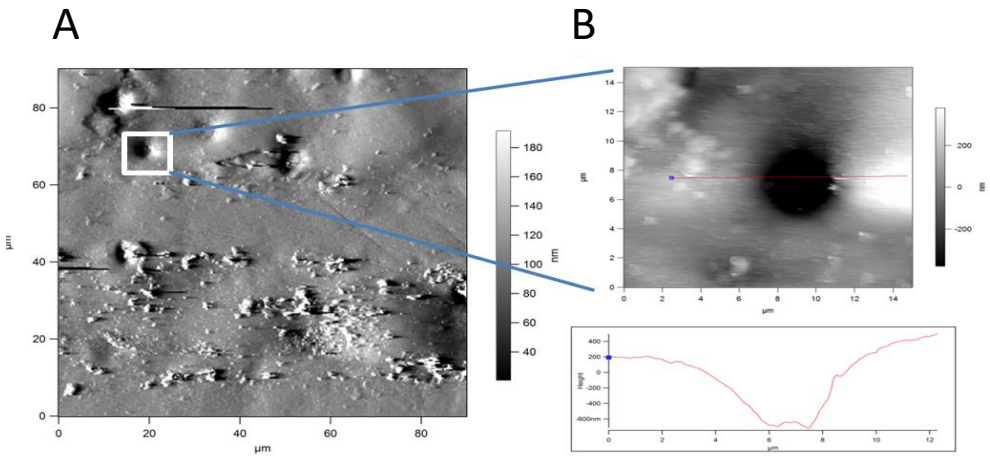

Figure 28 (A) AFM contact mode image of laser processed surface 500mmsec^{-1}, 9ns, 4W, 12 passes highlighting a high level of unwanted features and surface pit. (B) Profile of pit found in A.

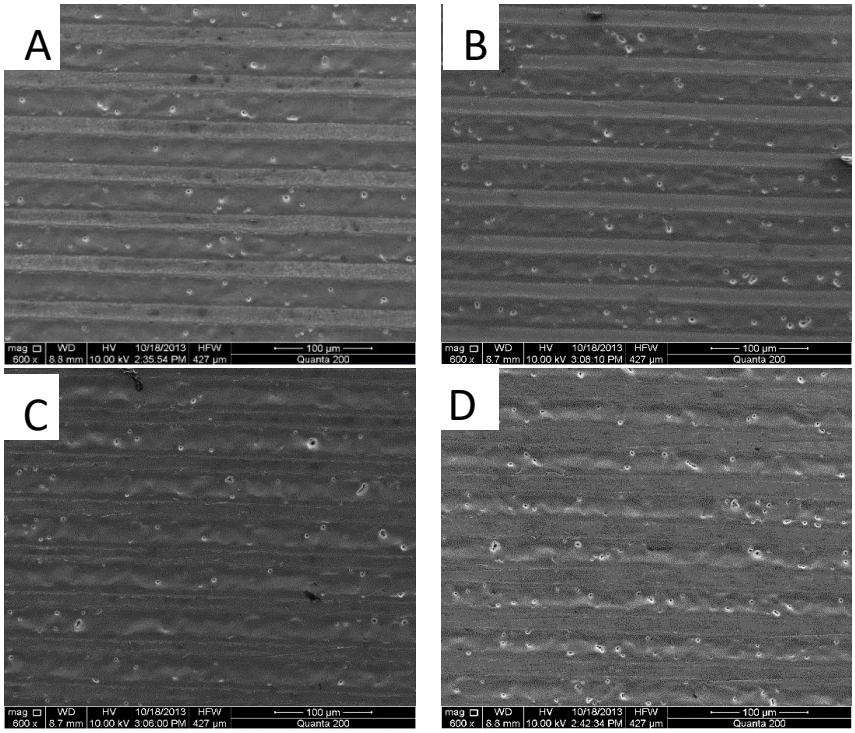

Figure 29 SEM images of laser processing 4W, 9ns, 20 passes, 500kHz. Shows defined edge to features, clearly distinct from non-processed areas with very little extra features seen. Pitting however is still apparent.

The features generated by the laser processing varied in size (Figure 30) and rose and fell in a rolling hill theme across the laser patterned path. The surface features were measured using the white light microscope software to determine the maximum feature height (Sz) This was identified to be approximately 8.97µm. The mean width of the feature path was approximately 32.2µm (+/- 0.9, n=30). This is due to the spot size of the laser and is a limiting factor in developing feature size. The approximate width between the feature paths was approximately 16.5µm (+/-0.88, n=30).

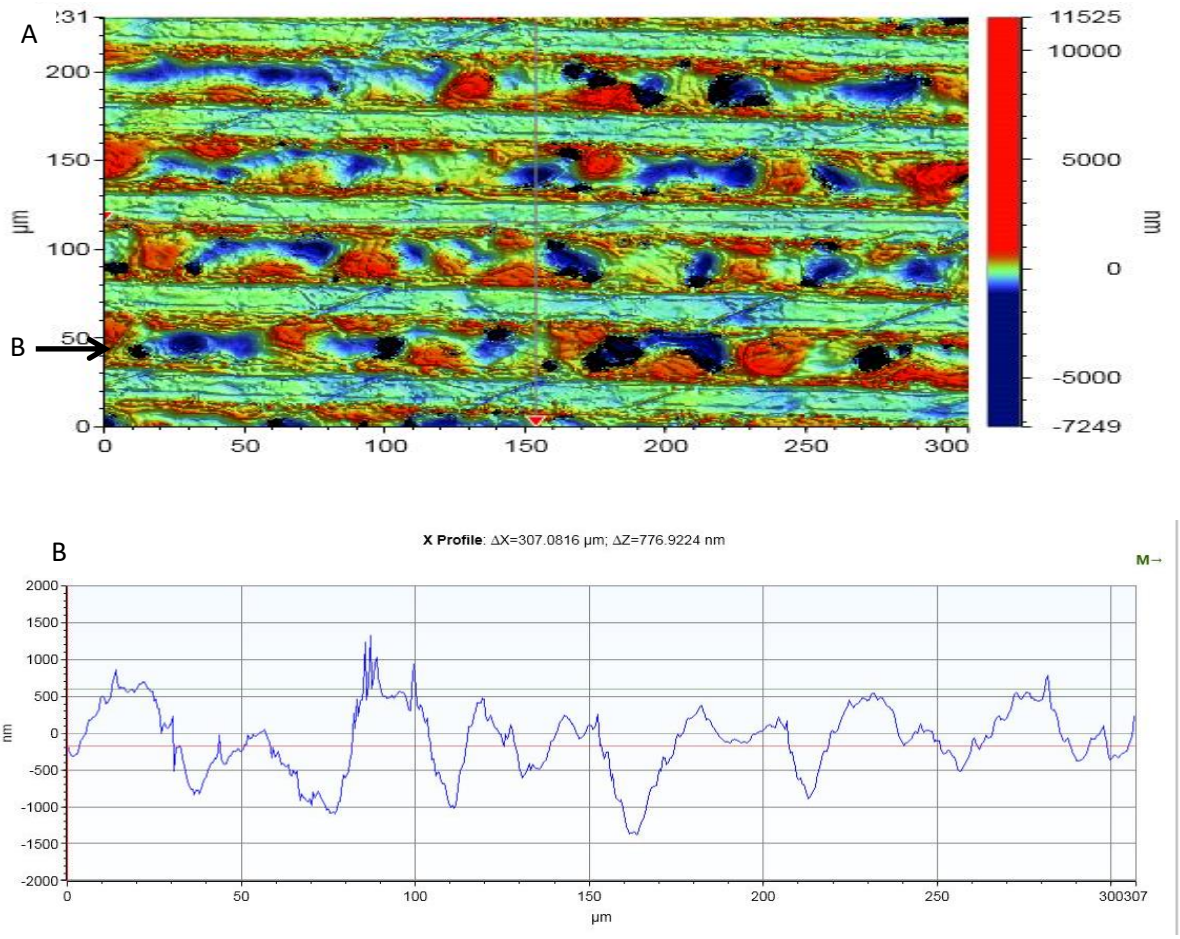

Figure 30 (A) White light interferometer image of laser processed surface in a plane view (×10). From the colour coding of image, the rolling hill formation is evident. (B) X profile of laser processed area, identified through arrow on image (A) showing a distinct height changes across area. Colour bar represents size gradient.

6.4 Identification of nano scratches on the surface and their development into useable surfaces

During polishing the stainless steel mould (prior to laser processing) it was identified that the surface was a highly scratched. Feature size of these scratches was found to decrease as the polish paper grain size decreased. Interestingly, these features seemed quite uniform in size and direction. When these features were imaged, it was found that the 1200B polishing paper produced surfaces with sub-micron sized features in the z-direction (Figure 31 A&B).

Features of a comparable size are found in the ECM, which is a 3D scaffold, to which cells in the human body anchor onto in order to form tissues. Therefore, using silicon carbide polishing paper and a METASERV universal polisher, stainless steel moulds were developed resulting in mean feature sizes in the z direction of 270nm ±15nm. The surface generated by the METASERV universal polisher also showed a relatively high degree of directionality with features largely orientating in the same direction.

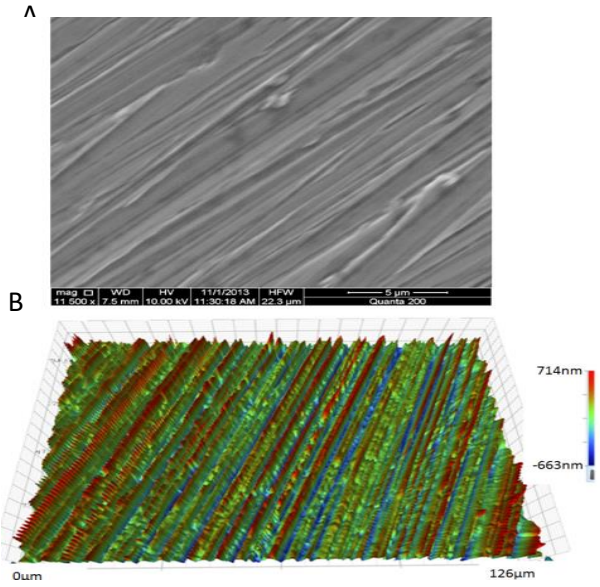

Figure 31 (A) SEM images of 1200B polished metal via universal polisher (×11500) (B) White Light Interferometer image of the 1200B polished metal (×50). Colour bar represents size gradient.

In the human body the ECM appears to be randomly organised with respect to direction. Therefore, new stainless steel moulds were developed, the surfaces were polished in the same manner as the 1200 linear surface but after reaching that stage they were manually polished using the 1200b grade paper to give scratches in a more random orientation (see Figure 32). When analysed the mean height value for the random surface was 480nm ±39nm.

Having established these three surface for use to test the effect on cell behaviour the next stage was to produce the polymer casts of the surface. These casts would need to accurately

represent the moulds, though being an inverse cast the heights of the features should still be the same.

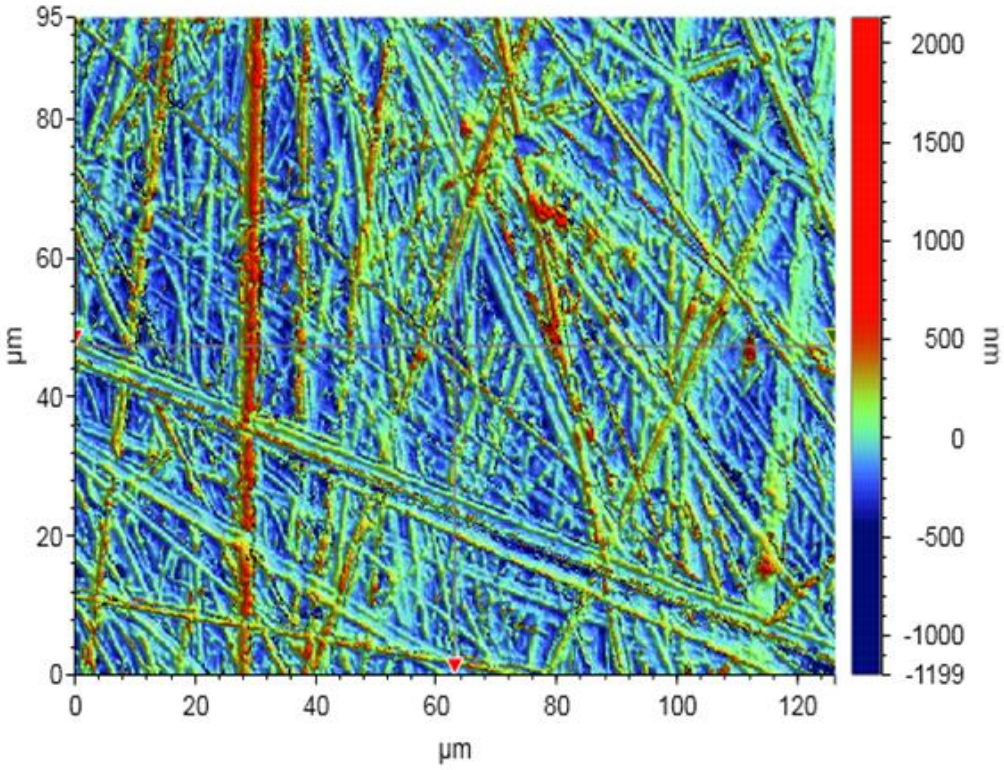

Figure 32 White light interferometer image of 1200 universal polisher random polished metal in a plane view (×50). Colour bar represents size gradient.

6.5 Production of polymer casts and the accuracy to the metal moulds

The laser processed and the nano-scratched steel substrates were to be used as moulds to cast polymer substrates, to culture cells in order to determine which substrate would have the greatest effect on enhancing or reducing cell adhesion, proliferation and migration.

When casting polymers from the steel surfaces the resulting surface have inverse features of the steel mould. These features are comparable in size to collagen fibrils found within the ECM [51] and also to those produced by more advanced techniques such as electrospinning

[99]. Measurements of the feature height and surface roughness of the polymers compare favourably with those of the stainless steel moulds. Polymer casts of the stainless steel moulds were also imaged using a white light interferometer, in order to determine the accuracy of the casts compared to the moulds. Figure 33 shows 3D images taken from the polymer casts, comparative measurements for peak height and feature width were taken from the laser surface, while for the polished surface just peak was identified using the instrument software. It was found that feature geometry and feature sizes were near identical to those of the laser processed surface. The polymer surface had features of an Sz value of 15.43µm, with mean measurements of 31.9µm (n=30, ± 1.54) for laser processed area width and 16.8µm, (n=30, ± 1.32) for the non-processed area. This showed a high similarity with the mould surface which had values of 32.2µm (+/- 0.9, n=30) and 16.5µm (+/-0.88, n=30) respectively. This similarity in the cast surfaces enabled the progression of this research into the testing of cell behaviour on the cast polymer surfaces.

Figure 33 demonstrates the Bruker software that was used to determine surface roughness parameters (Sa and Sz) for all polyurethane surfaces. As can be seen from Table 4, laser processing produced surfaces having significantly greater surface roughness values compared to the surfaces produced by polishing (as indicated by the higher S values). Abrasive polishing in a directional manner resulted in surfaces having the least overall surface roughness.

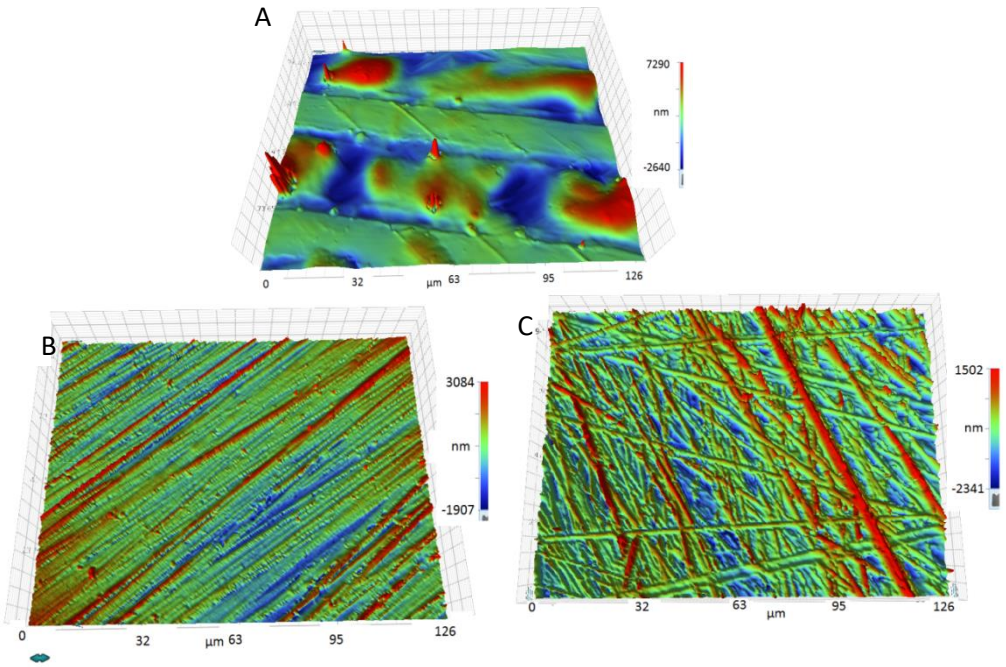

Figure 33 Polymer casts of the stainless steel moulds (A) Laser processed surface (B) Linear polished surface (C) Randomly polished surface. All images are (×50). Colour bar represents size gradient.

Table 6 Sa, and Sz measurements for the polymer casts taken via white light interferometry (N=5 from each surface)

Roughness of Polymer Substrates (µm)		
	Sa	Sz
Unprocessed	0.013	0.4
Laser	0.32	15.43
Directional	0.08	3.5
Random	0.17	5.6

Analysis of surface roughness properties (Table 4) found the mean surface roughness (Sa) for the laser processed surface to be almost twice that of the randomly polished surface.

Similarly, the mean maximum peak value (Sz) for the laser processed surface, were found to be greater than the polished surface.

The laser processed surface was produced using a directional scan pattern to try and produce a ploughed-field effect. Therefore, one might expect the Sa values to be lower compared to the random surface. However, this was not the case, as the laser surface was found to have a Sa value approximately twice of that of the randomly organised polymer surface (Table 4). Upon closer inspection of the laser processed surfaces, it becomes apparent that the processed areas are not uniform and display an undulating pattern along the processed areas (see Figure 24A). This seems to have resulted in the laser processed surface having a less ordered surface than may be expected and which may have contributed to the enhanced roughness and cell adhesion.

Having established the accuracy of the casts and thus the ability to reproduce on a large scale the next stage was to test the surfaces for their effect on modifying cell behaviour. Two cell lines were used LL24 fibroblast and BAE-1 endothelial, the effect the surfaces had on their ability to adhere, proliferate and migrate.

6.6 Effect of different feature types on modifying cell behaviour

The next stage of my research was to investigate whether the previously mentioned surfaces have any effect on cell behaviour. These tests for adhesion, proliferation and migration were done in triplicate and statistically analysed to determine any significant difference within the results.

6.6.1 Investigating the Effect of Surface Patterning on LL24 Cell Adhesion

In order to determine if the processed surfaces affected cell adhesion an MTT assay (colorimetric assay that relates absorbance to viable relative cell density) was carried out 2-hours post cell seeding. As can be seen from Figure 34, both the laser processed surface and the randomly polished surface were found to promote very similar levels of cell adhesion as indicated by absorbance values (absorbance values for the laser processed surface of 0.39 versus 0.4 for the polished surface, respectively). A one way anova t-test found the level of cell adhesion on the random surface to be significantly greater compared to the cells growing on the unprocessed surface and directional surfaces ($p<0.05$).

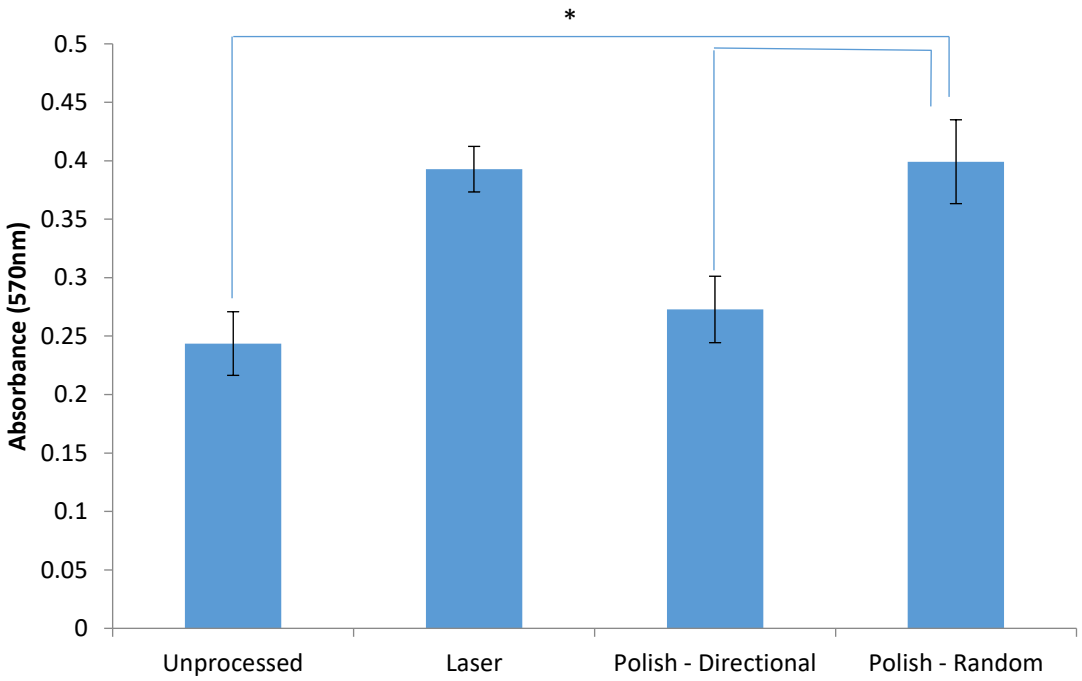

Figure 34 MTT assay results for cell adhesion showing absorbance for cells attached to the different surfaces. Error bars represent standard error of the mean.* $p<0.05$.

The unprocessed surface and the polished-directional surfaces were found to promote the least cell adhesion. The MTT assay revealed the absorbance values to be very similar for these two surfaces (0.23 versus 0.27, respectively), thus indicating a similar level of cell retention on these surfaces after 2 hours (Figure 28). Analysis of the surface roughness values for these two surfaces (discussed in 6.5) revealed them to have a similar mean surface roughness (Sa).

In vivo, the ECM is randomly organised in three-dimensions [100] and thus has greater similarity with the randomly polished surface compared to the more uniform topography of the other surfaces. Figure 34 shows that both the laser processed surface and the randomly polished surface were found to promote very similar levels of cell adhesion. They both also showed increased levels of cell retention when compared to the linear polished and un-patterned surfaces. Therefore, these results suggest that for the surfaces described here, feature directionality may be more important than surface roughness in promoting cell adhesion. This suggested effect of directionally ordered surfaces having a significant effect upon cell adhesion agrees with the previous work of others. For example, Biggs *et al* [68] used electron beam lithography and a polymer injection moulding process to generate arrays of nano-pits having varying degrees of order and found that highly ordered symmetry reduced adhesion, when compared to more randomly ordered surfaces. Similarly, Curtis *et al* [16] used electron beam lithography, followed by dry etching, to generate ordered and random arrays of micro-pillars and micro-pits on fused silica and found that ordered topography reduces fibroblast cell adhesion very markedly. The effect of topography on cell responses has been examined on the genetic level, Dalby *et al* 2005 investigated which genes were up/down regulated following seeding of fibroblasts on columns. Their work demonstrates that surface topography can have an effect on the expression of proteins that

are linked with cell behaviours including cell proliferation, ECM modelling and cytoskeleton production [101].

6.6.2 Investigating the Effect of Surface Patterning on LL24 Cell Proliferation

In order to compare the effects of the different surfaces upon cell proliferation an MTT test was performed after 24, 48 and 72 hours. Figure 35 shows that after 24, 48 and 72 hours, cells were found to proliferate steadily on all surfaces. After 24 hours the level of cell proliferation was similar for the unprocessed, laser processed and randomly polished surfaces, while cells growing on the directional polished surface displayed the least proliferation. Following 48 hours, cell growth was greatest on the randomly polished surface, followed by the laser processed surface, unprocessed surface and the directionally polished surface respectively. This trend was the same after 72 hours, however the differences were more pronounced (figure 29). There was no significant difference seen between the values ($p>0.05$)

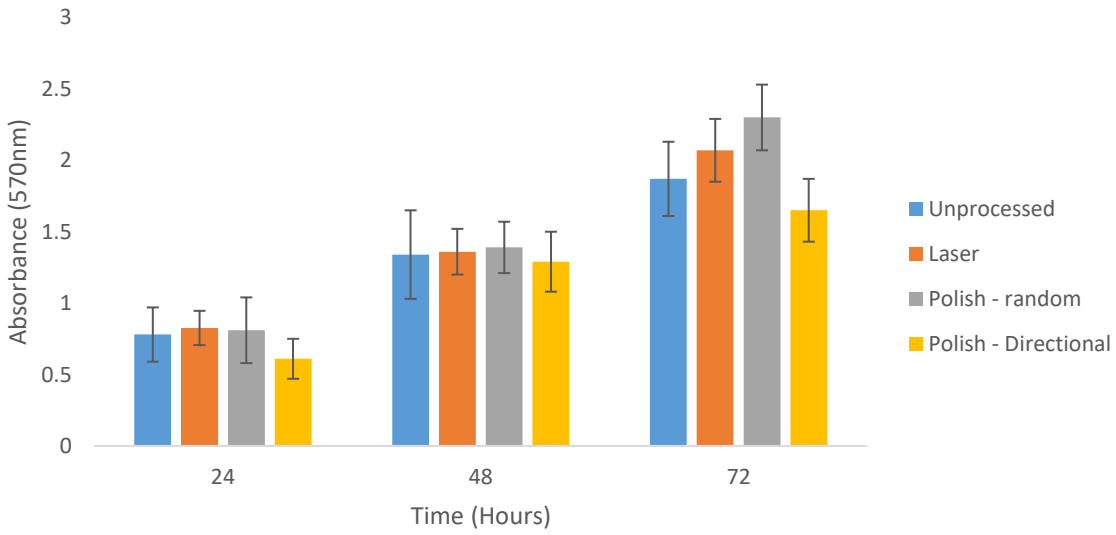

Figure 35 Proliferation MTT assay results showing mean absorbance versus time (hours) for different processed surfaces 9 (n=9). Error bars represent standard error of the mean.

These results mimic the cell adhesion results, in that the surfaces that produced the greatest adhesion (random-polish and laser processed) also produced the greatest level of cell proliferation. This would be expected, as one of the first biological responses of a cell to a surface is adhesion. This followed by cell flattening, elongation, migration and proliferation. Therefore, modulating cell adhesion also modulates cell proliferation. It has been reported that micro-roughness can have a negative effect on cell proliferation compared to flatter surfaces [102, 103]. This was not the case here, as the laser processed surface which had characteristic micro-roughness, encouraged a greater level of adhesion and proliferation compared to the directionally processed which had nano-roughness characteristics. It should be noted however that the studies of Kim *et al* [102] and Sader *et al* [103] used a different cell type, namely osteoblast-like cells growing on treated titanium rather than polyurethane as used here, thus highlighting the response of different cells to different surface having different materials properties. The trend presented in figure 35 of increased cell number on the random and laser surfaces was found to be repeatable however; statistical analysis found the difference in the mean absorbance of the cells growing on the unprocessed surface, not to be significant when compared to that of the cells growing on the surfaces produced by laser and abrasive polishing ($p>0.05$). This may be a result of the small sample size; this could be expanded upon to determine if the trend is maintained while also increasing the chance of any differences seen being significant. Dalby *et al* 2002 demonstrated that when seeded on 13nm islands fibroblasts are affected on the gene expression level for processes including cytoskeleton organisation, extracellular matrix production, DNA transcription, and cellular signalling [104].

6.6.3 Investigating the Effect of Surface Patterning on LL24 Cell migration

To compare the effects of the different surfaces on cell migration, fibroblast cells were seeded onto the various surfaces and left for 2 hours. They were then imaged every fifteen minutes over a 4-hour period. This allowed the mean migration distance to be determined for the different populations of cells (n=90 for each surface, with 30 cells tracked from 3 separate experiments). Interestingly, those surfaces which promoted the greatest adhesion and proliferation (i.e. those with the greatest surface roughness) were found to limit the migration distance. Overall, the directionally polished surface produced the greatest mean cell migration distance, followed by the unprocessed surface, randomly polished and laser processed surface respectively (Figure 36). This basic trend was found to be repeatable. However, when compared to the unprocessed surface mean cell migration distance was found not to be statistically significant ($P<0.05$).

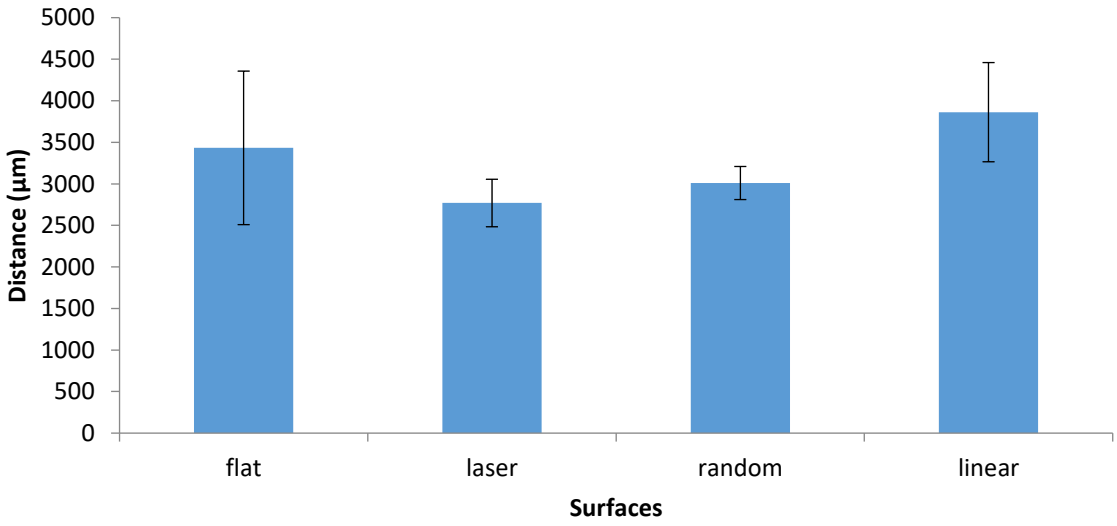

Figure 36 Mean cell migration distance (µm) for LL24 cells (n=90) growing on the different surfaces over a 4-hour period. Error bars represent standard deviation.

These results showed that those surfaces which promoted the greatest adhesion and proliferation (i.e. those with the greatest surface roughness) were found to limit the migration distance. Overall, the directionally polished surface produced the greatest mean cell migration distance, followed by the unprocessed surface, This work agrees with similar work in this area. For example, Hamilton *et al* [105] generated grooves on fused silica via photolithography. These grooves were designed to vary in depth from between 80nm - 9µm and vary in width from 2 - 20µm. It was found that chondrocyte cells did not spread appreciably on any groove size. However, cells were found to show accelerated movement on grooves having a depth of 750nm when compared to flat surfaces [105]. This suggests that surface feature size does indeed have an effect cell migration, specifically that submicron scale features promote the migration rate, whereas micron-sized features inhibit cell migration. Overall the laser processed surface used here, which has the largest feature size, produced the lowest level of cell migration, which would support the work of Hamilton *et al*.

Upon visual inspection of the time-lapse videos, it was observed that those cells growing on the unprocessed (video file 1), directionally polished (video file 2) and randomly polished surfaces (video file 3) migrated in a more random manner. In contrast, those cells growing on the laser produced surface (video file 4) were found mainly to be confined to either the laser processed grooves, or to the unprocessed areas and were observed to mainly migrate either along the groove, or along the unprocessed area. In contrast, relatively few cells were seen to migrate in a direction running perpendicular to the grooves, which may be due to the feature heights being too large for the cells to navigate across. Images of these clips can be seen in appendix 7.

It should also be noted that cells growing on the laser processed surface had a different morphology than those growing on both the flat and directional polymer surfaces; exhibiting

less spread. Similarly, cells growing on the randomly organised polished surface were also observed to move less freely when compared to those cells growing on both the flat and directionally polished polymer surfaces (see video files). Thus it can be concluded that the limitation imposed upon the direction of cell movement here has resulted in a reduced cell migration distance and thus a decrease in cell velocity.

6.7 Expansion of polishing method to produce different sized scratched surfaces for cell modification analysis

6.7.1 Development of scratched surfaces

As mentioned previously, studies have shown that increasing the surface roughness can enhance cell adhesion. Clearly, this is not the case with the directionally polished surface compared to the unprocessed surface. It may be that the size of the surface topographical features was too small and the frequency of the features was too high to be recognised by the cells; which may be reflected by the similar Ra values between the unprocessed surface and the directionally polished surface. To explore this further, directionally polished surfaces were prepared using larger grit sizes than the original super fine 1200B silicon carbide abrasive paper, now ranging between the coarser 120-600 grit sizes. This resulted in significantly larger feature sizes (although still sub-micron) and also larger values for Ra (Table 5). However, these coarser surfaces did not enhance cell adhesion when compared to polishing with the original finest 1200B grit size (cell adhesion was similar). Also, the directional polymer surfaces developed using polishing paper with a greater grit size than 1200, were found to have much greater surface roughness compared to the randomly organised polymer surface. However, they still promoted less cell adhesion than was the case for the random surface.

Table 7 Height values for polished surfaces (µm). Values taken using white light interferometer.

Silicon paper grade for surface polishing	1200	600	500	400	320	120
Sz	3.5024	3.18	6.38	7.07	10.88	10.56
sem	0.23	0.32	0.31	0.52	1.07	0.41
Sa	0.082	0.12	0.28	0.12	0.35	1.25

6.7.2 Investigating the Effect of Surface Polishing Pattern on LL24 Cell Adhesion

In order to determine if these new surfaces had an effect on cell adhesion the MTT assay was performed. Figure 37 shows that the patterned surfaces have a higher level of cell retention when compared to the unprocessed polymer. However, this was not found to be statistically significant, ($p>0.05$). Within the different polished surfaces, a drop in the level of cell retention was seen at the 400 graded samples. There is no obvious explanation for this to happen, the 400 surface has values that are similar to the other surfaces so the drop in cell retention is unexpected. These experiments were repeated three times and each time this basic trend was observed.

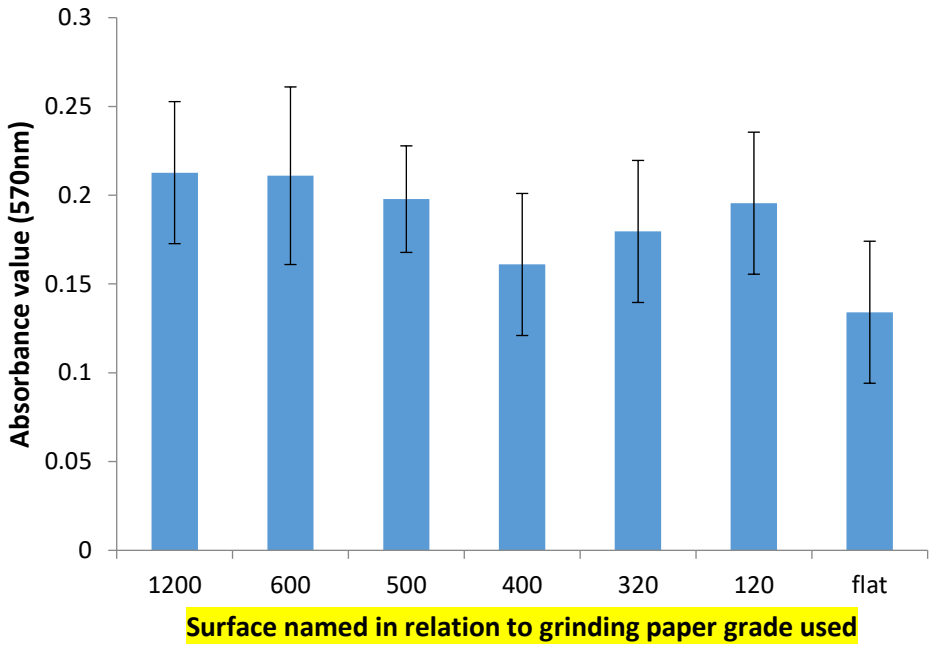

Figure 37 MTT assay results for cell adhesion showing absorbance for cells attached to the different surfaces 9 (n=9). Error bars represent standard error of the mean.

Research has shown that when well fibroblast cells attach to surface they spread out across it; this is typically seen on flat surfaces as opposed to those with developed features [98]. Fibroblast cells on decreasing groove size have been shown to be effected less as the groove size decreases for adhesion, orientation and migration [106], this potentially maybe due to the ability for cells to attachment within smaller grooves [107] on the order of 1-10 micron level. Research done by Walboomers *et al* 2000 has shown that when seeded on to grooved surfaces 1-10um wide a lower initial attachment was observed but 4h after seeding, cell numbers on the grooves increases when compared to smooth un-patterned polymer. Their reasoning behind this was an initial hampering of the formation of organized cell substrate contact junctions on textured surfaces which can result in reduced attachment percentages [108]. What has also been observed is that as surface roughness increased a corresponding increase was seen in cell attachment [109], this would support the results seen here that the

rough scratched surfaces showed increased cell adhesion compared to the un-patterned polymer.

6.7.3 Investigating the Effect of Surface Polishing Pattern on LL24 Cell proliferation

In order to determine whether the surfaces have any effect on cell proliferation MTT assays were performed after 24h, 48h and 72hs. As can be seen from figure 38 when comparing the surfaces at each of the time points there is no significant difference between them ($p>0.05$). When looking at each individual surface across the three time points it was determined that between 24 and 48h there was no significant difference seen for any surface ($p>0.05$). Some difference was seen between the 24 and 72h time points, the 1200, 600, 320, 120 and non-patterned surfaces all showed a significant difference between those time points ($p>0.05$). Between 48 and 72 only the 120 surface showed a significant difference ($p<0.05$).

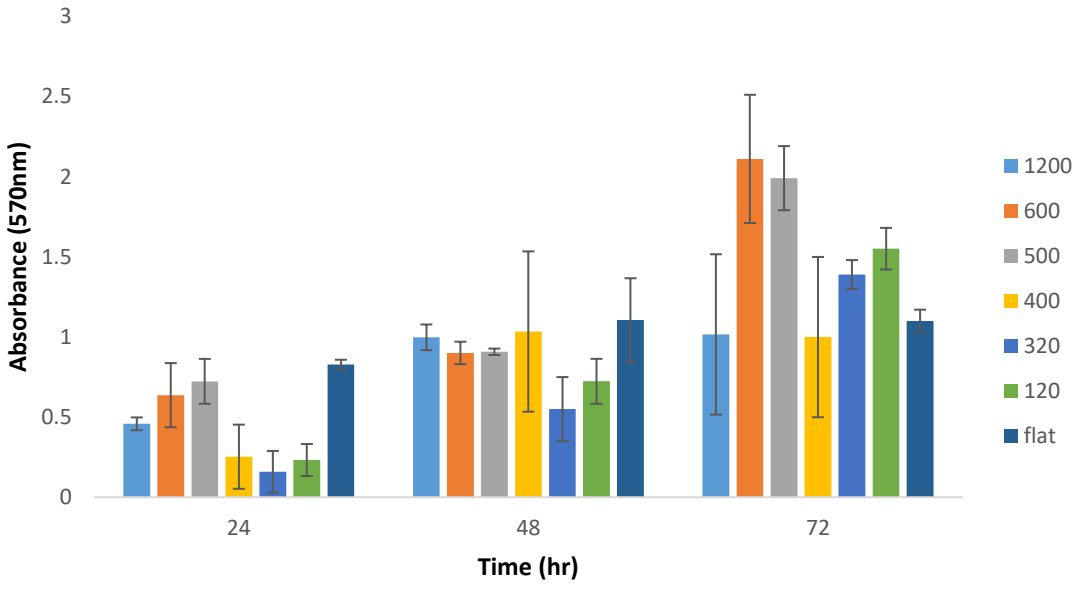

Figure 38 MTT proliferation assay results showing mean absorbance versus time (hours) (n=9). Error bars represent standard error of the mean.

The proliferative tests showed no significant differences between the surfaces at any of the time points or any difference between the surfaces across the three time points. The reason no significant difference was seen between the surfaces may be a result of the size of the scratches, research has shown that larger grooves promote cell proliferation over small or no features [27, 110] [94, 111]. This suggests that it is the submicron size of the scratches that is limiting the proliferative effect of the surfaces, had the scratches been larger there may have been a difference seen. What has also been shown is that increasing the surface area does not link to increase in cell number [107], this also suggests a reason for the lack of difference seen.

6.7.4 Investigating the Effect of Surface Polishing Pattern on LL24 Cell Migration

Figure 39 shows the tracking data for the difference polished surfaces. It shows that there was a trend for a decrease in cell migration from the smallest sized surface features (1200) to the largest (120), this difference was shown to be significant ($p<0.05$). When comparing whether the surfaces made any significant difference to cell migration it was determined that the 1200, 600 and 500 surface show no significant difference with any other surface ($p>0.05$). The 400 surface is seen to be significantly different to the 600, 500, 320 and 120 ($p<0.05$) with a larger migration distance shown, but is not different to 1200 or the flat surfaces ($p>0.05$) of which it shows similar values. The 320 and 120 surfaces showed the lowest cell migration and these results were significantly different to the other surfaces.

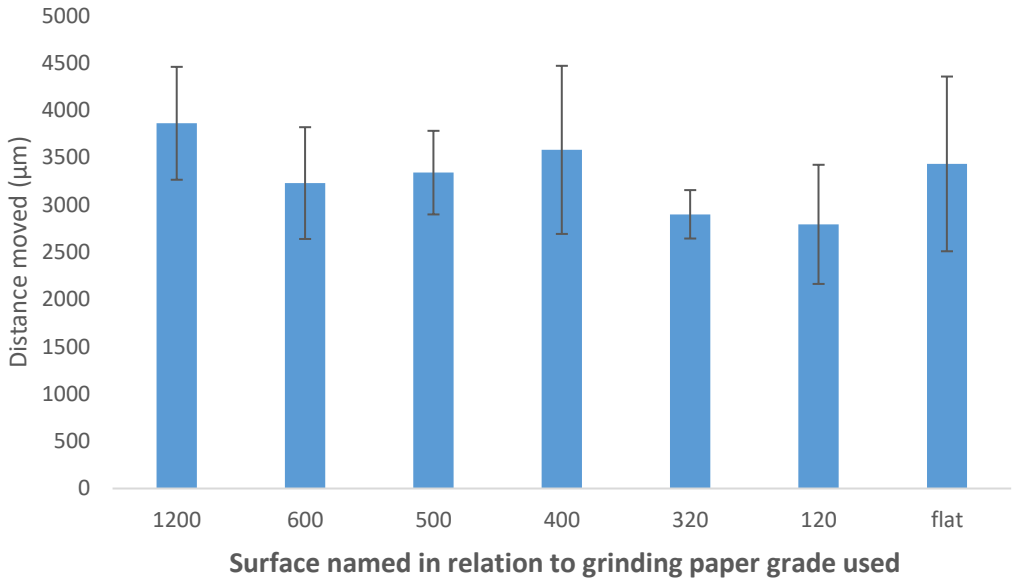

Figure 39 Mean cell migration distance (µm) for LL24 cells (n=90) growing on the different surfaces over a 4-hour period. Error bars represent standard deviation.

The results for the migration tests showed a trend for a decrease in the distance travelled by cell as the feature size increased. There was also a decrease in cell migration for the 320 and 120 surfaces when compared to the flat surface. This trend between decreases in migration with increased feature size has been demonstrated before Lercec *et al* 2013, they suggest that the reason for such a result is due to a reduction in physical confinement when cells can sit between grooves on the ridges, this then promotes migration. When cells are forced in closer neighbouring interaction cell-cell contacts are more likely to form, this inhibits migration [112]. Conversely independent research has shown that fibroblast migration increases on microgrooves [113] and that cells can be directed via grooves [106], more strongly if exposed to grooves of smaller width or greater depth. When investigating the reasoning behind migration and grooves Lee *et al* investigated the changes in gene regulation, there research showed that p27 was up regulated; they suggest that p27 is involved in the regulation of cell migration [110].

6.8 Results of BAE-1 Cell Responses to patterned Polyurethane and Non-patterned Polyurethane

6.8.1 Investigating the Effect of Surface Patterning on BAE-1 cell adhesion

Following work investigating the effect of the different patterned surfaces on fibroblast behaviour it was decided that the experiments would be repeated using a different cell line which originates from a different tissue namely BAE-1 cells.

To investigate the effect of the different patterned surfaces compared to the non-patterned on BAE-1 cell adhesion an MTT assay was carried out 6 hours post seeding. This investigation shows that cells attached with a much greater efficiency on the laser and random surfaces compared to the laser and non-patterned surfaces (figure 40). The laser surface had an adsorption value of 0.25, this was a greater value when compared to the random surface which had an adsorption value of 0.15. The MTT assay will produce a value that will correspond with the cell number on the surface being tested, a larger cell number will produce a larger adsorption value. Both these surfaces show a much greater value when compared to the linear and non-patterned which had adsorption values of 0.055 and 0.058 respectively. There was no statistical difference between the absorbance values ($p>0.05$)

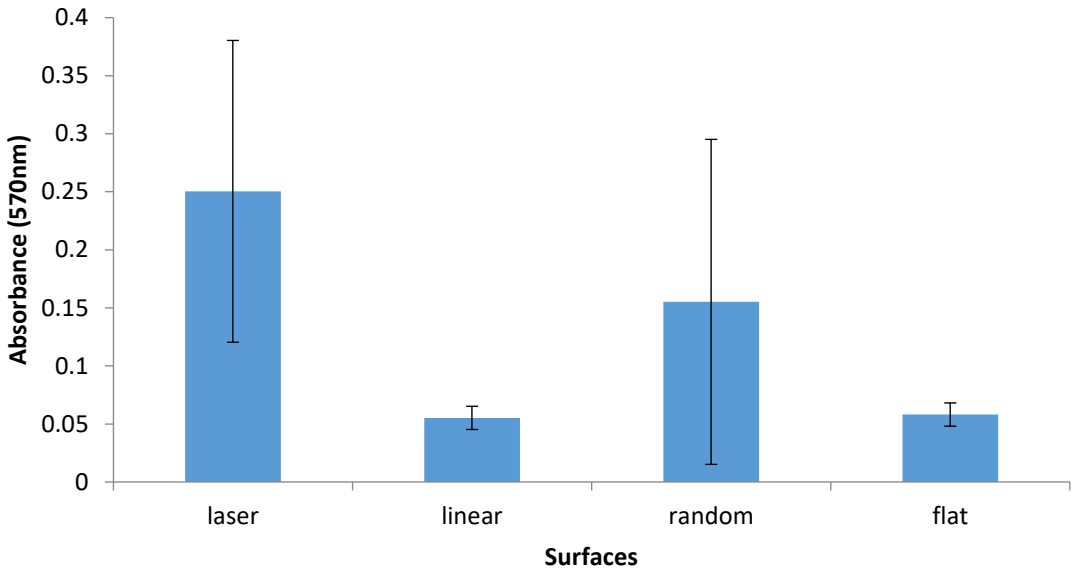

Figure 40 MTT assay results for BAE-1 cell adhesion showing absorbance for cells attached to the different surfaces (n=9). Error bars represent standard error of the mean.

When compared to the LL24 results on the same surface there is an obvious decrease in cell number for the BAE-1 testing. Though the trend is similar with higher adsorption value for the laser and random surface over the linear and non-patterned the values are all much smaller suggesting that though the cells showed improved adherence to those same surfaces the BAE-1 as a whole do not adhere well to them.

The BAE-1 adhesion results for the different scratched surfaces show that there was no significant difference between cell retention on any of the surfaces (figure 41). There was a trend for a decrease in cell number when comparing the scratched surfaces with the non-patterned one this however was not significant. When compared to the LL24 adhesion results the apparent drop in cell retention on the non-patterned surface was similar, however there was no other similarity seen.

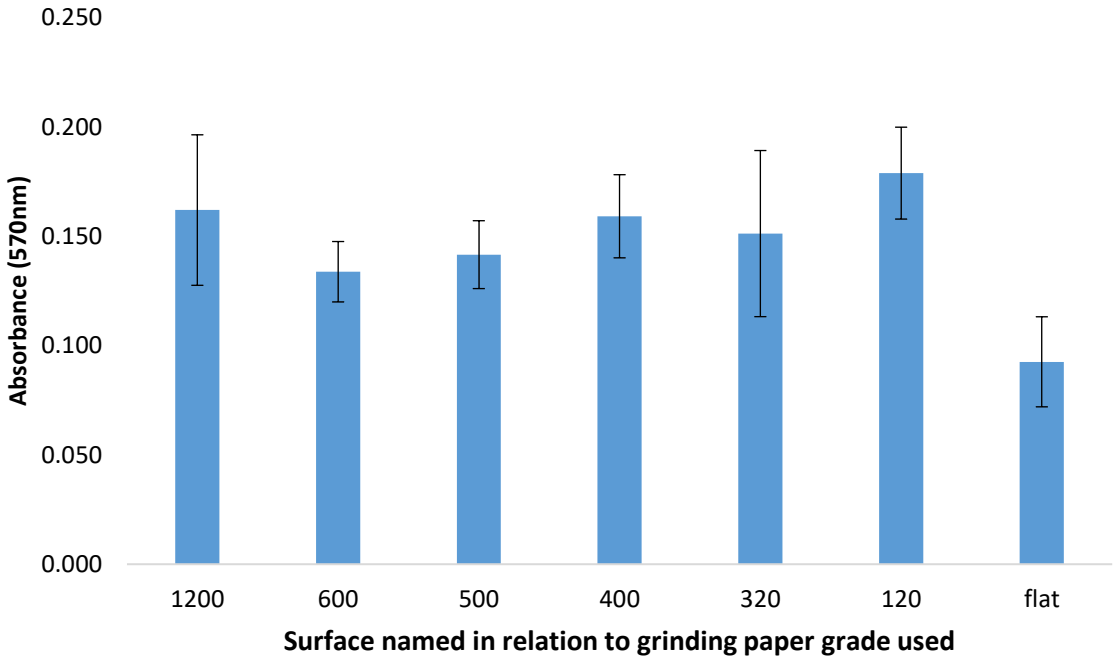

Figure 41 MTT assay results for BAE-1 cell adhesion showing absorbance for cells attached to the different polished surfaces (n=9). Error bars represent standard error of the mean.

Cell adhesion is the first response to a surface, to test the adhesive effect of the different patterned surfaces MTT assays were performed 6h post-cell seeding. This investigation demonstrated that when seeded on to the laser and random scratched surfaces the cells showed greater adherence then when compared to the linear and non-patterned surface as seen in figure 35. These results suggest a potential use in surface implants for inhibiting endothelial cell adhesion, Re *et al* demonstrated that endothelial cell survival is linked to cell adhesion. When examining human umbilical vein endothelial cells (HUVECs) it was found that when seeded on surfaces coated with low concentrations of fibronectin or vitronectin the cells were unable to attach and underwent apoptosis, this was in contrast to when seeded onto surface coated in high concentrations of fibronectin and vitronectin were cells flattened and retained viability [114].

When comparing the number of cells that adhered to the different scratched surfaces a similar result is seen when comparing the non-patterned surfaces in both experiments. They both resulted in low absorbance values and therefore low cell number. The linear surface or 1200 in this case showed a significant increase in absorbance value of 0.16, nearly a 3-fold increase on the previous result. The other surfaces showed similar absorbance results suggesting that there was no obvious effect of the differences in feature height or surface roughness on the cells ability to adhere to it.

6.8.2 Investigating the Effect of Surface Patterning on BAE-1 Proliferation

In order to compare the effects of the different surfaces upon cell proliferation an MTT test was performed after 24, 48 and 72 hours. Figure 42 shows that after 24, 48 and 72 hours, cells were found to proliferate steadily on all surfaces. After 24 hours there was no significant difference between cell numbers on the different surfaces as shown by the similarity in adsorption values ($p<0.05$). Following 48 hours, this similarity in cell number had continued with increased cell growth on all surfaces but no significant difference between them ($p<0.05$). This trend was the same after 72 hours, with no significant different seen between the different surfaces ($p<0.05$) however a difference can be seen in figure 35 between the polished surface and the others, there is a drop in adsorption value which would indicate a decrease in cell number when compared to the other surfaces. When compared to the LL24 results there is no similarity in trend, the only favourable comparison would be when looking at the polished surface which showed the lowest cell number when compared to the other surfaces with both cell lines.

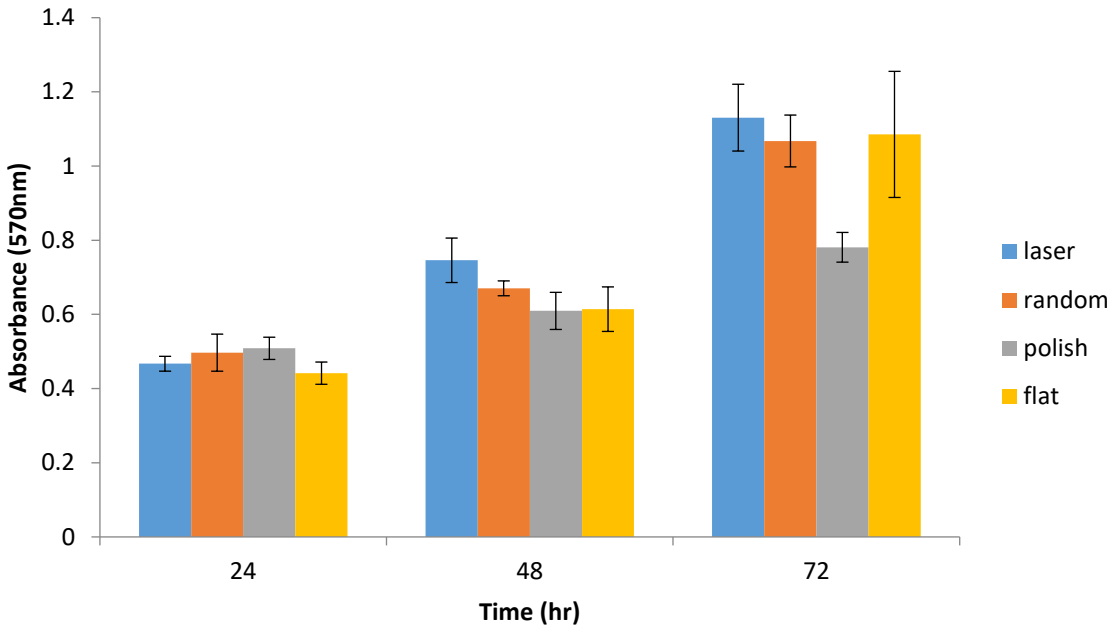

Figure 42 MTT BAE-1 cell proliferation assay results showing mean absorbance versus time (hours) (n=9). Error bars represent standard error of the mean.

This test was repeated using the different polished surfaces 1200, 600, 500, 400 320 and 120. Figure 43 shows that at 24 hours there was some differences seen in cell number, the 1200 surface showed the lowest cell number and was significantly different with the 320 and non-patterned surface ($p>0.05$). The 400, 320 and non-patterned surfaces showed the highest cell number though when statistically analysed only the 400 surface showed a significant difference compared to the other surfaces showing a difference with the 500, 320, 120 and flat surfaces. At 48 hours the non-patterned surface showed the highest cell number, while the 400 surface the lowest though there was no significant difference seen between any of the surfaces suggesting similar cell numbers. At 72 hours the trend for increased cell number on the non-patterned surface continues as well as the 400 surface showing the lowest cell number. The only significant differences seen was between the adsorption values of the 400 surface and the flat surface ($p>0.05$).

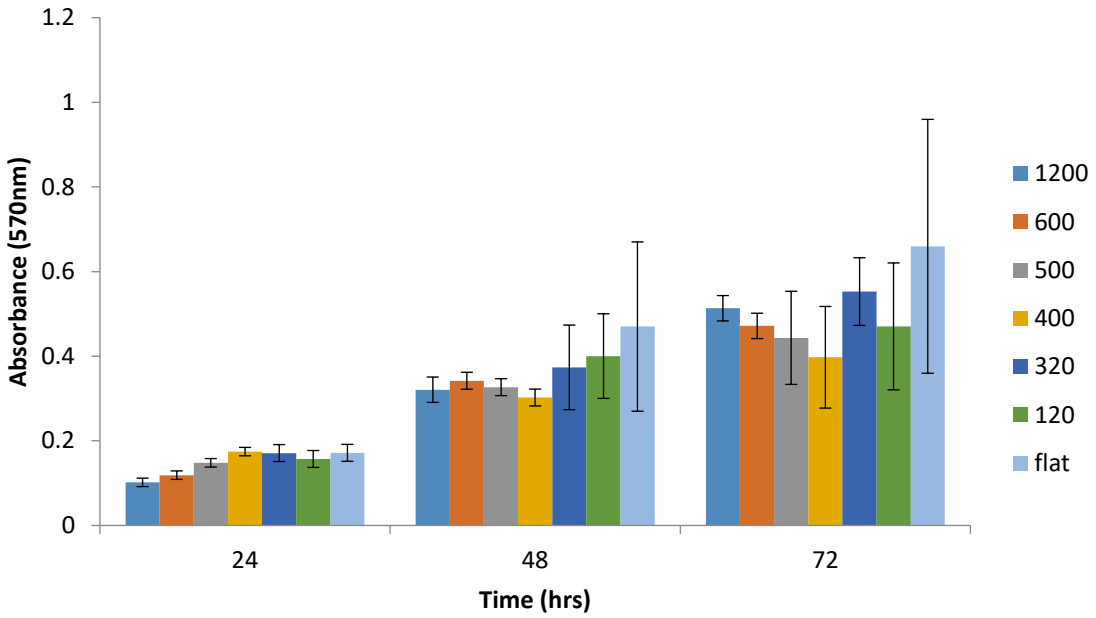

Figure 43 MTT BAE-1 cell proliferation assay results showing mean absorbance versus time (hours) (n=9). Error bars represent standard error of the mean.

When comparing the BAE-1 and LL24 scratched proliferation results there is no similarity between results, the LL24 cells showed an increased cell number on the 600 and 500 surface whereas the BAE-1 show an increased cell number on the flat surface. This suggests a difference in preference for the cells, with the fibroblast cells preferring the scratched rougher surfaces while the endothelial cells the non-patterned non rough surface.

Testing endothelial cell proliferation can be linked to implant integration, an essential step in stent implantation is the re-endothelisation of the implant following its placement. It is sustained through the wound healing process were cells proliferate and migrate to close the wound [115]. This research demonstrated that when seeded on to the different patterned surfaces (laser, linear and random) all surfaces showed cell number increase across the three time points (24, 48 and 72h) as seen on figure 36. The laser, random and non-patterned surfaces all showed similar levels of proliferation, it is only the linear surface that shows any obvious difference, at the 72h time point it shows a considerable drop in cell number when

compared to the other surfaces. When this experiment was repeated using the different scratched surfaces 24 hours after seeding with the 400 and 320 surfaces showed the greatest cell number, the surfaces with the lowest cell number were the 1200 and 600 surfaces those with the smallest feature height. After 48 and 72 hours this has changed with the non-patterned surface showing the greatest cell number with the 400 surface dropping down to the lowest sell number. There seems to be a link between cell adhesion and cell proliferation, both tests have shown the polished surface to negatively impact endothelial cell survival. The results suggest that the laser and random surface promote cell survival, the non-patterned surface is the only surface not to follow that trend with low adhesive qualities and yet a higher level of cell proliferation.

6.8.3 Investigating the Effect of Surface Patterning on BAE-1 Cell Migration

To compare the effects of the different surfaces on cell migration, BAE-1 cells were seeded onto the various surfaces and left overnight. They were then imaged every fifteen minutes over a 4-hour period. This allowed the mean migration distance to be determined for the different populations of cells (n=30 for each surface bar the random which was 25). Figure 44 shows the tracking data for the difference polished surfaces. It shows that the non-patented surface promoted cell migration to a much greater extent than the other surfaces, with a total accumulated distance covered of 3386µm. The laser, polished and random surfaces had similar values of 1932, 2059 and 2078µm respectively all of which were much less than the non-patterned surface.

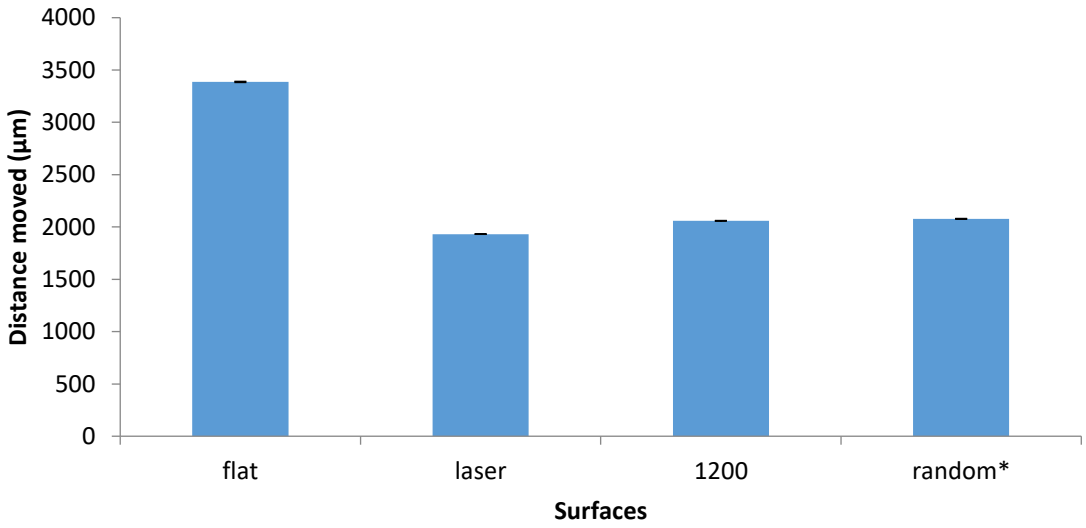

Figure 44 Mean cell migration distance (µm) for BAE-1 cells (n=30, 25 for random surface) growing on the different surfaces over a 4-hour period. Error bars represent standard deviation.

When comparing the migration values to the LL24 results there is a clear difference, the LL24 cells showed a greater distance covered on the polished and non-patterned surface. This showed a converse relationship between migration and adhesion for the fibroblast cells which had reduced cell adhesion on those surfaces. The BAE-1 cells showed increased migration on the non-patterned surface, but as the cells showed reduced adhesion on the linear surface as well and this is not represented in the migration results the same relationship between adhesion and migration is not seen.

As can be seen from figure 45, for the different scratched surfaces the surface that promoted the greatest cell migration was the 500 surface, followed by the flat surface. The 600 surface showed the next highest migration distance, while the surfaces prepared using the 1200, 400, 320 and 120 showed a similar level of cell migration.

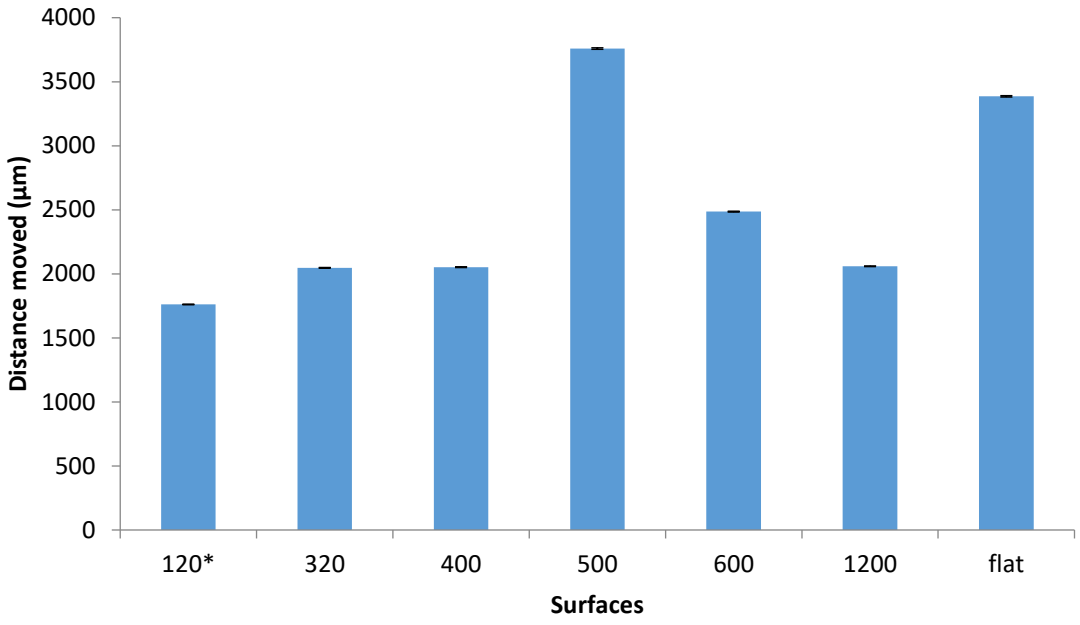

Figure 45 Mean cell migration distance (µm) for BAE-1 cells (n=30) growing on the different surfaces over a 4-hour period. Error bars represent standard deviation.* 120 value was taken from n=23 samples.

Live cell tracking was performed to investigate the effect the different surface has on cell migration. After following 90 cells over 4 hours there was a measurable difference between the un-patterned surface and the other surfaces. When the cumulative distance was determined the laser, polished and random surfaces had similar distance values of 1932, 2059 and 2078µm respectively. There was a great difference between those surfaces and the non-patterned surface, which had a cumulative distance, covered value of 3386µm, this is approximately 1000µm further than the other surfaces. There is no clear link between the three experiments, though the adhesive and proliferative surfaces showed some similarity this does not carry forward to the migration results.

When the live cell tracking was repeated using the different scratched surface it was determined that it was the 500 surface that prompted migration to the greatest extent with a value of 3759µm. The remaining surfaces showed a much reduced level of cell migration,

the 600 surface had a distance covered value of 2486µm, the remaining surfaces had similar values, of approximately 2000µm. The 120 surface showed the lowest cell migration distance with only approximately 1700µm covered.

6.9 Investigating Machine Grinding as a patterning method for modifying cell behaviour

6.9.1 Surface patterning using Machine Grinding

A third technique, machine grinding was used as a comparative method for producing micro grooves. This method is similar to surface polishing in that it is a low-tech method that can be carried out without the need for expensive equipment and does not involve multiple stages/complicated processes.

Surface patterns were created on the stainless steel moulds via a single pass across the samples by the dressed wheel at the different wheel depths to generate a 'ploughed field' feature effect as is seen in Figure 46. The different surface patterns were designated M1, M2, M3 and M4 for the 2, 4, 6 and 10µm wheel dressing depth respectively. The profiles show a pattern of peaks and troughs across the surface that varies in height. The width of the features also varies which results in channels that run along the surface that are not identical across each surface or across the different surfaces as can be seen in Figure 50. The stainless steel moulds were then used to produce a polymer cast which were designated P1, P2, P3 and P4, being identifiable with respect to their corresponding metal counterparts.

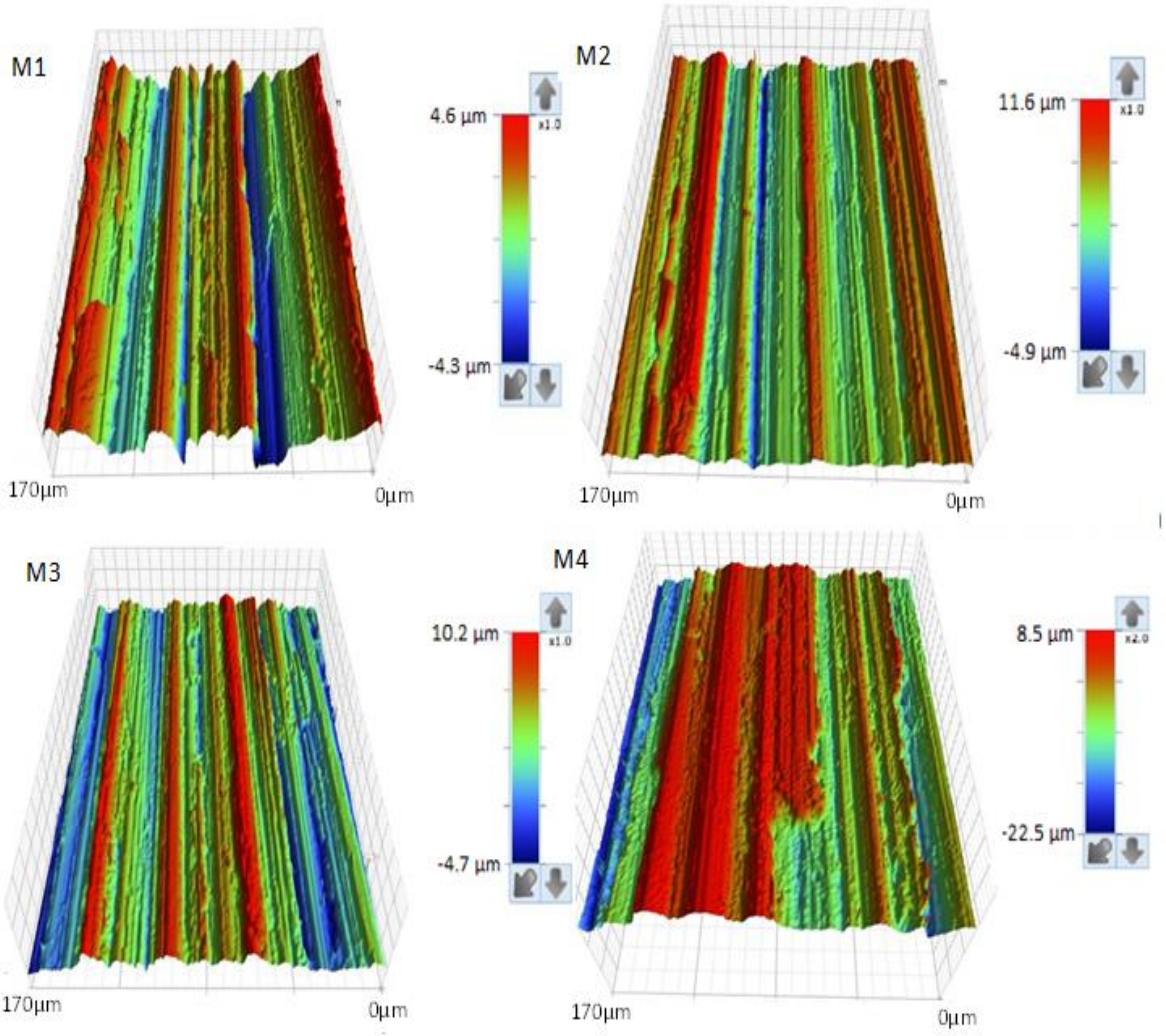

Figure 46 White light interferometer microscope images. All images were taken at ×25 magnification. Colour bar represents size gradient.

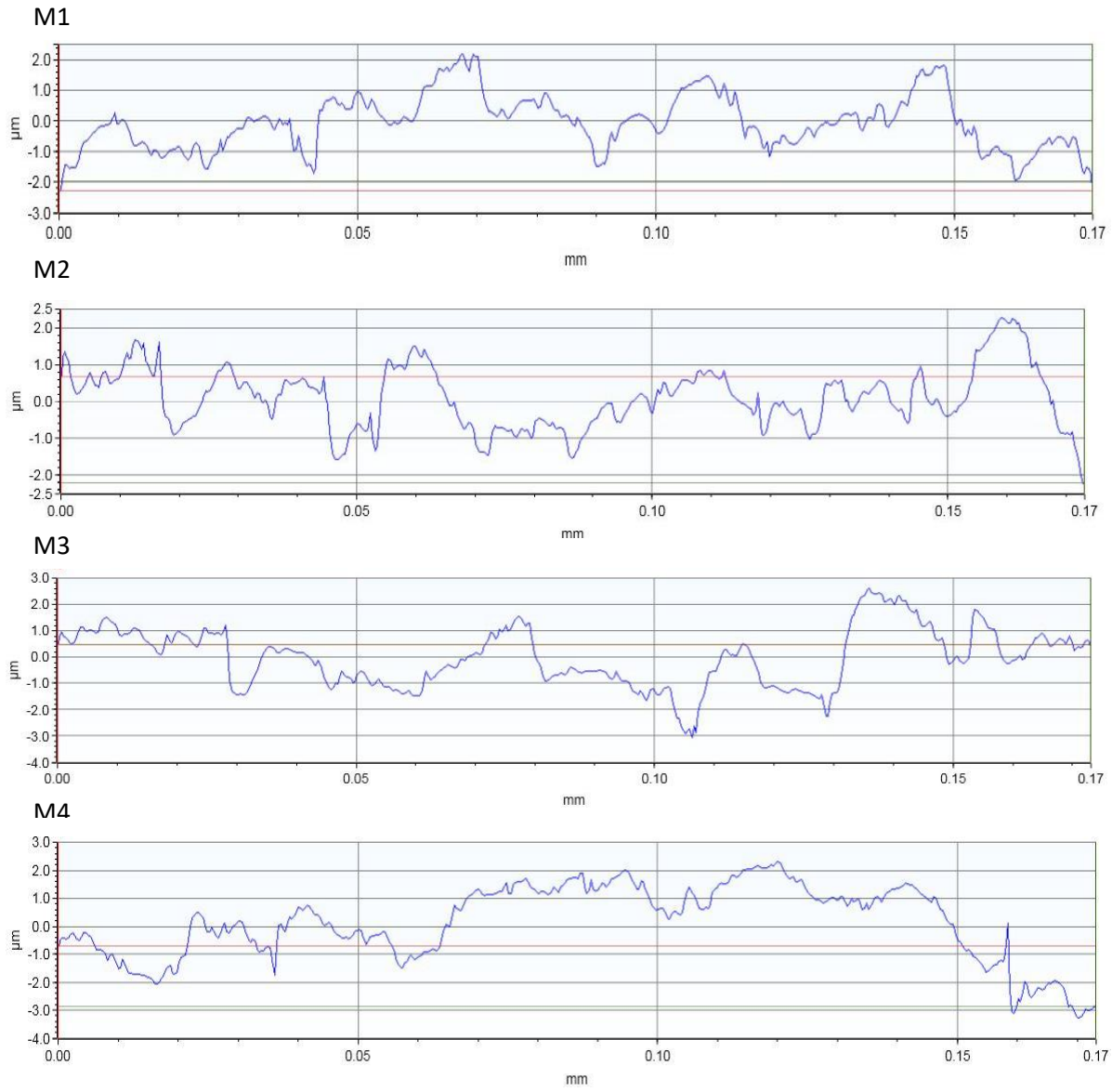

Figure 47 White light interferometer microscope surface profiles. All images were taken at ×25 magnification.

6.9.2 Surface Characterisation of Ground Surfaces

To compare the different ground surfaces to each other and their 'inverse' polymer cast, the surfaces were imaged using a white light interferometer microscope. This allowed for surface height measurements to be obtained. As can be seen from Figure 48, there is an increase in the maximum height of surface features (Sz) as the dressing depth increases. When comparing this result to the polymer are some clear discrepancys, the Sz values for the polymer surfaces are all much higher then the corresponding mould. Also while the overall trend is for the feature height to increase from P1 to P4 there is a significant drop for P2 and P3 which show a similar Sz value.

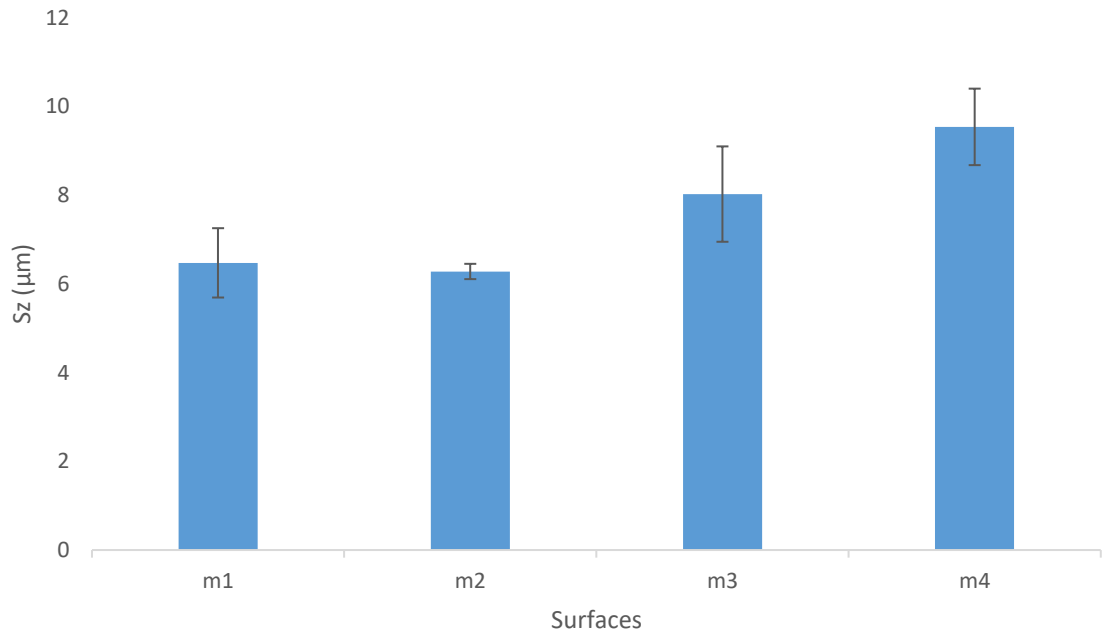

Figure 48 Sz values of ground metal samples. Measurements achieved via surface profiles taken by white light interferometer 50× magnification. Error bars represent standard error of the mean.

Further analysis was performed on the surfaces using a white light interference microscope in order to determine mean surface roughness (Sa) (Table 6). The average Sa values for the ground metal surfaces were found to be 0.766, 0.744, 0.876 and 1.361 respectively. The average Sz values for the metal casts were 6.473, 6.279, 8.024, and 9.538 for the same respective surfaces. Table 6 shows that there is a correlation between the increase in Sz and an increase in Sa. There is a small drop in the values between surfaces M1 and M2, were the wheel depth was 2 and 4µm respectively, but as the feature height increased to 6 and 10µm the values for Sa also increased, resulting in a positive trend between surface height and the analysis values.

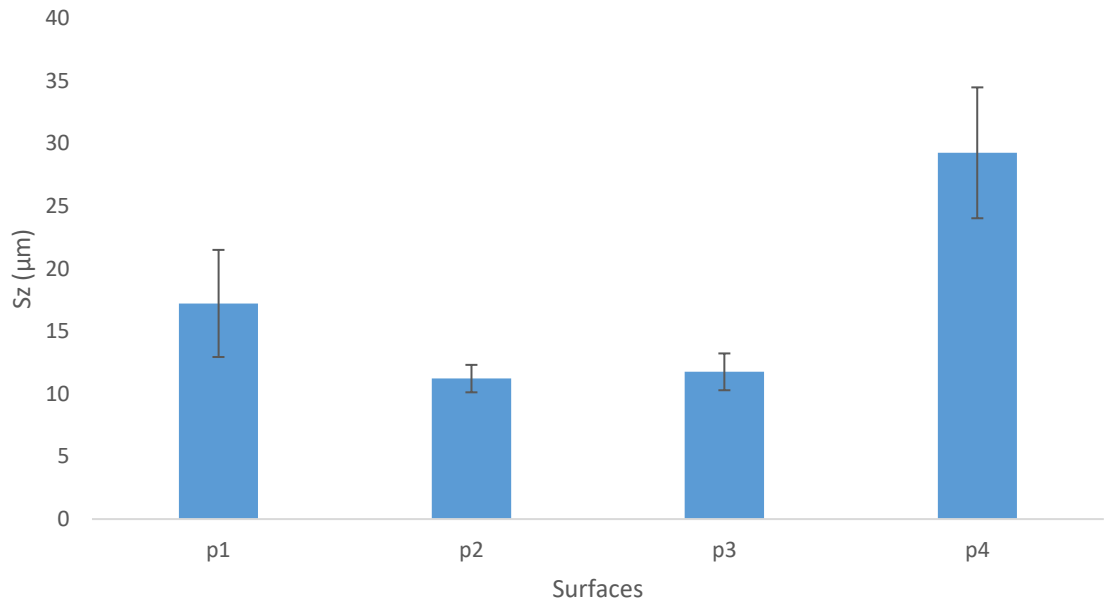

Figure 49 Sz values of inverse polymer casts of metal moulds. Measurements taken via white light interferometer. Error bars represent standard error of the mean.

Surface analysis was also performed on the inverse polymer casts and the Ra, Rt and Rz values can been seen in Table 6. It can be seen that, in a similar fashion to the stainless steel moulds, the values show a trend to increase from the lowest feature height value to the

largest. However Table 6 also shows that for casts P2 and P3 the mean feature height values are lower compared to P1, but still show an increase in mean height through to P4. This is not seen for the metal moulds (Figs 48 and 49) suggesting that this discrepancy may be as a result of the casting processes, where possibly the liquid polymer is not filling the mould accurately, hence resulting in this difference in values.

Table 8 Mean height, Sa and Sz measurements for metal moulds and polymer casts taken via white light interferometer. For all values N=5. All values are in µm.

		Surface analysis		sem	
Surface	Depth of cut	Sz	Sa	Sz	Sa
m1	2 µm	6.473	0.766	0.781	0.071
m2	4 µm	6.279	0.744	0.172	0.043
m3	6 µm	8.024	0.876	1.074	0.053
m4	10 µm	9.538	1.361	0.862	0.163
p1	2 µm	17.226	0.841	4.277	0.051
p2	4 µm	11.222	0.819	1.096	0.094
p3	6 µm	11.762	0.783	1.469	0.067
p4	10 µm	29.259	1.314	5.226	0.104

6.9.3 Investigating the effect of Machine Ground patterns on LL24 Cell Adhesion

In order to determine how the different machine ground surfaces affected cell adhesion a MTT adhesion assay was performed two hours after the cells were seeded on to the surfaces. Figure 50 shows that there is a clear difference between the adhesion of the cells to the flat unprocessed polymer compared to the ground surfaces. The results show that on the unprocessed polymer, less cells had adhered to the surface after two hours compared to all of the processed surfaces. There is also an observable difference between the different machine ground surfaces where we see an increase in cell adhesion as depth of cut increases up until surface P3 (Figure 50).

.

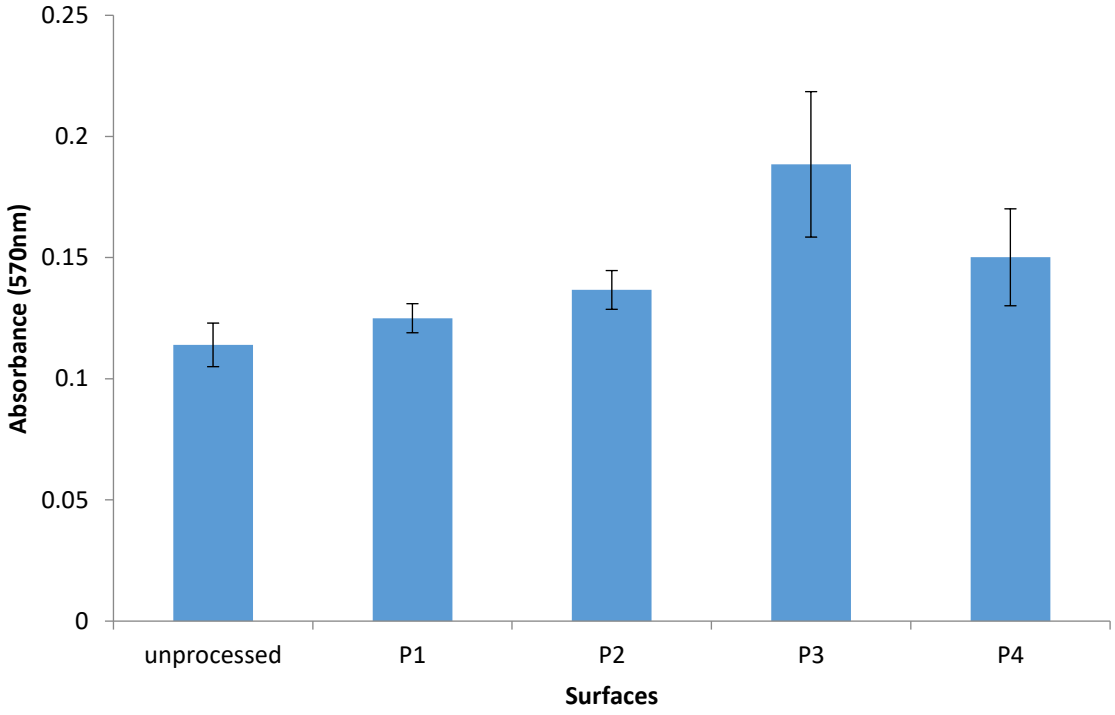

Figure 50 MTT LL24 cell adhesion assay, results showing mean absorbance versus time (hours) (n=9). Error bars represent standard error of the mean.

When analysing the effects of surface topography on cell adhesion, there is a clear difference between the un-patterned surface and the machine ground surfaces. The effect of surface topography on cell adhesion is linked to an effect known as 'contact guidance', were cells are able to sense their immediate environment and react to it [98]. This is seen with the ground polymer surfaces which show an increased level of adhesion when compared to the unprocessed polymer, hence suggesting a link between the surface features and the cells ability to adhere to the surface. The P3 surface shows a higher level of cell adhesion than the other ground surfaces, and this may be linked to the surface analysis results in which P3 has low values for Ra, Rt and Rz. This finding links to other work which shows that increases in surface roughness can have a negative impact on fibroblast cell adhesion and may potentially

prevent initial adaption of the cells to surface [116]. This effect is possibly linked to the number of focal adhesion contacts being formed between the cell and the surface as Grossner-Schreiber *et al*. had previously shown that there were an increased number of focal adhesion contacts on surfaces with a lower Ra value. However, this is not seen for the unprocessed polymer, which shows a lower [117] level of adhesion and also shows much lower surface analysis values. These results suggest that cells are able to attach to the machine ground surface much more quickly than is the case for the unprocessed polymer surface, as the MTT test was performed after a duration of only 2h. If this attachment time was increased, a similar attachment level may be seen. The effect of surface topography on cell behaviour has been shown previously, with cell alignment shown when cells are seeded onto grooved surfaces [112, 118] as well as when being seeded onto highly ordered nanopits that effect cytoskeleton organisation [68]. Fibroblasts, in particular, have been shown to adhere with more affinity, when exhibiting a well-spread, flattened morphology (i.e. on a flat surface) [119]. Results have also been shown were surface topography has a negative impact on fibroblast cell adhesion [16, 108].

6.9.4. Investigating the effect of Machine Ground patterns on LL24 Cell Proliferation

In order to compare the effects of the various different surfaces upon cell proliferation an MTT test was performed after 24, 48 and 72 hours. Figure 51 shows that after 24, 48 and 72 hours cells were found to proliferate steadily on the unprocessed surface, as indicated by the increase of the absorbance values. This trend was also observed with surface P4, although the cell proliferation rate was much lower compared to the unprocessed sample. In contrast, cells did not seem to proliferate on surfaces P1 and P2, as cell number remained relatively steady over time on these surfaces, while surface P3 was only found to promote proliferation

after 72 hours. These results indicate that the manipulation of surface features, their size and distribution, generated through machine grinding, can be used to control the proliferation rate of fibroblast cells.

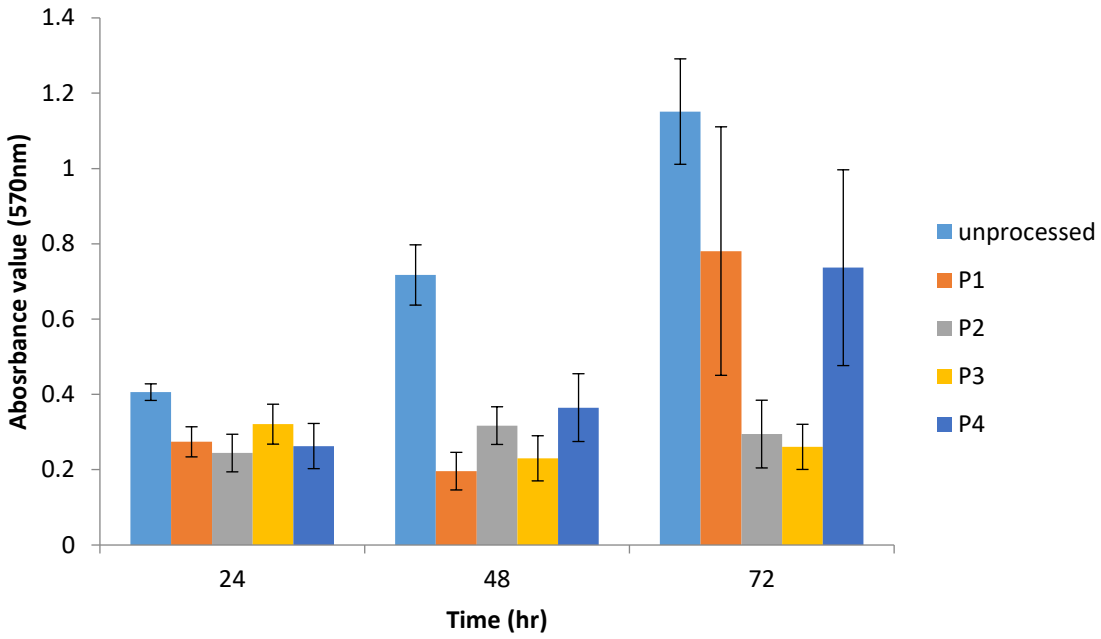

Figure 51 MTT LL24 cell proliferation assay, results showing mean absorbance versus time (hours) (n=9). Error bars represent standard error of the mean.

When analysing the effects of surface topography on cell proliferation, there is also a difference between the responses of cells grown on the unprocessed polymers, compared with those grown on the machine ground surfaces. The unprocessed polymer promotes cell growth to a greater extent when compared to the other surfaces at the 24- and 48-h time points. These results support previous research that shows that increased surface roughness impaired fibroblast cell growth [109]. They can also be linked to previous research showing similarities in that fibroblast cells that were seeded onto patterned surfaces resulted in the down regulation of transcription factors and genes involved with proliferation, while also being linked to a decrease in cell spreading [101]. However, there is no significant difference

between the machine ground surfaces when comparing at the same time points. After 72 h, the P1and P2 surfaces show an increased level of cell growth, suggesting that the cells growing on those surfaces have been able to settle and begin spreading on the surface, hence promoting the process of proliferation. When comparing the cell number across the three discrete time duration points, there is no significant difference for surfaces P2 and P3, suggesting limited to no cell proliferation on these surfaces. That the unprocessed polymer and P1 seem to promote cell growth to a greater extent may be due to the smaller size of their features, as previous research has shown that cells prefer smaller features over larger regarding proliferation. Kolind *et al*. showed that fibroblasts exhibit improved proliferation on pits with smaller gap sizes (ones that they could cover easily) when compared to pits with larger gap sizes [93].

6.9.5 Investigating the effect of Machine Ground patterns on LL24 Cell Proliferation

To compare the effect of machine ground surfaces on cell migration, fibroblast cells were seeded onto the surfaces and left to attach for two hours, before being imaged every 15 minutes for four hours. This allowed us to track cell movement over time. The distance moved was determined through the sum total of the distance moved by each cell after four hours. Figure 52 shows that cells on surfaces P2 and P3 moved considerably further when compared to the other surfaces, moving a distance of around 4900 and 4200µm respectively. The unprocessed surface, surface P1 and surface P4 showed similar distances moved after the 4 hour period, but these were all under 3000µm, showing a significant reduction in distance moved compared to P2 and P3.

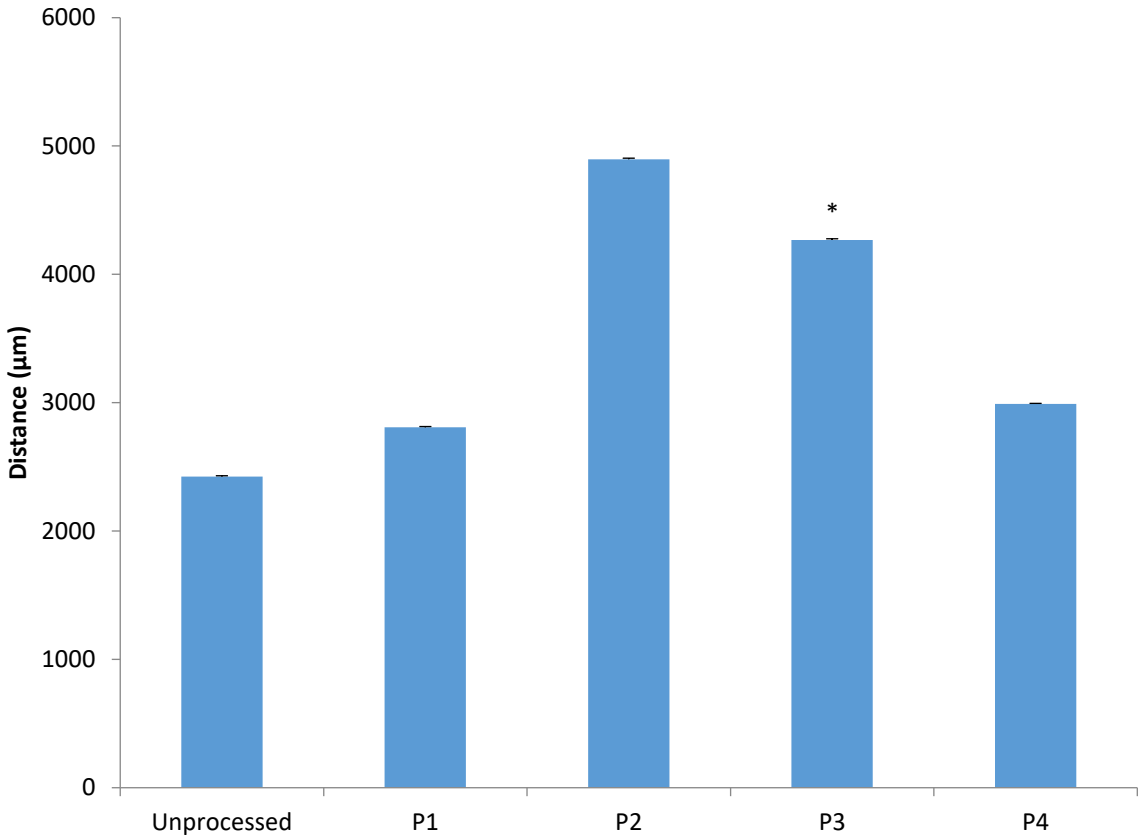

Figure 52 The total distance moved in microns by 30 cells over 4hours (*n=27). Error bars represent standard deviation.

When comparing the ability of the cells to migrate on the surfaces, it was found that all machine ground surfaces enhanced cell migration when compared to the unprocessed surface. These results mirror the adhesion studies, were the surfaces that showed enhanced adhesion also seem to promote greater cell migration across the surface. When comparing these results to the surface analysis values, it could be suggested that the surfaces with lower values for Ra, Rt and Rz and feature height promote cell adhesion and migration. However, this is not seen for surface P4, which despite showing the largest values for the surface analysis shows a more enhanced level of cell migration and adhesion when compared to surface P1. The effect of surface features on cell migration has been seen before; Clark *et al*.

showed that when cells encountered topological steps, as the height of the step increased, there was a significantly decreased crossing frequency, with more cells turning back rather than climbing up the substrate surface feature [60]. The effect of substrate surface features on cell migration can also be seen in the work by Hamilton *et al*., were fibroblast cells were seen to hug groove walls in order to turn their entire body around corners [95].

Chapter 7 - Conclusion

7.1 Optimization and development of the different feature types using three different patterning methods

This present study aimed to compare the features produced from three different processing methods; laser patterning, surface polishing and machine grinding.

- Using laser technology an undulating pattern was generated with a mean peak height of 1.89µm, a mean width of the feature path was approximately 32.2µm, approximate width between the feature paths was approximately 16.5µm (+/-0.88, n=30).
- The polished surfaces were developed through the use of a surface polisher and different grades of polishing paper to produce a range of surfaces. They were named after the paper that was used to generate the features; 1200, 600, 500, 400, 320 and 120.
- A single surface based on the 1200 paper was generated but with features in a random orientation, the lack of uniformity to the features increased it similarity to the ECM. This surface enables a direct comparison between the ordered and non-ordered feature types.
- The machine ground features were to provide a proof of concept on whether the use of machine grinding can provide features that are comparable in size to more established patterning methods
- The surfaces produced were based on the depth of cut used on the grinding wheel before being used to run across the steel.

7.2 Investigating LL24 and BAE-1 responses to laser patterned, polished and machine ground surface features

The main objective of this thesis was to take the surfaces produced using the different patterning methods and compare their ability to modify cell behaviours. These behaviours were adhesion, proliferation and migration and could be tested through the use of MTT assays and live cell tracking.

- When comparing the laser, polished and random surfaces, LL24 cells have enhanced levels of adherence on the laser and random surfaces.
- A link between the three behaviours was established, the surfaces that promoted cell adhesion (laser and random) also promoted cell proliferation while the surfaces that seemed to hinder these behaviours (linear and non-patterned) promoted cell migration.
- These results seem to follow the nature of LL24 cells which typically follow a pathway of adhesion followed by proliferation.

When comparing the different sized scratched surfaces, the results showed that:

- All surfaces promoted cell adhesion when compared to the non-patterned surface.
- The proliferation and migration results show some correlation, this suggests a link between cell proliferation and a lack of cell migration.

The BAE-1 cell results showed different trends:

- Though the surfaces would promote and hinder cell behaviours all surfaces showed a reduction in cell number when compared to the LL24 results.
- This suggests that as a whole the BAE-1 cells do not find the surfaces as preferable as the LL24 cells.

- The adhesion results showed the same trend as the LL24 were preferable adherence was seen on the laser and random surfaces as opposed to the linear and non-patterned.
- The proliferation results showed a link between the polished surface and a reduction in cell survival with a drop in cell proliferation as well as adhesion.
- There was no similar reduction seen for the non-patterned surface which showed similar proliferation levels to the laser and random surfaces. What was found when analysing the migration results was that the non-patterned surfaces promoted BAE-1 migration.

The BAE-1 results for the polished surfaces showed:

- A similar trend to the LL24 with increased adhesion on all the polished surfaces when compared to the non-patterned.
- In contrast to this the proliferation results showed a decrease in cell number on all patterned surfaces compared to the non-patterned.
- The migration results showed no conclusive trend ran through out the BAE-1 results, they showed that the BAE-1 cells showed enhanced migration on the flat compared to most other surfaces.

The grinding results were part for a fit for purpose study on the suitability of using machine grinding to pattern surfaces for modifying cell behaviour.

- The adhesion results showed that the LL24 cells adhered better on the ground surfaces than the non-patterned surfaces.
- The proliferation tests demonstrated that the cells were able to reproduce to a much greater effect on the non-patterned surface than the ground. The proliferation results also showed that the P2 and P3 surfaces drastically reduced cell proliferation, with

results similar between the 48 and 72h time periods. This is interesting as it shows these two surfaces to be the only ones investigated to do so.

- When analysing cell migration, a similar trend was discovered between proliferation and migration were P2 and P3 the surfaces that drastically reduced cell proliferation were the ones to promote cell migration.
- When looking at the results as whole a similar trend for fibroblast cells is seen, the surfaces that promote adhesion also promote migration.
- This is seen with P2 and P3 which show higher levels of adhesion and migration while also exhibiting limited proliferation.
- While the non-patterned surface that shows limited adhesion promotes cell proliferation, this is also seen for P1 and P4.

Chapter 8 - Recommendations for future work

8.1 Investigating cell morphology and formation of structural proteins to support MTT data

The MTT results present a picture on which surfaces the cells respond to favourably by demonstrating which they adhere to and proliferate on with a greater degree. It can be reasoned why they have responded as they do through previous research, regarding cell responses to similar surfaces in feature type, size or surface roughness. However, to understand why the cells behaviour has occurred further analysis is required.

To support the MMT data cell staining can be performed, through the use of fluorescent antibodies to visualize actin, vinculin and the cell membrane. This can be done at specific time points following cell seeding. By staining actin it will provide information on the internal cell structure of the cell while on the different surfaces. This would provide information on whether the cell is aligning along the features of the scratched surface or moulding itself around the undulating features of the laser patterned surface of maintaining random. Actin staining will also provide information on the formation of focal adhesions, where they form will provide information on how the cell interacts with the surface.

Cell membrane staining will support the adhesion MMT data, by staining the cell membrane and using the confocal microscopes ability to perform Z stacking images cell height can be determined. Both the fibroblast cells and endothelial cells spread across the surface when well attached, by investigating the heights of cells on the surface the cell preference for the surface can be inferred.

8.2 Investigating wound healing assays and migration under flow conditions to bolster migration data

The current migration data provides information on the distances travelled by cells after a set time period given for the cells to settle on the surface. The data enables the surfaces that hinder or promote cell migration to be identified, however this provide information that is linked to the cell type. Wound healing assays are were the time taken for cells to re-cover an area of space following reaching confluence can be determined would provide a link to the fibroblasts natural role to cover wounds. These assays can be performed both with and against the features, this would suggest any ability for the surfaces to direct cell migration. Whether the cells cover the area quicker through moving along the features or over them.

Similarly, the endothelial cells migration information was based on static flow conditions, this is unnatural for the cells particularly these aortic based endothelial cells. There is the equipment to set up migration experiments with the flow set to mimic the flow of blood through the aorta. By replicating these conditions, a truer representation of the surfaces effect on endothelial cell migration can be determined and a suggestion for the surfaces suitability to be used in any stent based implant can be made.

Chapter 9 – References

1. Reece, J.B. and N.A. Campbell, *Campbell biology*. 2011, Boston: Benjamin Cummings / Pearson.
2. Yam, J.W., E.Y. Tse, and I.O. Ng, *Role and significance of focal adhesion proteins in hepatocellular carcinoma.* J Gastroenterol Hepatol, 2009. **24**(4): p. 520-30.
3. Recknor, J.B., J.C. Recknor, D.S. Sakaguchi, and S.K. Mallapragadaa, *Oriented astroglial cell growth on micropatterned polystyrene substrates.* Biomaterials, 2004. **25**(14): p. 2753-2767.
4. Turner, A.M.P., N. Dowell, S.W.P. Turner, L. Kam, M. Isaacson, J.N. Turner, H.G. Craighead, and W. Shain, *Attachment of astroglial cells to microfabricated pillar arrays of different geometries.* Journal of Biomedical Materials Research, 2000. **51**(3): p. 430-441.
5. Chen, Y.F., *Nanofabrication by electron beam lithography and its applications: A review.* Microelectronic Engineering, 2015. **135**: p. 57-72.
6. Curtis, A.S.G., N. Gadegaard, M.J. Dalby, M.O. Riehle, C.D.W. Wilkinson, and G. Aitchison, *Cells react to nanoscale order and symmetry in their surroundings.* Ieee Transactions on Nanobioscience, 2004. **3**(1): p. 61-65.
7. Ulerich, J.P., L.C. Lonescu, J.B. Chen, W.O. Soboyejo, and C.B. Arnold, *Modifications of Ti-6Al4V surfaces by direct-write laser machining of linear grooves - art. no. 645819.* Photon Processing in Microelectronics and Photonics VI, 2007. **6458**: p. 45819-45819.

8. Waugh, D.G. and J. Lawrence, *Wettability and osteoblast cell response modulation through UV laser processing of nylon 6,6.* Applied Surface Science, 2011. **257**(21): p. 8798-8812.

9. Vijayakumar, S.C., K. Venkatakrishnan, and B. Tan, *Manipulating mammalian cell by phase transformed titanium surface fabricated through ultra-short pulsed laser synthesis.* Experimental Cell Research, 2016. **340**(2): p. 274-282.

10. Goh, C., T., *Development of Laser Micro-fabricated Surfaces to Accelerate & Enhance Endothelial Cell Adhesion and Proliferation.* 2014.

11. Lincks, J., B.D. Boyan, C.R. Blanchard, C.H. Lohmann, Y. Liu, D.L. Cochran, D.D. Dean, and Z. Schwartz, *Response of MG63 osteoblast-like cells to titanium and titanium alloy is dependent on surface roughness and composition.* Biomaterials, 1998. **19**(23): p. 2219-2232.

12. Le Guehennec, L., A. Soueidan, P. Layrolle, and Y. Amouriq, *Surface treatments of titanium dental implants for rapid osseointegration.* Dental Materials, 2007. **23**(7): p. 844-854.

13. Valencia-Lazcano, A.A., T. Alonso-Rasgado, and A. Bayat, *Characterisation of breast implant surfaces and correlation with fibroblast adhesion.* J Mech Behav Biomed Mater, 2013. **21**: p. 133-148.

14. Reynolds, P.M., R.H. Pedersen, M.O. Riehle, and N. Gadegaard, *A Dual Gradient Assay for the Parametric Analysis of Cell-Surface Interactions.* Small, 2012. **8**(16): p. 2541-2547.

15. Ghibaudo, M., L. Trichet, J. Le Digabel, A. Richert, P. Hersen, and B. Ladoux, *Substrate Topography Induces a Crossover from 2D to 3D Behavior in Fibroblast Migration.* Biophysical Journal, 2009. **97**(1): p. 357-368.

16. Curtis, A.S.G., B. Casey, J.O. Gallagher, D. Pasqui, M.A. Wood, and C.D.W. Wilkinson, *Substratum nanotopography and the adhesion of biological cells. Are symmetry or regularity of nanotopography important?* Biophysical Chemistry, 2001. **94**(3): p. 275-283.

17. WojciakStothard, B., A. Curtis, W. Monaghan, K. Macdonald, and C. Wilkinson, *Guidance and activation of murine macrophages by nanometric scale topography.* Experimental Cell Research, 1996. **223**(2): p. 426-435.

18. Dalby, M.J., M.O. Riehle, H. Johnstone, S. Affrossman, and A.S.G. Curtis, *In vitro reaction of endothelial cells to polymer demixed nanotopography.* Biomaterials, 2002. **23**(14): p. 2945-2954.

19. Biggs, M.J.P., R.G. Richards, N. Gadegaard, C.D.W. Wilkinson, R.O.C. Oreffo, and M.J. Dalby, *The use of nanoscale topography to modulate the dynamics of adhesion formation in primary osteoblasts and ERK/MAPK signalling in STRO-1+enriched skeletal stem cells.* Biomaterials, 2009. **30**(28): p. 5094-5103.

20. Koo, S., R. Muhammad, G.S. Peh, J.S. Mehta, and E.K. Yim, *Micro- and nanotopography with extracellular matrix coating modulate human corneal endothelial cell behavior.* Acta Biomater, 2014. **10**(5): p. 1975-84.

21. Andersson, A.S., P. Olsson, U. Lidberg, and D. Sutherland, *The effects of continuous and discontinuous groove edges on cell shape and alignment.* Experimental Cell Research, 2003. **288**(1): p. 177-188.

22. Li, S.F., B.W. Tuft, L.J. Xu, M.A. Polacco, J.C. Clarke, C.A. Guymon, and M.R. Hansen, *Microtopographical features generated by photopolymerization recruit RhoA/ROCK through TRPV1 to direct cell and neurite growth.* Biomaterials, 2015. **53**: p. 95-106.

23. Alaerts, J.A., V.M. De Cupere, S. Moser, P.V.B. de Aguilar, and P.G. Rouxhet, *Surface characterization of poly(methyl methacrylate) microgrooved for contact guidance of mammalian cells.* Biomaterials, 2001. **22**(12): p. 1635-1642.

24. Karuri, N.W., T.J. Porri, R.M. Albrecht, C.J. Murphy, and P.F. Nealey, *Nano- and microscale holes modulate cell-substrate adhesion, cytoskeletal organization, and -beta1 integrin localization in SV40 human corneal epithelial cells.* IEEE Trans Nanobioscience, 2006. **5**(4): p. 273-80.

25. Wood, M.A., D.O. Meredith, and G.R. Owen, *Steps toward a model nanotopography.* IEEE Trans Nanobioscience, 2002. **1**(4): p. 133-40.

26. Clark, P., P. Connolly, A.S. Curtis, J.A. Dow, and C.D. Wilkinson, *Topographical control of cell behaviour: II. Multiple grooved substrata.* Development, 1990. **108**(4): p. 635-44.

27. Lee, S.W., S.Y. Kim, M.H. Lee, K.W. Lee, R. Leesungbok, and N. Oh, *Influence of etched microgrooves of uniform dimension on in vitro responses of human gingival fibroblasts.* Clin Oral Implants Res, 2009. **20**(5): p. 458-66.

28. Lenhert, S., M.B. Meier, U. Meyer, L. Chi, and H.P. Wiesmann, *Osteoblast alignment, elongation and migration on grooved polystyrene surfaces patterned by Langmuir-Blodgett lithography.* Biomaterials, 2005. **26**(5): p. 563-70.

29. Karuri, N.W., S. Liliensiek, A.I. Teixeira, G. Abrams, S. Campbell, P.F. Nealey, and C.J. Murphy, *Biological length scale topography enhances cell-substratum adhesion of human corneal epithelial cells.* J Cell Sci, 2004. **117**(Pt 15): p. 3153-64.

30. Liliensiek, S.J., S. Campbell, P.F. Nealey, and C.J. Murphy, *The scale of substratum topographic features modulates proliferation of corneal epithelial cells and corneal*

fibroblasts. Journal of Biomedical Materials Research Part A, 2006. **79**(1): p. 185-92.

31. Aguilar, C.A., Y. Lu, S. Mao, and S.C. Chen, *Direct micro-patterning of biodegradable polymers using ultraviolet and femtosecond lasers.* Biomaterials, 2005. **26**(36): p. 7642-7649.

32. Bolle, M. and S. Lazare, *Characterization of Submicrometer Periodic Structures Produced on Polymer Surfaces with Low-Fluence Ultraviolet-Laser Radiation.* Journal of Applied Physics, 1993. **73**(7): p. 3516-3524.

33. Inoue, S. and H. Sato, *Cell motility by labile association of molecules. The nature of mitotic spindle fibers and their role in chromosome movement.* J Gen Physiol, 1967. **50**(6): p. Suppl:259-92.

34. Roth, L.E. and E.W. Daniels, *Electron microscopic studies of mitosis in amebae. II. The giant ameba Pelomyxa carolinensis.* J Cell Biol, 1962. **12**: p. 57-78.

35. Ramaekers, F.C. and F.T. Bosman, *The cytoskeleton and disease.* J Pathol, 2004. **204**(4): p. 351-4.

36. Ingber, D.E. and J. Folkman, *Mechanochemical switching between growth and differentiation during fibroblast growth factor-stimulated angiogenesis in vitro: role of extracellular matrix.* J Cell Biol, 1989. **109**(1): p. 317-30.

37. Alberts, B., *Molecular biology of the cell*. 5th ed. Cytoskeleton. . 2008, New York: Garland Science.

38. Kleinsmith, L.J. and V.M. Kish, *Principles of cell and molecular biology*. 2nd ed. The Cytoskeleton and Cell Motility. 1995, New York: HarperCollins. xxviii, 810, 57 p.

39. Alberts, B., *Essential cell biology*. 3rd ed. Cytoskeleton. 2009, New York: Garland Science.

40. Lodish, H.F.B., Arnold. Kaiser, Chris A. Krieger, M. Bretscher, A. Ploegh, H. Amon. A. Scott, Matthew, P. , *Molecular cell biology*. 6th ed. Cell Organisation and Movement II. 2008, New York: W.H. Freeman.

41. Janmey, P., *Structure and dynamics of membranes*. Handbook of biological physics, Cell Membranes and the Cytoskeleton 1995, Amsterdam ; New York: Elsevier Science. v. <1A-1B, >.

42. Wozniak, M.A., K. Modzelewska, L. Kwong, and P.J. Keely, *Focal adhesion regulation of cell behavior.* Biochimica Et Biophysica Acta-Molecular Cell Research, 2004. **1692**(2-3): p. 103-119.

43. Pelham, R.J., Jr. and Y. Wang, *Cell locomotion and focal adhesions are regulated by substrate flexibility.* Proc Natl Acad Sci U S A, 1997. **94**(25): p. 13661-5.

44. Engler, A., L. Bacakova, C. Newman, A. Hategan, M. Griffin, and D. Discher, *Substrate compliance versus ligand density in cell on gel responses.* Biophysical Journal, 2004. **86**(1): p. 617-628.

45. DuFort, C.C., M.J. Paszek, and V.M. Weaver, *Balancing forces: architectural control of mechanotransduction.* Nat Rev Mol Cell Biol, 2011. **12**(5): p. 308-19.

46. Schwartz, M.A., *Integrins and extracellular matrix in mechanotransduction.* Cold Spring Harb Perspect Biol, 2010. **2**(12): p. a005066.

47. Lo, C.M., H.B. Wang, M. Dembo, and Y.L. Wang, *Cell movement is guided by the rigidity of the substrate.* Biophysical Journal, 2000. **79**(1): p. 144-152.

48. Solon, J., I. Levental, K. Sengupta, P.C. Georges, and P.A. Janmey, *Fibroblast adaptation and stiffness matching to soft elastic substrates.* Biophys J, 2007. **93**(12): p. 4453-61.

49. Trappmann, B., J.E. Gautrot, J.T. Connelly, D.G. Strange, Y. Li, M.L. Oyen, M.A. Cohen Stuart, H. Boehm, B. Li, V. Vogel, J.P. Spatz, F.M. Watt, and W.T. Huck, *Extracellular-matrix tethering regulates stem-cell fate.* Nat Mater, 2012. **11**(7): p. 642-9.

50. Wen, J.H., L.G. Vincent, A. Fuhrmann, Y.S. Choi, K.C. Hribar, H. Taylor-Weiner, S. Chen, and A.J. Engler, *Interplay of matrix stiffness and protein tethering in stem cell differentiation.* Nat Mater, 2014. **13**(10): p. 979-87.

51. Davies, J., *Extra Cellular Matrix.* Nature Publishing Group, 2001.

52. Martin, G.R. and R. Timpl, *Laminin and other basement membrane components.* Annu Rev Cell Biol, 1987. **3**: p. 57-85.

53. Kawabe, T.T., D.K. MacCallum, and J.H. Lillie, *Variation in basement membrane topography in human thick skin.* Anat Rec, 1985. **211**(2): p. 142-8.

54. Howat, W.J., J.A. Holmes, S.T. Holgate, and P.M. Lackie, *Basement membrane pores in human bronchial epithelium: a conduit for infiltrating cells?* Am J Pathol, 2001. **158**(2): p. 673-80.

55. Howat, W.J., T. Barabas, J.A. Holmes, S.T. Holgate, and P.M. Lackie, *Distribution of basement membrane pores in bronchus revealed by microscopy following epithelial removal.* J Struct Biol, 2002. **139**(3): p. 137-45.

56. Li, Y., Y. Zhu, H. Yu, L. Chen, and Y. Liu, *Topographic characterization and protein quantification of esophageal basement membrane for scaffold design*

reference in tissue engineering. J Biomed Mater Res B Appl Biomater, 2012. **100**(1): p. 265-73.

57. Demidova-Rice, T.N., M.R. Hamblin, and I.M. Herman, *Acute and impaired wound healing: pathophysiology and current methods for drug delivery, part 1: normal and chronic wounds: biology, causes, and approaches to care.* Adv Skin Wound Care, 2012. **25**(7): p. 304-14.

58. *A SHORT HISTORY OF PRINTING A2 - WIJNEKUS, F.J.M*, in *Dictionary of the Printing and Allied Industries (Second, Revised and Enlarged Edition)*, E.F.P.H. Wijnekus, Editor. 1983, Elsevier: Amsterdam. p. xiii-xxxvi.

59. Harriott, L.R., *Limits of lithography.* Proceedings of the IEEE, 2001. **89**(3): p. 366-374.

60. Clark, P., P. Connolly, A.S. Curtis, J.A. Dow, and C.D. Wilkinson, *Topographical control of cell behaviour. I. Simple step cues.* Development, 1987. **99**(3): p. 439-48.

61. Andersson, A.S., F. Backhed, A. von Euler, A. Richter-Dahlfors, D. Sutherland, and B. Kasemo, *Nanoscale features influence epithelial cell morphology and cytokine production.* Biomaterials, 2003. **24**(20): p. 3427-3436.

62. McMurray, R., M.J. Dalby, and N. Gadegaard, *Nanopatterned surfaces for biomedical applications*. 2011: INTECH Open Access Publisher.

63. Salem, A.K., R. Stevens, R.G. Pearson, M.C. Davies, S.J.B. Tendler, C.J. Roberts, P.M. Williams, and K.M. Shakesheff, *Interactions of 3T3 fibroblasts and endothelial cells with defined pore features.* Journal of Biomedical Materials Research, 2002. **61**(2): p. 212-217.

64. Okazaki, S., *High resolution optical lithography or high throughput electron beam lithography: The technical struggle from the micro to the nano-fabrication evolution.* Microelectronic Engineering, 2015. **133**: p. 23-35.

65. Hu, W.C., K. Sarveswaran, M. Lieberman, and G.H. Bernstein, *Sub-10 nm electron beam lithography using cold development of poly(methylmethacrylate).* Journal of Vacuum Science & Technology B, 2004. **22**(4): p. 1711-1716.

66. Teixeira, A.I., P.F. Nealey, and C.J. Murphy, *Responses of human keratocytes to micro- and nanostructured substrates.* Journal of Biomedical Materials Research Part A, 2004. **71**(3): p. 369-76.

67. Rajnicek, A.M., S. Britland, and C.D. McCaig, *Contact guidance of CNS neurites on grooved quartz: influence of groove dimensions, neuronal age and cell type.* J Cell Sci, 1997. **110**: p. 2905-2913.

68. Biggs, M.J.P., R.G. Richards, N. Gadegaard, C.D.W. Wilkinson, and M.J. Dalby, *Regulation of implant surface cell adhesion: Characterization and quantification of S-phase primary osteoblast adhesions on biomimetic nanoscale substrates.* Journal of Orthopaedic Research, 2007. **25**(2): p. 273-282.

69. Biggs, M.J.P., R.G. Richards, N. Gadegaard, R.J. McMurray, S. Affrossman, C.D.W. Wilkinson, R.O.C. Oreffo, and M.J. Dalby, *Interactions with nanoscale topography: Adhesion quantification and signal transduction in cells of osteogenic and multipotent lineage.* Journal of Biomedical Materials Research Part A, 2009. **91A**(1): p. 195-208.

70. Brown, M.S. and C.B. Arnold, *Fundamentals of Laser-Material Interaction and Application to Multiscale Surface Modification*, in *Laser Precision*

Microfabrication, K. Sugioka, M. Meunier, and A. Piqué, Editors. 2010, Springer Berlin Heidelberg: Berlin, Heidelberg. p. 91-120.

71. Gregson, V.G., *Laser Heat Treatment.* Laser materials processing, 1984. **3**: p. 201-234.

72. Zhang, D.L., TC; Zhang, JG; Ouyang, JH; , *The effects of heat treatment on microstructure and erosion properties of laser surface-clad Ni-base alloy.* Surface & Coatings Technology, 1999. **115**(2-3): p. 176-`83.

73. Ranjan, R., D.N. Lambeth, M. Tromel, P. Goglia, and Y. Li, *Laser texturing for low-flying-height media.* Journal of Applied Physics, 1991. **69**(8): p. 5745-5747.

74. Etsion, I., *State of the Art in Laser Surface Texturing.* Journal of Tribology, 2005. **127**(1): p. 248-253.

75. Kurella, A. and N.B. Dahotre, *Review paper: Surface Modification for Bioimplants: The Role of Laser Surface Engineering.* Journal of Biomaterials Applications, 2005. **20**(1): p. 5-50.

76. Clark, P., P. Connolly, A.S. Curtis, J.A. Dow, and C.D. Wilkinson, *Cell guidance by ultrafine topography in vitro.* J Cell Sci, 1991. **99 (Pt 1)**: p. 73-7.

77. Clark, P., G.A. Dunn, A. Knibbs, and M. Peckham, *Alignment of myoblasts on ultrafine gratings inhibits fusion in vitro.* International Journal of Biochemistry & Cell Biology, 2002. **34**(7): p. 816-825.

78. Waugh, D.G., J. Lawrence, D.J. Morgan, and C.L. Thomas, *Interaction of CO2 laser-modified nylon with osteoblast cells in relation to wettability.* Materials Science & Engineering C-Materials for Biological Applications, 2009. **29**(8): p. 2514-2524.

79. Waugh, D.G., J. Lawrence, and E.M. Brown, *Osteoblast cell response to a CO2 laser modified polymeric material.* Optics and Lasers in Engineering, 2012. **50**(2): p. 236-247.

80. Voisin, M., M. Ball, C. O'Connell, and R. Sherlock, *Osteoblasts response to microstructured and nanostructured polyimide film, processed by the use of silica bead microlenses.* Nanomedicine-Nanotechnology Biology and Medicine, 2010. **6**(1): p. 35-43.

81. Premnath, P., A. Tavangar, B. Tan, and K. Venkatakrishnan, *Tuning cell adhesion by direct nanostructuring silicon into cell repulsive/adhesive patterns.* Experimental Cell Research, 2015. **337**(1): p. 44-52.

82. Linez-Bataillon, P., F. Monchau, M. Bigerelle, and H.F. Hildebrand, *In vitro MC3T3 osteoblast adhesion with respect to surface roughness of Ti6Al4V substrates.* Biomol Eng, 2002. **19**(2-6): p. 133-41.

83. Lv, L., Y. Liu, P. Zhang, X. Zhang, J. Liu, T. Chen, P. Su, H. Li, and Y. Zhou, *The nanoscale geometry of TiO2 nanotubes influences the osteogenic differentiation of human adipose-derived stem cells by modulating H3K4 trimethylation.* Biomaterials, 2015. **39**: p. 193-205.

84. Mendonca, D.B., P.A. Miguez, G. Mendonca, M. Yamauchi, F.J. Aragao, and L.F. Cooper, *Titanium surface topography affects collagen biosynthesis of adherent cells.* Bone, 2011. **49**(3): p. 463-72.

85. Shimizu, K., H. Fujita, and E. Nagamori, *Alignment of skeletal muscle myoblasts and myotubes using linear micropatterned surfaces ground with abrasives.* Biotechnol Bioeng, 2009. **103**(3): p. 631-8.

86. Arizmendi, M., J. Fernandez, L.N.L. de Lacalle, A. Lamikiz, A. Gil, J.A. Sanchez, F.J. Campa, and F. Veiga, *Model development for the prediction of surface topography generated by ball-end mills taking into account the tool parallel axis offset. Experimental validation.* Cirp Annals-Manufacturing Technology, 2008. **57**(1): p. 101-104.

87. Denkena, B., V. Boss, D. Nespor, P. Gilge, S. Hohenstein, and J. Seume, *Prediction of the 3D Surface Topography after Ball End Milling and its Influence on Aerodynamics.* 15th Cirp Conference on Modelling of Machining Operations (15th Cmmo), 2015. **31**: p. 221-227.

88. Sato, K., *On the surface roughness in grinding.* Technology Reports, Tohoku University, 1955. **20**: p. 59-70.

89. Khare, S.K. and S. Agarwal, *Predictive modeling of surface roughness in grinding.* 15th Cirp Conference on Modelling of Machining Operations (15th Cmmo), 2015. **31**: p. 375-380.

90. Bozukova, D., C. Pagnoulle, R. Jerome, and C. Jerome, *Polymers in modern ophthalmic implants-Historical background and recent advances.* Materials Science & Engineering R-Reports, 2010. **69**(6): p. 63-83.

91. Mohan, C.C., K.P. Chennazhi, and D. Menon, *In vitro hemocompatibility and vascular endothelial cell functionality on titania nanostructures under static and dynamic conditions for improved coronary stenting applications.* Acta Biomater, 2013. **9**(12): p. 9568-77.

92. Reznickova, A., Z. Novotna, Z. Kolska, N.S. Kasalkova, S. Rimpelova, and V. Svorcik, *Enhanced adherence of mouse fibroblast and vascular cells to plasma modified polyethylene.* Mater Sci Eng C Mater Biol Appl, 2015. **52**: p. 259-66.

93. Kolind, K., A. Dolatshahi-Pirouz, J. Lovmand, F.S. Pedersen, M. Foss, and F. Besenbacher, *A combinatorial screening of human fibroblast responses on micro-structured surfaces.* Biomaterials, 2010. **31**(35): p. 9182-91.

94. Lee, M.H., J.H. Kang, and S.W. Lee, *The significance of differential expression of genes and proteins in human primary cells caused by microgrooved biomaterial substrata.* Biomaterials, 2012. **33**(11): p. 3216-34.

95. Hamilton, D.W., C. Oakley, N.A. Jaeger, and D.M. Brunette, *Directional change produced by perpendicularly-oriented microgrooves is microtubule-dependent for fibroblasts and epithelium.* Cell Motil Cytoskeleton, 2009. **66**(5): p. 260-71.

96. Berry, C.C., G. Campbell, A. Spadiccino, M. Robertson, and A.S.G. Curtis, *The influence of microscale topography on fibroblast attachment and motility.* Biomaterials, 2004. **25**(26): p. 5781-5788.

97. Ko, Y.G., C.C. Co, and C.C. Ho, *Directing cell migration in continuous microchannels by topographical amplification of natural directional persistence.* Biomaterials, 2013. **34**(2): p. 353-360.

98. Dalby, M.J., M.O. Riehle, S.J. Yarwood, C.D. Wilkinson, and A.S. Curtis, *Nucleus alignment and cell signaling in fibroblasts: response to a micro-grooved topography.* Exp Cell Res, 2003. **284**(2): p. 274-82.

99. Heath, D.E., J.J. Lannutti, and S.L. Cooper, *Electrospun scaffold topography affects endothelial cell proliferation, metabolic activity, and morphology.* J Biomed Mater Res A, 2010. **94**(4): p. 1195-204.

100. Wang, L. and R.L. Carrier, *Biomimetic topography: bioinspired cell culture substrates and scaffolds*. 2011: INTECH Open Access Publisher.

101. Dalby, M.J., M.O. Riehle, D.S. Sutherland, H. Agheli, and A.S. Curtis, *Morphological and microarray analysis of human fibroblasts cultured on nanocolumns produced by colloidal lithography.* Eur Cell Mater, 2005. **9**: p. 1-8; discussion 8.

102. Kim, H.J., S.H. Kim, M.S. Kim, E.J. Lee, H.G. Oh, W.M. Oh, S.W. Park, W.J. Kim, G.J. Lee, N.G. Choi, J.T. Koh, D.B. Dinh, R.R. Hardin, K. Johnson, V.L. Sylvia, J.P. Schmitz, and D.D. Dean, *Varying Ti-6Al-4V surface roughness induces different early morphologic and molecular responses in MG63 osteoblast-like cells.* Journal of Biomedical Materials Research Part A, 2005. **74A**(3): p. 366-373.

103. Sader, M.S., A. Balduino, G.D. Soares, and R. Borojevic, *Effect of three distinct treatments of titanium surface on osteoblast attachment, proliferation, and differentiation.* Clinical Oral Implants Research, 2005. **16**(6): p. 667-675.

104. Dalby, M.J., S.J. Yarwood, M.O. Riehle, H.J.H. Johnstone, S. Affrossman, and A.S.G. Curtsi, *Increasing fibroblast response to materials using nanotopography: morphological and genetic measurements of cell response to 13-nm-high polymer demixed islands.* Experimental Cell Research, 2002. **276**(1): p. 1-9.

105. Hamilton, D.W., M.O. Riehle, R. Rappuoli, W. Monaghan, R. Barbucci, and A.S.G. Curtis, *The response of primary articular chondrocytes to micrometric surface topography and sulphated hyaluronic acid-based matrices.* Cell Biology International, 2005. **29**(8): p. 605-615.

106. Biela, S.A., Y. Su, J.P. Spatz, and R. Kemkemer, *Different sensitivity of human endothelial cells, smooth muscle cells and fibroblasts to topography in the nano-micro range.* Acta Biomaterialia, 2009. **5**(7): p. 2460-6.

107. Walboomers, X.F., W. Monaghan, A.S.G. Curtis, and J.A. Jansen, *Attachment of fibroblasts on smooth and microgrooved polystyrene.* Journal of Biomedical Materials Research, 1999. **46**(2): p. 212-220.

108. Walboomers, X.F., L.A. Ginsel, and J.A. Jansen, *Early spreading events of fibroblasts on microgrooved substrates.* Journal of Biomedical Materials Research, 2000. **51**(3): p. 529-534.

109. Gomez-Florit, M., R. Xing, J.M. Ramis, S. Taxt-Lamolle, H.J. Haugen, S.P. Lyngstadaas, and M. Monjo, *Human gingival fibroblasts function is stimulated on machined hydrided titanium zirconium dental implants.* Journal of Dentistry, 2014. **42**(1): p. 30-38.

110. Lee, S.W., S.Y. Kim, I.C. Rhyu, W.Y. Chung, R. Leesungbok, and K.W. Lee, *Influence of microgroove dimension on cell behavior of human gingival fibroblasts cultured on titanium substrata.* Clin Oral Implants Res, 2009. **20**(1): p. 56-66.

111. Kim, S.Y., N. Oh, M.H. Lee, S.E. Kim, R. Leesungbok, and S.W. Lee, *Surface microgrooves and acid etching on titanium substrata alter various cell behaviors of cultured human gingival fibroblasts.* Clin Oral Implants Res, 2009. **20**(3): p. 262-272.

112. Leclerc, A., D. Tremblay, S. Hadjiantoniou, N.V. Bukoreshtliev, J.L. Rogowski, M. Godin, and A.E. Pelling, *Three dimensional spatial separation of cells in response to microtopography.* Biomaterials, 2013. **34**(33): p. 8097-104.

113. Oakley, C., N.A.F. Jaeger, and D.M. Brunette, *Sensitivity of fibroblasts and their cytoskeletons to substratum topographies: Topographic guidance and topographic compensation by micromachined grooves of different dimensions.* Experimental Cell Research, 1997. **234**(2): p. 413-424.

114. Re, F., A. Zanetti, M. Sironi, N. Polentarutti, L. Lanfrancone, E. Dejana, and F. Colotta, *Inhibition of Anchorage-Dependent Cell Spreading Triggers Apoptosis in Cultured Human Endothelial-Cells.* Journal of Cell Biology, 1994. **127**(2): p. 537-546.

115. Lee, J.S. and A.I. Gotlieb, *Understanding the role of the cytoskeleton in the complex regulation of the endothelial repair.* Histol Histopathol, 2003. **18**(3): p. 879-87.

116. Mustafa, K., B. Silva Lopez, K. Hultenby, A. Wennerberg, and K. Arvidson, *Attachment and proliferation of human oral fibroblasts to titanium surfaces blasted with TiO2 particles. A scanning electron microscopic and histomorphometric analysis.* Clin Oral Implants Res, 1998. **9**(3): p. 195-207.

117. Grossner-Schreiber, B., M. Herzog, J. Hedderich, A. Duck, M. Hannig, and M. Griepentrog, *Focal adhesion contact formation by fibroblasts cultured on surface-modified dental implants: an in vitro study.* Clin Oral Implants Res, 2006. **17**(6): p. 736-45.

118. Duncan, A.C., F. Rouais, S. Lazare, L. Bordenave, and C. Baquey, *Effect of laser modified surface microtopochemistry on endothelial cell growth.* Colloids Surf B Biointerfaces, 2007. **54**(2): p. 150-9.

119. Couchman, J.R., M. Hook, D.A. Rees, and R. Timpl, *Adhesion, growth, and matrix production by fibroblasts on laminin substrates.* J Cell Biol, 1983. **96**(1): p. 177-83.

120. Irving, M., M.F. Murphy, M.N. Morgan, F. Lilley, P. French, D.R. Burton, and P. Moran, *Machine grinding as an alternative method for creating functional surfaces for controlling cell behaviour.* International Journal of Advanced Manufacturing Technology, 2016. **87**(1-4): p. 1023-1031.

121. Irving, M., M.F. Murphy, F. Lilley, P.W. French, D.R. Burton, S. Dixon, and M.C. Sharp, *The use of abrasive polishing and laser processing for developing polyurethane surfaces for controlling fibroblast cell behaviour.* Materials Science & Engineering C-Materials for Biological Applications, 2017. **71**: p. 690-697.

Appendix 1 - Published paper:

Machine grinding as an alternative method for creating functional surfaces for controlling cell behaviour.

Michael Irving & Mark F. Murphy & Mike N. Morgan & Francis Lilley & Paul French & David R. Burton & Peter Moran

Abstract: There is extensive evidence to show that certain cellular behaviours including cell proliferation, migration and adhesion can be controlled by culturing cells on surfaces containing different micro-metre- and nanometre-scale features. This paper will introduce the use of machine grinding to generate surfaces with micro-sized features and their ability to affect cell behaviour. Results are presented which show that polyurethane castings of the ground surfaces can promote cell adhesion and migration. This study demonstrates the usefulness of surface grinding as a cost-effective method for generating functional surfaces for modifying cell behaviour.

[120]

Appendix 2 - Published paper:

The use of abrasive polishing and laser processing for developing polyurethane surfaces for controlling fibroblast cell behaviour.

Michael Irving & Mark F. Murphy & Mike N. Morgan & Francis Lilley & Paul French & David R. Burton & Peter Moran

Abstract: Studies have shown that surfaces having micro and nano-scale features can be used to control cell behaviours including; cell proliferation, migration and adhesion. The aim of this work was to compare the use of laser processing and abrasive polishing to develop micro/nano-patterned polyurethane substrates for controlling fibroblast cell adhesion, migration and proliferation. Laser processing in a directional manner resulted in polyurethane surfaces having a ploughed field effect with micron-scale features. In contrast, abrasive polishing in a directional and random manner resulted in polyurethane surfaces having sub-micron scale features orientated in a linear or random manner. Results show that when compared with flat (non-patterned) polymer, both the laser processed and abrasive polished surface having randomly organised features, promoted significantly greater cell adhesion, while also enhancing cell proliferation after 72 h. In contrast, the abrasive polished surface having linear features did not enhance cell adhesion or proliferation when compared to the flat surface. For cell migration, the cells growing on the laser processed and abrasively polished random surface showed decreased levels of migration when compared to the flat surface. This study shows that both abrasive polishing and laser processing can be used to produce surfaces having features on the nano-scale and micron-scale, respectively. Surfaces produced using both techniques can be used to promote fibroblast cell adhesion and

proliferation. Thus both methods offer a viable alternative to using lithographic techniques for developing patterned surfaces. In particular, abrasive polishing is an attractive method due to it being a simple, rapid and inexpensive method that can be used to produce surfaces having features on a comparable scale to more expensive, multi-step methods.

[121]

Appendix 3 - Raw surface analysis data

A 3.1 Laser patterned surface values

Peak Height	Width path	width non laser path
1.5	31.1	15
1.9	31.3	16
2.1	31.7	16
2.7	30.9	17
2.6	32.4	16
2.9	32.6	15
3.2	33	16
1.6	31.3	17
2.7	33.2	17
1.1	31.9	16
1.9	32.7	17
1	33.9	17
1.3	31.3	17
1.8	31.5	16
0.8	32.3	16
1.3	33.3	17
2.1	32.8	16
2.3	32.7	16
1.7	32.3	16
3	31.5	15
0.9	33.3	15
0.9	30.3	18
0.9	32.3	17
2.7	32.3	18
2.6	31.3	17
1.3	32.9	17
2.6	32.9	17
1.5	31.1	17
2.4	32.8	18
1.5	33.9	18

mean value	1.89	32.23	16.53
sd	0.71	0.90	0.88

sem	0.132	0.168	0.16

A 3.2 Polymer laser surface measurements

height of peaks	Non laser path	width of laser
1.8	16	31
0.6	18	31
1.4	16	32
1.4	15	34
1.5	15	31
0.9	18	31
1.3	17	31
1.3	17	33
1.2	17	31
1.6	18	34
1.9	17	28
1.9	17	29
1.1	15	32
2.3	15	32
0.8	19	33
1.8	19	32
1.3	17	34
1.2	16	34
1	18	31
3.3	19	30
1.4	19	35
1.9	18	33
0.9	17	33
1.2	16	34
1.5	17	32
0.8	15	31
1.6	15	32
1.1	16	32
0.5	15	31
0.9	17	31

mean value	1.38	16.8	31.93333
sd	0.547357	1.32665	1.547758
sem	0.102	0.25	0.29

A 3.3 Peak heights for Metal scratched surfaces

1200	600	500	400	320	120	random
0.597	0.433	0.46	0.184	0.414	0.316	0.98
0.575	0.244	0.261	0.243	0.395	0.412	0.64
0.221	0.307	0.699	0.465	0.369	0.172	0.43
0.191	0.435	0.523	0.543	0.27	0.543	0.43
0.147	0.397	0.395	0.164	0.369	0.27	0.38
0.311	0.16	0.309	0.266	0.172	0.454	0.38
0.217	0.264	0.421	0.229	0.277	0.711	0.18
0.385	0.326	0.355	0.387	0.442	0.308	0.46
0.304	0.415	0.518	0.241	0.478	0.438	0.33
0.315	0.356	0.481	0.623	0.511	0.353	0.95
0.314	0.898	0.512	0.268	0.312	0.453	0.56
0.245	0.432	0.383	0.356	0.365	0.545	0.5
0.226	0.217	0.244	0.297	0.225	0.453	0.26
0.342	0.185	0.986	0.191	0.345	0.267	0.61
0.195	0.42	0.715	0.29	0.167	0.356	0.67
0.2406	0.297	0.411	0.359	0.348	0.45	0.59
0.305	0.312	0.36	0.217	0.318	0.498	0.52
0.305	0.25	0.82	0.283	0.368	0.635	0.59
0.264	0.331	0.56	0.269	0.308	0.423	0.21
0.28	0.297	0.228	0.275	0.14	0.566	0.27
0.448	0.691	0.688	0.28	0.32	0.537	0.78
0.342	0.461	0.389	0.252	0.276	0.423	0.74
0.188	0.475	0.782	0.149	0.491	0.932	0.88
0.248	0.447	0.837	0.208	0.496	0.909	0.19
0.346	0.617	0.789	0.499	0.31	0.386	0.6
0.256	0.278	0.701	0.49	0.263	0.81	0.27
0.226	0.224	0.465	0.223	0.172	0.415	0.49
0.223	0.271	0.36	0.231	0.365	0.324	0.53
0.402	0.286	0.171	0.248	0.307	0.561	0.67
0.266	0.282	0.755	0.195	0.322	0.338	0.51
0.457	0.213	0.407	0.279	0.266	0.793	0.3
0.42	0.53	0.505	0.35	0.495	0.57	0.18
0.31	0.25	0.486	0.337	0.158	0.511	0.39
0.149	0.3	0.223	0.233	0.314	1.726	0.27
0.36	0.416	0.436	0.286	0.35	1.417	0.92
0.151	0.325	0.386	0.187	0.478	1.154	0.42

0.266	0.174	0.473	0.415	0.263	0.588	0.27
0.121	0.328	0.393	0.168	0.271	0.622	0.33
0.103	0.344	0.313	0.172	0.221	0.779	0.59
0.173	0.207	0.361	0.322	0.442	1.302	0.49
0.186	0.477	0.468	0.577	0.387	0.719	0.43
0.212	0.308	0.87	0.259	0.296	0.679	0.26
0.242	0.733	0.357	0.311	0.236	0.536	0.49
0.227	0.306	0.606	0.148	0.333	0.463	0.64
0.316	0.437	0.327	0.17	0.209	0.765	0.37
0.167	0.284	0.461	0.203	0.432	0.784	0.51
0.338	0.173	0.666	0.244	0.309	1.88	0.39
0.283	0.381	0.831	0.196	0.327	0.845	0.61
0.329	0.359	0.44	0.385	0.244	0.676	0.36
0.171	0.308	0.634	0.212	0.288	0.955	0.3

Mean peak value	0.278112	0.35722	0.50442	0.28758	0.32468	0.64044	0.4824

A 3.4 Metal Ra values for scratched surfaces

	Ra							
	laser	**120**	**320**	**400**	**500**	**600**	**1200**	**random**
	0.328	1.116	0.307	0.149	0.235	0.122	0.088	0.162
	0.316	1.295	0.337	0.154	0.249	0.133	0.085	0.16
	0.288	1.452	0.255	0.115	0.255	0.126	0.079	0.157
	0.359	1.504	0.378	0.154	0.317	0.125	0.088	0.177
	0.308	1.31	0.29	0.157	0.311	0.122	0.085	0.168
Mean	0.3198	1.3354	0.3134	0.1458	0.2734	0.1256	0.085	0.1648

A 3.5 Metal Rz values for scratched surfaces

	Rz							
	laser	**120**	**320**	**400**	**500**	**600**	**1200**	**random**
	5.575	7.627	3.25	2.836	2.917	1.98	2.159	2.913
	5.786	14.707	3.215	2.389	3.134	2.242	1.906	2.679
	5.939	11.222	3.183	2.026	3.162	2.921	1.796	2.789
	7.69	13.701	3.469	2.967	3.576	1.836	2.178	2.649
	5.728	9.157	3.537	2.937	3.173	2.272	2.01	2.784
Mean	6.1436	11.2828	3.3308	2.631	3.1924	2.2502	2.0098	2.7628

A 3.6 Metal Rt values for scratched surfaces

	Rt						
	laser	**120**	**320**	**400**	**500**	**600**	**1200**	**Random**
	7.573	9.63	3.673	3.63	3.441	2.991	2.83	3.521
	8.545	16.091	3.688	2.678	4.447	3.581	2.542	3.595
	8.731	15.244	4.523	2.515	3.83	3.41	2.655	3.2264
	11.412	15.253	4.204	4.062	4.025	2.659	3.205	3.159
	8.589	9.609	5.416	3.65	4.037	2.821	2.467	3.464
Mean	8.97	13.1654	4.3008	3.307	3.956	3.0924	2.7398	3.39308

A 3.7 Polymer peak height values for scratched surfaces

120	**320**	**400**	**500**	**600**	**1200**	**random**
2.72	0.73	0.43	0.63	0.61	0.32	0.87
3.04	0.58	0.33	1.07	0.45	0.24	0.46
1.82	0.85	0.68	1.23	0.28	0.25	0.65
2	0.75	0.28	0.89	0.25	0.32	0.42
1.22	0.3	0.24	1.01	0.32	0.19	0.36
1.82	0.8	0.26	0.75	0.36	0.21	0.29
1.27	0.74	0.32	0.78	0.48	0.21	0.6
0.8	0.86	0.14	0.57	0.34	0.15	1.4
1.4	0.83	0.3	0.65	0.23	0.22	0.58
0.37	0.36	0.91	0.85	0.33	0.25	0.15
0.69	0.25	0.37	0.57	0.24	0.17	0.2
0.94	0.36	0.39	0.66	0.49	0.16	0.32
1.12	0.13	0.83	0.5	0.5	0.23	0.51
0.64	0.27	0.29	1.4	0.59	0.09	0.23
1.12	0.38	0.43	1.19	0.44	0.27	0.33
2.41	1.1	0.38	0.5	0.42	0.27	0.29
1.09	0.35	0.47	0.89	0.51	0.29	0.29
2.36	0.81	0.25	0.27	0.56	0.42	0.57
2.77	0.99	0.35	0.63	0.26	0.22	0.34
0.89	0.35	0.35	0.73	0.36	0.31	0.36
1.71	0.43	0.3	0.61	0.32	0.18	0.29
0.93	0.42	0.65	0.59	0.42	0.31	0.46

2.68	0.19	0.35	0.76	0.49	0.23	0.29
1.11	0.43	0.32	1.14	0.41	0.25	0.58
1.7	0.43	0.61	0.72	0.45	0.16	0.36
1.09	0.53	0.44	0.39	0.89	0.29	0.4
0.5	0.97	0.39	0.55	0.62	0.27	0.52
2.27	0.88	0.54	0.47	0.75	0.18	0.72
2.09	0.36	0.23	0.29	0.39	0.21	1.28
1.31	0.43	0.58	1.18	0.7	0.19	0.25
0.49	0.83	0.48	0.69	0.66	0.42	0.6
1.67	0.49	0.47	0.9	0.7	0.23	0.71
2.32	0.55	0.42	0.72	0.63	0.17	0.26
0.61	0.67	0.43	0.83	0.82	0.12	0.22
1.83	0.61	0.65	0.57	0.79	0.17	0.44
1.35	0.31	0.83	0.57	0.6	0.31	0.31
1.94	1.33	0.69	0.65	0.48	0.21	0.3
3.61	0.77	0.41	0.43	0.69	0.37	1.64
2.31	0.59	0.39	0.68	0.74	0.39	1.65
1.15	0.87	0.29	0.36	0.45	0.21	0.36
1.88	0.38	0.79	0.34	0.89	0.34	0.5
0.85	0.38	0.48	0.43	0.66	0.26	0.49
0.98	1.15	0.19	0.61	1.1	0.21	0.72
0.93	0.32	0.43	0.41	0.62	0.25	0.67
1.19	0.5	0.26	0.48	0.84	0.13	0.54
2.11	0.79	0.35	0.85	1.29	0.29	0.44
0.64	0.29	0.59	0.72	1	0.41	0.58
1.89	0.24	0.29	0.69	0.26	0.22	0.48
1.99	0.31	0.81	0.64	0.42	0.19	0.26
1.3	0.52	0.29	0.51		0.18	0.35

mean values	1.5384	0.5752	0.439	0.691	0.553061	0.2428	0.5178
sd	0.74	0.28	0.18	0.25	0.23	0.08	0.33
sem	0.1	0.04	0.03	0.04	0.03	0.01	0.05

A 3.8 Polymer Ra for scratched surfaces

Ra

laser	**120**	**320**	**400**	**500**	**600**	**1200**	**random**
0.327	1.489	0.31	0.125	0.316	0.126	0.081	0.186
0.322	1.009	0.318	0.135	0.316	0.121	0.081	0.18
0.329	1.054	0.318	0.115	0.27	0.117	0.088	0.167
0.302	1.36	0.334	0.11	0.266	0.138	0.081	0.173
0.324	1.374	0.476	0.124	0.278	0.137	0.081	0.175

Mean	0.3208	1.2572	0.3512	0.1218	0.2892	0.1278	0.0824	0.1762

A 3.9 Polymer Rz for scratched surfaces

	Rz							
	laser	**120**	**320**	**400**	**500**	**600**	**1200**	**random**
	11.069	9.068	8.582	4.368	5.862	2.029	2.151	4.351
	10.748	9.7644	6.542	7.357	5.129	2.317	2.284	3.95
	12.328	9.102	7.084	4.389	5.248	1.976	2.392	5.228
	10.84	8.555	5.899	4.661	4.279	3.115	2.888	4.712
	10.952	9.368	7.916	5.59	4.828	2.636	2.673	4.523
Mean	11.1874	9.17148	7.2046	5.273	5.0692	2.4146	2.4776	4.5528

A 3.10 Polymer Rt for scratched surfaces

	Rt							
	laser	**120**	**320**	**400**	**500**	**600**	**1200**	**random**
	14.882	10.79	14.808	7.088	7.394	2.848	2.708	5.332
	16.05	11.245	8.617	8.867	5.875	3.157	3.601	4.086
	15.643	10.674	10.582	5.574	6.722	2.544	3.443	7.446
	14.65	8.99	9.283	6.721	5.631	4.392	4.176	5.371
	15.939	11.113	11.144	7.077	6.296	2.994	3.584	5.467
Mean	15.4328	10.5624	10.8868	7.0654	6.3836	3.187	3.5024	5.5404

Appendix 4 - Raw cell MTT data

A 4.1 MTT proliferation raw data LL24 different patterning

24h							Mean
laser	0.6585	0.7965	0.3895	0.7885	1.0915	1.2295	0.825667
polish	0.215353	0.1	0.396353	0.763353	0.926353	0.892353	0.548961
random	0.141611	0.216611	0.836611	0.971611	1.642611	1.171611	0.830111
flat	0.522833	0.171833	0.368833	0.954833	1.168	1.341	0.754556

48h							Mean
laser	0.9295	0.9355	1.3695	1.9085	1.6485	1.3855	1.362833
polish	1.002353	1.038353	1.096353	2.100353	2.042353	1.569353	1.474853
random		0.963611	1.149611	1.369611	2.042353	1.569353	1.418908
flat	0.918833	1.140833	0.455833	2.325833	1.621833	2.279833	1.457167

72h							Mean
laser	1.5785	1.5605	1.6845	2.8075	2.2645	2.5445	2.073333
polish	1.529353	1.735353	1.373353	2.535353	2.669353	2.193353	2.00602
random	2.463611	2.416611	1.928611	1.759611	3.320611	2.039611	2.321444
flat	1.483833	1.906833	1.642833	2.802833	2.820833	2.831833	2.248167

combined	24	48	72	sem	sem	sem
laser	0.825667	1.362833	2.073333	0.12	0.16	0.22
polish	0.515186	1.474853	2.00602	0.14	0.21	0.22
random	0.830111	1.418908	2.321444	0.23	0.18	0.23
flat	0.754556	1.457167	2.248167	0.19	0.31	0.26

A 4.2 MTT proliferation raw data LL24 scratched surfaces

24h				Mean	sem
1200	0.380833	0.505833	0.486833	0.457833	0.04
600	0.328667	0.415667	1.165667	0.636667	0.2
500	0.965833	0.488833	0.713833	0.722833	0.14
400	0.667083	0.089083	0.002083	0.25275	0.2
320	0.001667	0.420667	0.053667	0.158667	0.13
120	0.11825	0.16725	0.41125	0.23225	0.1
flat	0.7819	0.8069	0.8939	0.827567	0.03

48h				Mean	sem
1200	1.090833	1.058833	0.842833	0.9975	0.08
600	0.880667	0.789667	1.029667	0.9	0.07
500	0.940833	0.878833	0.901833	0.907167	0.02
400	0.071083	1.236083	1.793083	1.033417	0.5
320	0.270667	0.346667	1.030667	0.549333	0.2
120	0.76125	0.46825	0.94025	0.72325	0.14
flat	0.8269	0.8699	1.6209	1.1059	0.26

72h				Mean	Sem
1200	0.172833	1.122833	1.750833	1.0155	0.5
600	2.090667	2.746667	1.493667	2.110333	0.4
500	1.737833	1.890833	2.341833	1.990167	0.2
400	1.713083	0.131083	1.152083	0.99875	0.5
320	1.538667	1.234667	1.393667	1.389	0.09
120	1.61425	1.73225	1.30425	1.55025	0.13
flat	1.0349	1.0179	1.2469	1.0999	0.07

combined	24	48	72	Sem	Sem	Sem
1200	0.457833	0.9975	1.0155	0.04	0.08	0.5
600	0.636667	0.9	2.110333	0.2	0.07	0.4
500	0.722833	0.907167	1.990167	0.14	0.02	0.2
400	0.25275	1.033417	0.99875	0.2	0.5	0.5
320	0.158667	0.549333	1.389	0.13	0.2	0.09
120	0.23225	0.72325	1.55025	0.1	0.14	0.13
flat	0.827567	1.1059	1.0999	0.03	0.26	0.07

A 4.3 Migration mean data for three repeats

					av	sd	
flat	3483.429	4331.307	2483.49	flat	3432.742		924
laser	2455.341	2836.412	3015.499	laser	2769.084		286
random	3127.659	2779.75	3121.403	random	3009.604		199
linear	4322.365	3186.43	4077.893	linear	3862.229		597

Appendix 5 – BAE-1 raw data

A 5.1 BAE-1 raw adhesion MTT data

										Mean	SD	SEM
laser	0.330	0.119	1.259	0.079	0.090	0.069	0.089	0.086	0.129	0.250	0.39	0.13
linear	0.105	0.065	0.028	0.037	0.052	0.031	0.067	0.054	0.061	0.055	0.02	0.01
random	0.000	0.044	0.012	0.048	0.031	1.152	0.016	0.043	0.047	0.155	0.39	0.14
flat	0.047	0.085	0.088	0.061	0.018	0.042	0.028	0.061	0.091	0.058	0.03	0.01

A 5.2 BAE-1 raw adhesion MTT data scratched surfaces

1200	0.264	0.159	0.216	0.233	0.589	0.144	0.099	0.074	0.070	0.112	0.098	0.061
600	0.238	0.162	0.150	0.148	0.206	0.170	0.147	0.152	0.083	0.041	0.074	0.055
500	0.251	0.100	0.084	0.190	0.140	0.166	0.260	0.111	0.055	0.086	0.091	0.136
400	0.281	0.282	0.210	0.182	0.244	0.202	0.137	0.083	0.049	0.081	0.081	0.147
320		0.222	0.301		0.200	0.520	0.174	0.076	0.065	0.053	0.118	0.051
120	0.216	0.251	0.348	0.307	0.226	0.236	0.157	0.143	0.102	0.115	0.077	0.086
flat	0.206	0.175	0.180	0.185	0.193		-0.024	0.048	0.055	0.062	0.065	0.016

			Mean	SEM
0.123	0.109	0.083	0.162	0.034
0.123	0.139	0.120	0.134	0.014
0.189	0.128	0.136	0.142	0.016
0.135	0.113	0.161	0.159	0.019
0.076	0.057	0.050	0.151	0.038
0.156	0.131	0.129	0.179	0.021
0.033	0.062	0.040	0.093	0.021

A 5.3 BAE-1 raw proliferation MTT data

24h										Mean	SD	SEM
laser	0.448	0.445	0.359	0.440	0.536	0.430	0.455	0.486	0.601	0.467	0.07	0.02
random	0.440	0.397	0.691	0.609	0.540	0.628	0.244	0.465	0.457	0.497	0.14	0.05
polish	0.359	0.487	0.564	0.476	0.646	0.648	0.467	0.488	0.438	0.509	0.09	0.03
flat	0.473	0.563	0.406	0.475	0.499	0.369	0.341	0.497	0.354	0.442	0.08	0.03

48h										Mean	SD	SEM
laser	0.894	0.514	0.628	0.701	0.496	0.986	0.767	0.705	1.019	0.746	0.19	0.06
random	0.705	0.628	0.683	0.620	0.724	0.701	0.654	0.564	0.752	0.670	0.06	0.02
polish	0.591	0.556	0.881	0.565	0.629	0.814	0.510	0.445	0.490	0.609	0.15	0.05
flat	0.801	0.905	0.575	0.497	0.739	0.428	0.518	0.639	0.427	0.614	0.17	0.06

72h	Mean	SD	SEM

laser	1.232	0.966	1.016	0.878	0.883	1.092	1.207	1.765	1.133	1.131	0.37	0.09
random	0.906	0.865	0.863	1.260	1.052	1.370	1.312	0.896	1.083	1.068	0.2	0.07
polish	0.966	0.715	0.859	0.941	0.708	0.737	0.618	0.820	0.661	0.781	0.12	0.04
flat	1.061	0.869	2.414	0.696	1.046	0.985	0.905	0.866	0.928	1.085	0.5	0.17

	MEAN			SEM		
combined	24	48	72	24	48	72
laser	0.467	0.745889	1.130556	0.02	0.06	0.09
random	0.496893	0.670226	1.06756	0.05	0.02	0.07
polish	0.508534	0.609423	0.780979	0.03	0.05	0.04
flat	0.44162	0.614064	1.085286	0.03	0.06	0.17

A 5.4 BAE-1 raw 1 raw proliferation MTT data scratched surfaces

24h										Mean	SEM	SD
1200	0.144	0.127	0.112	0.142	0.092	0.102	0.064	0.082	0.051	0.102	0.01	0.03
600	0.148	0.127	0.112	0.130	0.062	0.104	0.182	0.118	0.083	0.119	0.01	0.04
500	0.123	0.216	0.184	0.118	0.175	0.124	0.116	0.126	0.150	0.148	0.01	0.04
400		0.111	0.070	0.073	0.086	0.068	0.049	0.075	0.027	0.070	0.01	0.02
320	0.186	0.198	0.184	0.191	0.189	0.041	0.158	0.235	0.159	0.171	0.02	0.05
120	0.173	0.209	0.228	0.141	0.081	0.136	0.174	0.180	0.092	0.157	0.02	0.05
flat	0.207	0.179	0.258	0.124	0.163	0.135	0.102	0.135	0.245	0.172	0.02	0.05

48h										Mean	SEM	SD
1200	0.509	0.398	0.283	0.356	0.309	0.361	0.183	0.239	0.249	0.321	0.03	0.09
600	0.380	0.440	0.360	0.351	0.289	0.265	0.307	0.336	0.346	0.342	0.02	0.05
500	0.312	0.448	0.385	0.321	0.324	0.273	0.329	0.289	0.260	0.327	0.02	0.06
400	0.289	0.419	0.351	0.233	0.353	0.243	0.243	0.335	0.252	0.302	0.02	0.07
320	0.436	0.464	0.477	0.335	0.326	0.364	0.412	0.053	0.497	0.374	0.05	0.13
120	0.385	0.391	0.425	0.396	0.389	0.376	0.311	0.354	0.575	0.400	0.05	0.14
flat	0.298	0.437	0.419	0.349	0.423	0.313	1.060	0.418	0.516	0.470	0.08	0.2

72h										Mean	SEM	SD
1200	0.711	0.469	0.439	0.495	0.617	0.444	0.549	0.496	0.399	0.513	0.03	0.09
600	0.667	0.445	0.472	0.502	0.485	0.367	0.469	0.433	0.400	0.472	0.03	0.08
500	0.508	0.570	0.567	0.426	0.363	0.520	0.295	0.445	0.296	0.443	0.04	0.11

400	0.445	0.555	0.441	0.229	0.338	0.247	0.291	0.511	0.518	0.398	0.04	0.12
320	0.532	0.615	0.667	0.466	0.586	0.574	0.406	0.515	0.615	0.553	0.03	0.08
120	0.148	0.665	0.546	0.393	0.485	0.539	0.410	0.434	0.613	0.470	0.05	0.15
flat	0.442	0.669	0.400	0.618	0.662	0.523	0.778	1.351	0.497	0.660	0.09	0.29

	Mean			SEM		
combined	24	48	72	24	48	72
1200	0.101844	0.320844	0.513289	0.01	0.03	0.03
600	0.118911	0.342022	0.471578	0.01	0.02	0.03
500	0.148067	0.326844	0.4434	0.01	0.02	0.04
400	0.174556	0.302333	0.397556	0.01	0.02	0.04
320	0.171089	0.373644	0.552756	0.02	0.05	0.03
120	0.157178	0.400289	0.4704	0.02	0.05	0.05
flat	0.171667	0.47	0.659667	0.02	0.08	0.09

Appendix 6 – Grinding data

A 6.1 Peak heights for different ground metal surfaces

M1	M2	M3	M4
3.93	1.22	2.25	1.69
2.44	1.58	2.09	1.36
1.35	2.02	1.79	1.56
1.38	0.82	0.85	2.41
0.81	1.22	0.52	1.26
1.18	1.53	0.96	1.05
1.12	1.01	0.69	1.09
1.04	1.39	0.56	0.60
1.17	0.83	1.27	0.74
1.41	1.21	0.96	1.49
2.87	0.67	0.80	2.20
0.94	0.63	3.17	0.65
3.40	0.48	3.46	0.89
1.11	1.23	0.83	2.38
0.46	0.29	0.57	1.15
0.66	2.47	0.86	1.68
1.18	1.87	3.22	1.06
1.17	0.92	2.29	0.99
0.31	1.28	3.89	2.03
0.51	0.99	1.74	1.04
1.07	2.18	1.23	1.72
0.87	0.87	2.43	1.23
1.52	0.84	3.08	1.52
1.61	0.57	1.07	1.19
0.78	1.02	1.29	3.03
0.85	0.65	1.37	2.14
0.16	3.22	1.98	1.05
0.69	0.80	0.78	1.00
0.67	1.79	1.34	0.59
2.95	2.89	2.15	3.78
0.64	0.81	3.66	1.09
0.87	1.11	3.79	1.07
2.16	0.66	1.26	1.64
1.57	0.17	1.08	0.93
1.09	1.16	2.55	2.09
0.92	2.92	1.71	2.64
1.74	3.73	1.06	3.32
1.40	2.76	1.21	2.77
0.74	1.09	0.74	1.48

0.92	0.26	0.98	0.97
1.58	0.97	1.12	1.19
2.34	2.55	2.57	0.75
0.53	2.41	3.28	1.46
0.43	0.59	0.77	1.13
1.41	0.42	2.09	0.99
0.55	1.55	0.85	1.58
1.35	2.89	1.95	1.21
0.95	2.86	2.04	1.43
1.20	0.85	2.07	0.98
1.47	0.52	1.32	1.89
1.33	0.21	0.72	0.81
1.32	1.88	1.54	1.86
0.18	2.31	2.63	2.14
1.02	1.23	2.95	1.15
0.54	1.48	2.13	4.68
0.66	1.28	1.61	1.15
1.46	1.44	2.19	3.18
0.54	1.34	1.33	2.52
0.56	1.89	1.06	2.72
1.08	2.30	0.89	1.65
1.76	1.72	0.22	1.55
1.42	1.13	1.15	1.59
1.09	1.82	1.89	2.81
0.58	1.52	0.59	1.84
1.18	0.78		1.71
2.54	1.41		1.26
1.37	1.23		6.02
0.62	2.26		2.96
0.92	2.17		3.78
1.25	0.99		1.96
2.70	0.96		1.19
1.27	1.01		2.42
1.53	0.46		2.18
1.35	0.47		3.45
0.42	2.03		2.81
1.08	2.73		1.96
0.69	0.89		2.05
1.31	0.51		2.33
2.19	0.58		2.41
0.64	1.00		4.65
0.41	1.29		4.05
1.31	1.16		2.23
0.88	0.60		2.84
2.59	1.33		1.22
0.95	0.79		2.16

	1.33	0.86		0.72
	0.48	2.31		2.28
	2.64	2.03		2.57
	0.76	1.48		1.19
	0.75	0.86		1.47
	0.68	0.49		1.97
	0.63	0.71		2.26
	0.89	0.90		1.23
	0.66			2.27
	0.72			
	2.39			
	0.54			
	1.13			
	3.18			
	1.02			
	1.44			
	1.98			
	1.21			
	1.47			
Mean	1.23	1.34	1.66	1.88
SD	0.72	0.768	0.919	0.985
SEM	0.07	0.079	0.115	0.102

A 6.2 Peak heights for different ground polymer surfaces

P1	P2	P3	P4
0.82	0.46	1.46	0.56
1.14	0.99	1.60	0.43
2.06	1.23	0.75	0.66
0.97	0.89	1.94	1.04
1.08	1.85	0.88	0.55
2.57	1.8	1.05	1.46
0.52	0.46	1.28	2.49
2.04	0.66	2.25	0.96
0.68	1.14	1.74	0.92
0.6	0.63	0.45	2.58
0.38	0.67	0.88	1.86
0.83	0.97	2.30	2.84
1.24	0.29	1.37	0.88
0.33	0.47	0.76	0.95
0.64	1.07	0.31	2.64
0.87	0.89	1.53	2.36
0.84	0.51	0.53	2.96
0.75	0.39	1.18	5.36
1.15	1.67	0.61	4.57

0.69	0.83	0.74	3.12
1.39	0.65	0.46	1.34
1.88	0.42	0.53	0.72
1.93	0.82	1.39	1.79
1.72	0.29	0.48	3.21
1.09	0.34	0.13	1.67
0.88	0.37	0.57	2.26
0.47	1.01	1.29	1.15
0.75	0.48	2.19	2.63
1.17	0.46	1.42	1.74
1.32	1.45	0.85	1.21
0.87	0.42	1.20	1.27
0.55	2.09	2.24	1.63
0.43	0.78	1.69	1.19
0.37	0.69	0.64	1.02
1.59	0.29	2.00	0.99
1.45	0.84	3.71	2.09
0.65	0.37	0.73	1.02
0.76	0.67	1.79	0.67
1.4	0.64	3.39	2.35
1.51	1.57	2.87	2.48
0.87	0.81	1.30	1.51
0.89	0.86	1.54	1.14
1.09	0.79	1.09	1.37
2.69	0.44	1.04	1.96
2.37	0.38	0.69	1.89
0.98	0.65	1.34	3.16
2.05	0.53	1.47	1.72
0.58	0.34	1.32	1.74
0.92	1.09	1.36	1.74
1.99	0.26	1.63	0.68
2.73	0.81	0.93	0.96
0.65	1.71	1.92	0.96
1.19	1.43	1.58	0.52
0.91	0.37	0.43	1.77
0.79	0.62	1.47	3.27
1.42	1.57	1.24	0.74
2.65	0.5	1.40	1.01
2.46	0.46	1.18	1.25
2.33	1.51	0.49	1.35
1.65	1.74	0.41	0.81
1.49	2.07	0.50	1.05
1.68	0.48	0.81	0.86
0.82	0.47	0.37	0.53
1.08	0.48	1.18	1.04
0.26	0.89	1.44	1.98

1.59	1.57	1.27	1.54
1.83	1.23	0.65	0.52
0.88	1.09	0.63	2.43
0.91	2.21	0.63	1.48
0.76	1.49	0.28	0.79
1.6	0.53	1.82	3.21
0.67	0.7	0.95	0.85
1.45	0.99	0.74	0.47
0.56	0.98	0.62	2.53
1.69	1.67	0.64	0.78
1.13	1.38	0.53	0.64
0.98	0.63	0.67	0.56
1.12	0.46	0.83	0.79
1.22	0.63	0.72	1.36
1.35	1.29	0.33	0.59
1.49	0.67	1.13	1.22
2.15	1.37	1.03	1.59
0.86	0.49	0.64	2.03
3.47	1.5	0.85	2.27
0.55	0.72	1.14	2.54
1.13	0.38	1.10	4.09
0.83	0.84	0.87	1.47
0.98	0.77	0.98	2.15
1.68	0.42	1.07	2.78
0.69	0.33	1.64	1.17
1.09	0.38	0.57	1.33
0.93	0.36	1.08	1.27
0.69	1.1	2.00	2.07
0.59	0.37	0.63	2.81
0.77	0.32	1.22	2.03
1.1	2.55	0.53	1.26
0.79	0.43	1.17	1.58
0.4	1.17	1.74	1.39
1.96	0.46	2.82	2.01
2.04	1.39	1.51	2.85
0.73	1.34	0.94	3.63
0.52	1.36	0.65	5.47
0.47	0.53	0.85	4.02
0.32	0.54	0.73	2.26
0.38	1.1	1.02	2.12
0.7	0.82	0.83	0.74
0.73	1.66	3.15	0.69
1.19	0.34	0.42	
0.98	0.64	0.54	
0.85	0.85	0.99	
0.87	0.76	0.49	

2.47	0.73	1.11
0.95	0.75	1.14
2.26	0.98	1.32
0.69	0.56	1.24
0.92	0.8	2.99
2.46	2.08	0.67
1.56	0.74	1.69
0.74	0.99	2.13
1.36	0.65	0.97
0.86	0.36	1.45
1.33	1.85	1.76
3.39	0.71	0.89
1.5	0.88	1.86
0.76	1.78	1.95
	1.85	0.70
	1.28	0.49
	0.42	0.85
	0.45	1.82
	0.77	1.75
	0.25	1.11
	0.56	1.11
	0.42	0.37
	0.65	0.45
	1.6	0.55
	0.86	0.48
	1.53	0.43
	2.99	0.45
	2.54	1.07
	0.73	0.75
	1.26	
	1.7	
	1.34	
	1.11	
	1.84	
	0.82	
	0.82	
	0.61	
	0.55	
	1.18	
	0.59	
	1.74	
	1	
	0.71	
	1.07	
	1.91	
	1.24	

		1.25		
		1.36		
		0.63		
		0.65		
		1.73		
Mean	1.19872	0.941111	1.15	1.71972
SD	0.656	0.539	0.657	1.03
SEM	0.059	0.042	0.056	0.099

A 6.3 Metal Ra values for ground surfaces

Ra						Mean	SD	SEM
M1	0.735	0.454	0.768	0.994	0.789	0.748	0.193	0.086
M2	0.711	0.657	0.901	0.687	0.766	0.7444	0.962	0.043
M3	0.941	0.743	1.05	0.822	0.824	0.876	0.12	0.034
M4	0.991	1.091	1.438	1.36	1.924	1.3608	0.365	0.163

A 6.4 Metal Rz values for ground surfaces

Rz								
M1	6.735	4.32	5.03	7.49	5.488	5.8126	1.29	0.575
M2	6.066	5.512	6.033	5.419	5.771	5.7602	0.292	0.132
M3	6.24	6.123	7.279	6.006	8.188	6.7672	0.942	0.421
M4	7.045	6.423	9.219	7.581	10.455	8.1446	1.657	0.741

A 6.5 Metal Rt values for ground surfaces

Rt								
M1	7.465	4.474	5.139	8.809	6.481	6.4736	1.748	0.782
M2	6.788	5.744	6.454	6.146	6.265	6.2794	1.748	0.782
M3	6.957	6.778	7.801	6.364	12.221	8.0242	2.4	1.07
M4	11.159	7.035	10.859	7.883	10.758	9.5388	1.928	0.862

A 6.6 Polymer Ra values for ground surfaces

Ra								
P1	0.786	0.933	0.952	0.865	0.699	0.847	0.105	0.047
P2	0.972	1.079	0.784	0.542	0.718	0.819	0.212	0.095
P3	0.629	0.996	0.879	0.734	0.678	0.7832	0.151	0.068
P4	1.125	1.298	1.12	1.762	1.374	1.3358	0.262	0.117

A 6.7 Polymer Rz values for ground surfaces

Rz								
P1	6.977	9.432	7.851	19.546	17.487	12.2586	5.83	2.61
P2	9.37	8.935	8.151	5.73	8.329	8.103	1.41	0.632
P3	6.324	11.58	9.818	8.054	8.582	8.8716	1.967	0.879
P4	24.64	32.581	14.57	23.518	21.242	23.3102	6.49	2.9

A 6.8 Polymer Rt values for ground surfaces

Rt								
P1	8.7	14.626	8.874	30.647	23.283	17.226	9.57	4.28
P2	11.08	10.047	11.866	8.243	14.877	11.2226	2.45	1.09
P3	7.75	12.717	16.497	11.999	9.841	11.7608	3.29	1.47
P4	30.983	46.844	11.471	28.922	24.978	28.6396	12.69	5.68

A 6.9 Adhesion raw data for ground surfaces

							Mean	SD	SEM
Flat	0.134	0.109	0.145	0.111	0.107	0.079	0.114	0.023	0.009
P1	0.139	0.141	0.119	0.108	0.113	0.131	0.125	0.014	0.006
P2	0.145	0.107	0.136	0.133	0.165	0.136	0.136	0.02	0.008
P3	0.154	0.143	0.136	0.165	0.170	0.361	0.189	0.086	0.03
P4	0.116	0.194	0.123	0.206	0.110		0.150	0.05	0.02

A 6.10 Proliferation raw data for ground surfaces

24h										Mean	SD	SEM
Flat	0.436	0.534	0.419	0.429	0.373	0.292	0.413	0.408	0.352	0.406	0.066	0.022
P1	0.052	0.384	0.288	0.338	0.169	0.299	0.391	0.324	0.218	0.274	0.11	0.04
P2	0.139	0.186	0.353	0.565	0.227	0.238	0.224	0.094	0.170	0.244	0.14	0.05
P3	0.227	0.171	0.375	0.317	0.679	0.431	0.179	0.269	0.239	0.321	0.159	0.053
P4	0.655	0.116	0.043	0.379	0.155	0.399	0.292	0.210	0.118	0.263	0.19	0.06

48h										Mean	SD	SEM
Flat	0.877	0.750	0.623	0.573	0.301	0.541	1.122	0.880	0.785	0.717	0.24	0.08
P1	0.049	0.334	0.241	0.029	0.076	0.032	0.367	0.295	0.339	0.196	0.15	0.05
P2	0.350	0.490	0.248	0.387	0.304	0.132	0.083	0.449	0.411	0.317	0.14	0.05
P3	0.284	0.186	0.060	0.636	0.282	0.260	0.125	0.142	0.100	0.230	0.17	0.06
P4	0.050	0.052	0.694	0.147	0.466	0.201	0.760	0.408	0.503	0.365	0.27	0.09

72h										Mean	SD	SEM
Flat	1.570	1.438	1.290	0.665	0.604	1.511	0.587	1.124	1.576	1.151	0.42	0.14
P1	2.521	2.502	0.063	0.604	0.300	0.614	0.204	0.158	0.060	0.781	1	0.33
P2	0.852	0.103	0.337	0.016	0.018	0.278	0.094	0.253	0.705	0.295	0.29	0.09
P3	0.270	0.242	0.578	0.504	0.073	0.354	0.163	0.074	0.088	0.261	0.19	0.06
P4	1.742	2.200	0.905	0.292	0.993	0.127	0.053	0.102	0.219	0.737	0.79	0.26

combined	24	48	72		24	48	72
Flat	0.406	0.717222	1.151167		0.022	0.08	0.14
P1	0.274	0.196111	0.780667		0.04	0.05	0.33
P2	0.244222	0.317111	0.294611		0.05	0.05	0.09
P3	0.321	0.230222	0.260667		0.053	0.06	0.06
P4	0.262857	0.364889	0.7365		0.06	0.09	0.26

Appendix 7 – cell images on surfaces

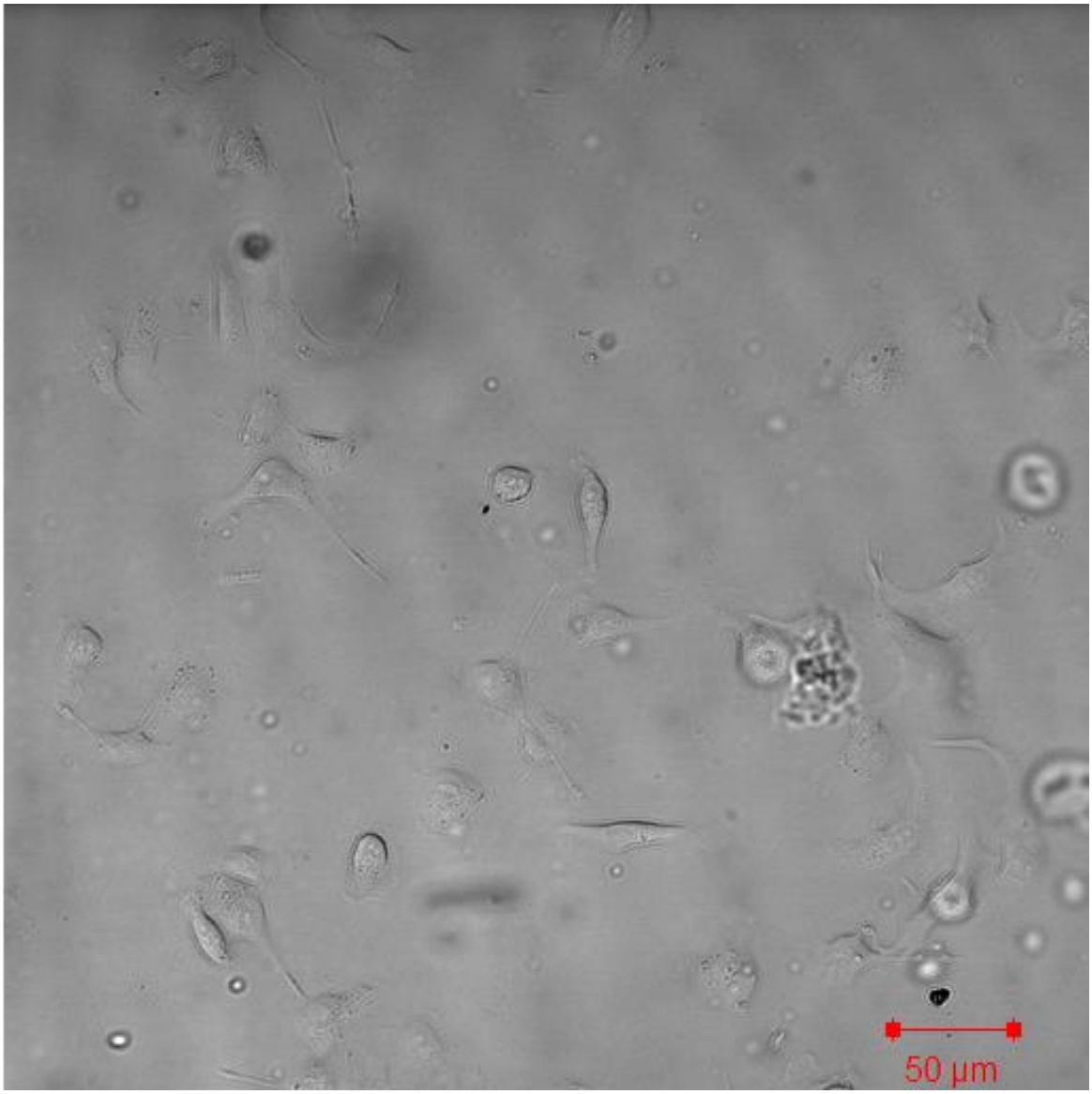

Image of LL24 fibroblasts on a non-patterned polymer surface during time-lapse photography for migration testing

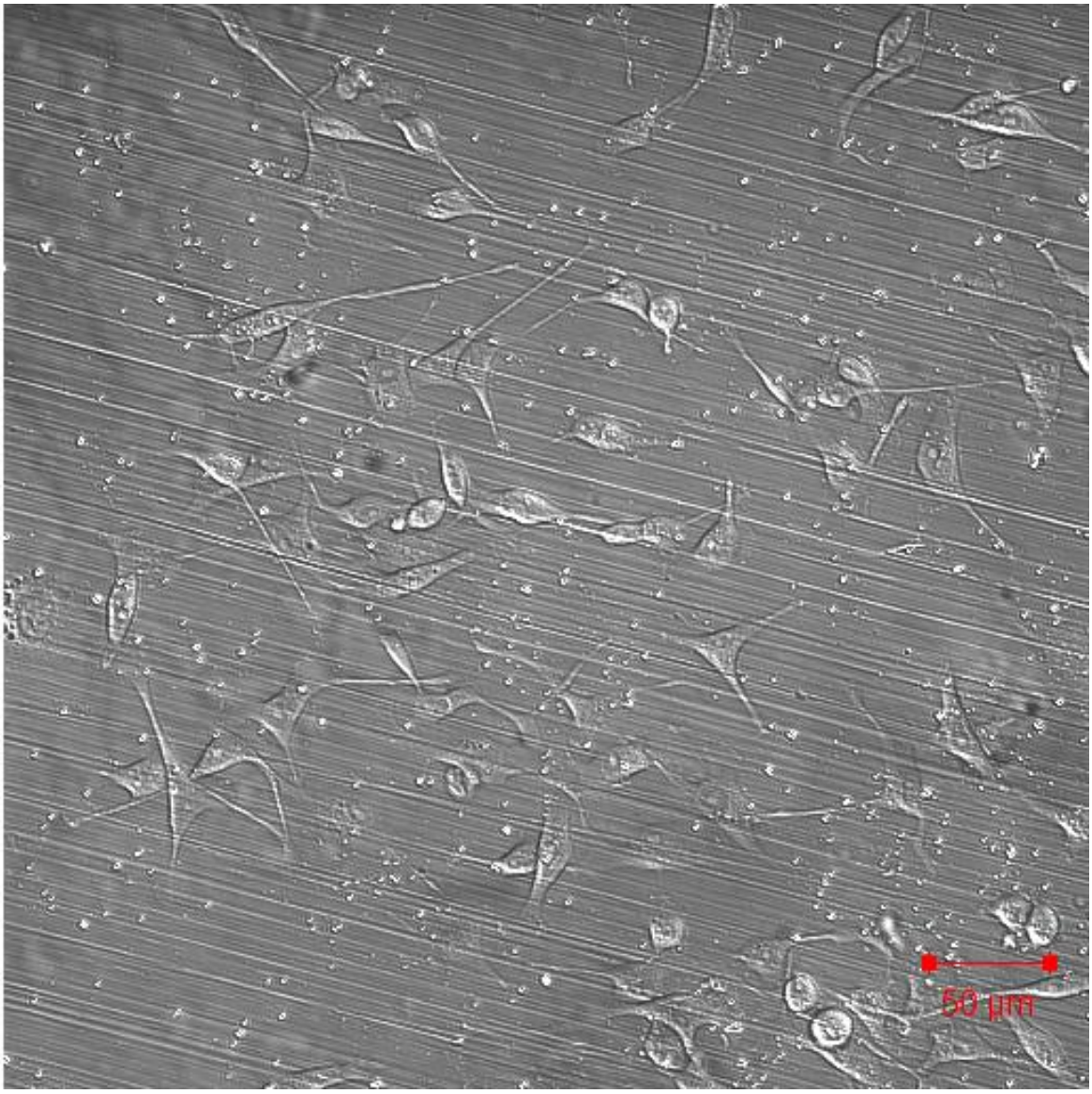

Image of LL24 fibroblasts on a linear polished polymer surface during time-lapse photography for migration testing

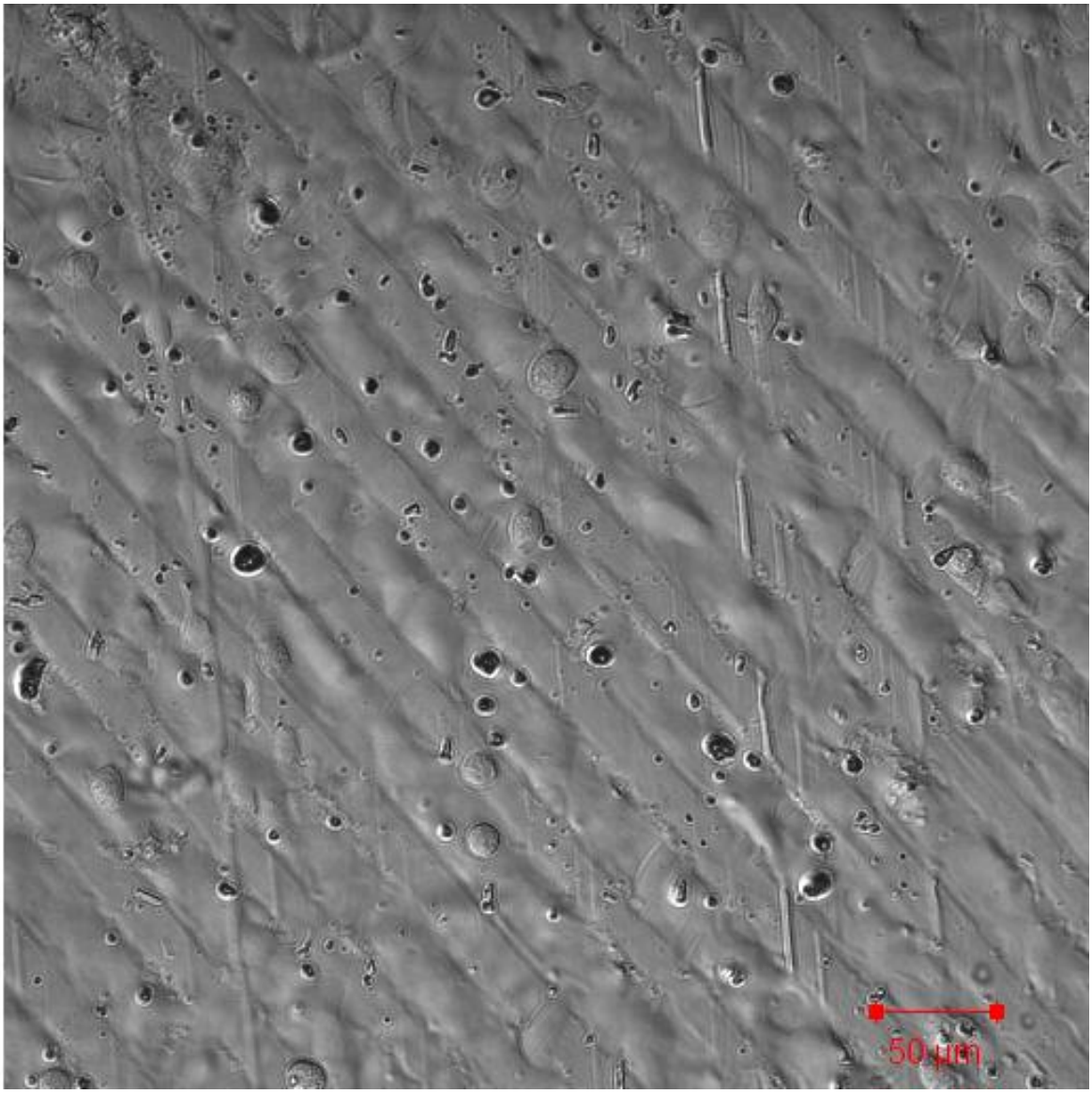

Image of LL24 fibroblasts on a laser patterned polymer surface during time-lapse photography for migration testing

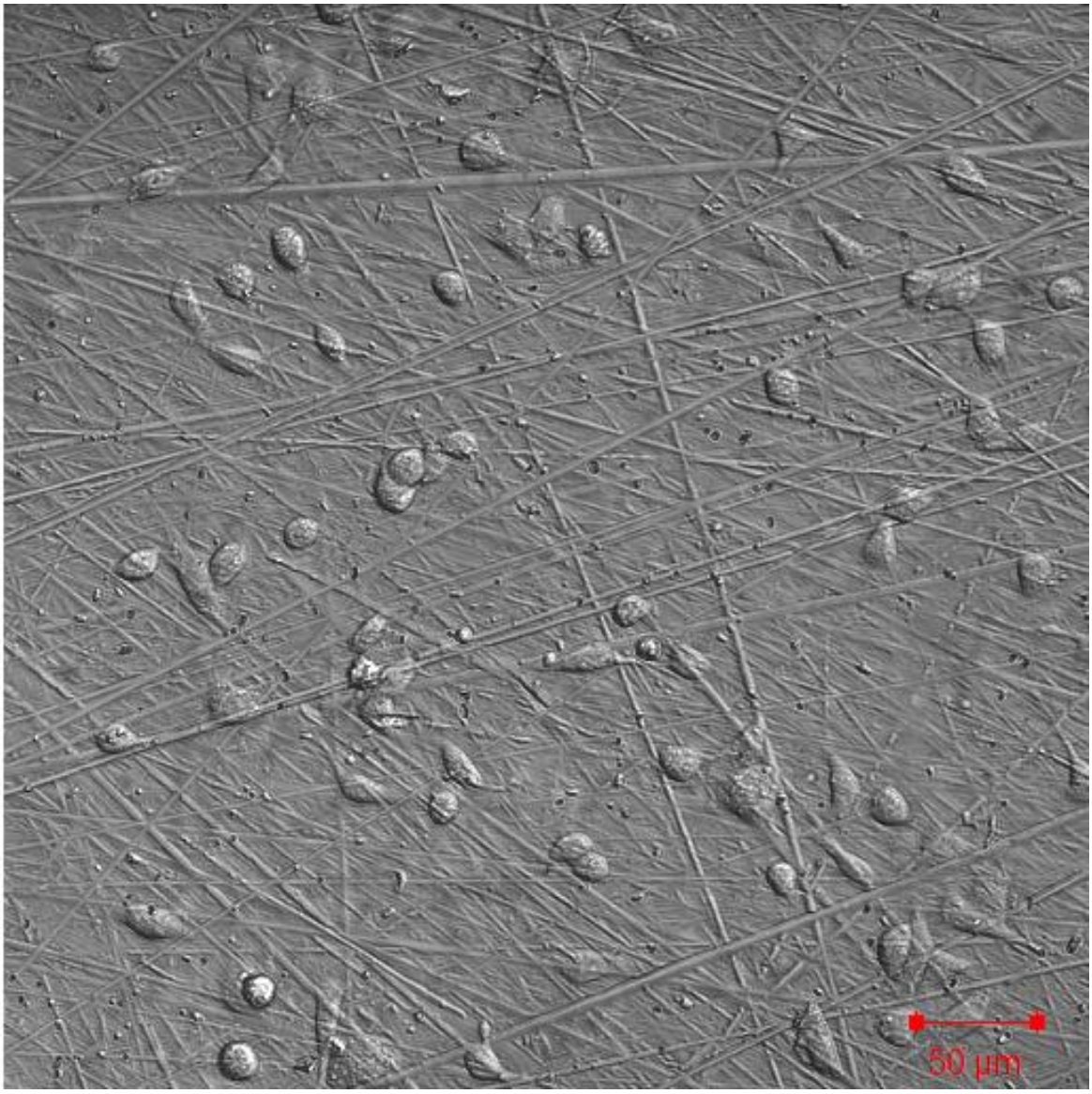

Image of LL24 fibroblasts on a random polished polymer surface during time-lapse photography for migration testing